Spring 2017

Volumetric error compensation for 5-axis machine tools

Jennifer Ruth Creamer

Department: Mechanical and Aerospace Engineering

VOLUMETRIC ERROR COMPENSATION FOR 5-AXIS MACHINE TOOLS

by

JENNIFER RUTH CREAMER

A DISSERTATION

Presented to the Faculty of the Graduate School of the

MISSOURI UNIVERSITY OF SCIENCE AND TECHNOLOGY

In Partial Fulfillment of the Requirements for the Degree

DOCTOR OF PHILOSOPHY

in

MECHANICAL ENGINEERING

2017

Approved

Douglas A. Bristow, Co-advisor

Robert G. Landers, Co-advisor

James B. Castle

Ming Leu

Xiaoping Du

V. Samaranayake

PUBLICATION DISSERTATION OPTION

This dissertation has been prepared using the Publication Option. The content of pages 4-36 have been published in the ASME Journal of Manufacturing Science and Engineering. The contents of pages 37-66 have been published in the International Journal of Advanced Manufacturing Technology. Opening and closing sections have been added for purposes normal to dissertation writing.

ABSTRACT

This work presents a geometric error compensation method for large 5-axis machine tools. The compensation method presented here uses tool tip measurements recorded throughout the axis space to construct a position-dependent geometric error model that can easily be used for error compensation. The measurements are taken using a laser tracker, permitting rapid error data gathering at most locations in the axis space. First two model types are compared for generating table-based error compensation and experimental results are presented. Table-based compensation is then extended to machine tool controller types with restrictions on the number or combination of compensation tables using an artificial intelligence method. The overall methodology is then extended to the integration of additional instruments. A particular strength of the proposed methodology is the simultaneous generation of a complete set of compensation tables that accurately captures complicated kinematic errors independent of whether they arise from expected and unexpected sources.

ACKNOWLEDGMENTS

Over the past seven years, I have received support and encouragement from many people. Many thanks are due to my advisors, Dr. Doug Bristow and Dr. Robert Landers, for supporting this work throughout my time at Missouri S&T and providing guidance along the way. Special thanks are due to Dr. James Castle for aiding me in my transition to industry and helping me navigate finishing my graduate work while working full time. I would like to thank my dissertation committee of Dr. Ming Leu, Dr. Xiaoping Du, and Dr. V. Samarayanake for their support. I would also like to thank Sam Easley for the countless hours he put in over the years facilitating experiments on machine tools throughout Boeing and Dr. Phil Freeman for laying the foundation for this work and providing advice and feedback throughout. Finally, I would like to thank Dr. Joan Broderick for providing me with invaluable undergraduate research experience that inspired me to go on to pursue a graduate degree. Funding for this work was generously provided by the Center for Aerospace Manufacturing Technologies at Missouri University of Science and Technology, the National Science Foundation (NSF, grant CMMI-1335340), and the Department of Education (DOE, grant P200A120062). Resources for experiments were provided by Boeing Research and Technology.

TABLE OF CONTENTS

LIST OF ILLUSTRATIONS

LIST OF TABLES

SECTION

1. INTRODUCTION

Monolithic parts have become increasingly common in the aerospace industry. Figure 1.1 shows an example of such a part. These parts can be beneficial in decreasing the amount of hand work and number of fasteners, but also increases part complexity and the demand for tight tolerances over longer distances, so new strategies for improving the accuracy of these machines is needed.

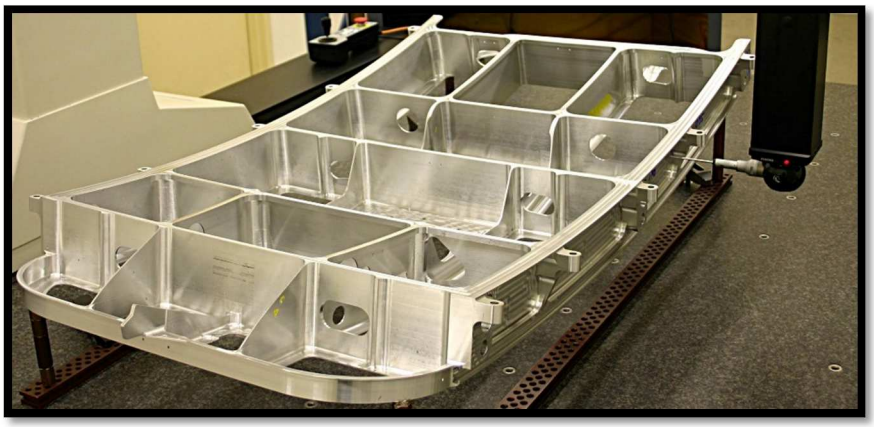

Figure 1.1: An example of a monolithic part that combines smaller components with features requiring tight tolerances.

Additionally, many machine shops have aging. The accuracy of machine tool is typically improved through calibration or mechanical adjustment since machine tools are very repeatable. Machine tool accuracy may also change over time due to wear or collisions with a work part or table, so calibration is a part of regular maintenance. Calibration common practice in the industry, but based on techniques developed originally for three-axis machine tools. Three-axis machine tools often used direct measurement methods since they have only linear axes. Direct measurement methods are

measurement methods that attempt to isolate an individual error. These methods can be more time consuming and are not as suited to more complex machines. Sartori and Zhang [1] and Schwenke et al [2] both give an overview of direct measurement methods. ISO 230-1 describes the current practice for machine tool calibration [3]. These methods generally calibrate the three linear axes individually, then measure the rotary axes separately. Calibration of the rotary axes uses indirect measurement, which uses measurement of the tooltip position, rather than a direct measurement of individual errors. Indirect measurement types are summarized in [4], including instruments such as a ball bar [5, 6] or the R-test [7, 8]. The ball bar has traditionally been used to identify errors between two linear axes, but has been extended to rotary axes in Tsustsumi and Saito [5], Zargarbashi and Mayer [6], and Lei et al [9]. Some less common instruments include the cross grid encoder, "capball", developed by Zargarbashi and Mayer [6], and "non-bar," developed by Jywe et al [10]. These methods assume perfectly calibrated linear axes so that the errors of the rotary axes can be isolated. There are several problems with this approach. First, assumptions are being made that the errors on each axis can be separated from one another and that after the linear axes are calibrated, their errors have no further influence on the rotary axes. In addition to this, each of these individual errors requires a different instrument and/or setup, and a full calibration can require several weeks to complete according to experts inside Boeing. In response to this, Dr. Phil Freeman and Sam Easley developed a method to calibrate a machine tool using a laser tracker in a single setup and implement compensation through a real-time inverse Jacobian based algorithm [11]. This work was completed through a Metals Affordability Initiative project, and won a Defense award in 2006 as a ground breaking technology. The real-time algorithm was developed in conjunction with Siemens, and as a result can only be implemented on the Siemens 840D. Even without this specific restriction, the real-time algorithm requires deep access to the control, and will not work on many controller types. However, most controllers have some type of position dependent look up tables meant to be used for geometric error compensation.

This work presents a method for generating optimal table-based compensation for a variety of controllers and presents results on multiple machines. Paper I presents a general method for creating optimal table-based compensation from tool tip

measurements taken with a laser tracker and provides experimental results on a 5-axis machine tool in a laboratory setting.

Section 2 presents results using the methodology presented in Section 2 on six additional machines. Two of these machines are Boeing Defense production, two are Boeing Commercial production, one is an additional Boeing lab machine, and one is a NASA production machine.

Paper II presents and extension of the table-based compensation methodology proposed in Paper I to multiple controller types. Table-based compensation method developed previously assumes that all tables will be available on a machine tool controller, and this is frequently not the case, particularly on older controllers. There is often some freedom in how the available tables are assigned, so what is the best way to assign them for a specific machine. An artificial intelligence methodology is presented to solve this problem.

Section 3 addresses concerns about laser tracker accuracy and presents methods to mitigate any issue with instrument accuracy as well as a way of integrating other measurement instruments. Some studies raise concerns about the accuracy of laser trackers being inadequate for machine tool calibration. While it is true that laser trackers are less accurate than some traditional instruments like interferometers, there are techniques for mitigating noisy measurements. Additionally, the laser tracker is used to measure volumetric error, which tends to be larger than the errors of an individual axis. The accuracy of the laser tracker does impact the number of measurements required and to some extent the model accuracy, so ways to integrate more accurate instruments at sensitive poses or to better use the information available are needed. This section experiments with using native spherical coordinate measurements from the laser tracker and their uncertainties in a maximum likelihood estimator.

PAPER

I. TABLE-BASED VOLUMETRIC ERROR COMPENSATION FOR LARGE 5-AXIS MACHINE TOOLS

J. Creamer[1], D.A. Bristow[2], R.G. Landers[2], P. Freeman[3], S. Easley[1]

[1]Boeing Research and Technology, St. Louis, MO

[2]Department of Mechanical and Aerospace Engineering,
Missouri University of Science and Technology, Rolla, MO

[3]Boeing Research and Technology, Charleston, NC

ABSTRACT

This paper presents a geometric error compensation method for large 5-axis machine tools uses tool tip measurements recorded throughout the axis space to construct an explicit model of a machine tool's geometric errors from which a corresponding set of compensation tables are constructed. The measurements are taken using a laser tracker, permitting rapid error data gathering at most locations in the axis space. Two position-dependent geometric error models are considered in this paper. The first model, referred to as the six degree-of-freedom model, utilizes a six degree-of-freedom kinematic error description at each axis, and the second model, referred to as the axis perturbation model, describes geometric errors as small perturbations to the axis commands. The parameters of both models are identified from the measurement data using a maximum likelihood estimator. Compensation tables are generated by projecting the error model onto the compensation space created by the compensation tables available in the machine tool controller. Experimental results on a commercial 5-axis machine tool are presented and analyzed. Compensation using the first model is found to reduce the mean volumetric error of a validation data set from 551 to 38 μm, a 93.1% reduction. Compensation using the second model reduced the mean volumetric error for the same validation data set to 43 μm, a 92.2% reduction. Despite significant differences in the machine tool error descriptions, both methods produce similar results, within the repeatability of the machine tool. Reasons for this unexpected result are discussed. Analysis of the models and compensation tables reveals significant complicated, and unexpected kinematic

behavior in the experimental machine tool. A particular strength of the proposed methodology is the simultaneous generation of a complete set of compensation tables that accurately captures complicated kinematic errors independent of whether they arise from expected and unexpected sources.

Keywords: 5-axis machine tools, geometric errors, volumetric error compensation

1. INTRODUCTION

The trend towards the manufacture of large monolithic parts in the aircraft and other industries is driving the demand for high accuracy from 5-axis machine tools. One of the largest sources of machine tool inaccuracy is geometric errors, which are typically corrected through regular calibration. Five-axis machine tools are known to have 41 basic geometric errors [1] and standard methods for measuring these errors are well established. Many of these methods separate measurement of the three linear axes from the two rotary axes. The basic geometric errors are then typically isolated and directly measured individually, particularly those associated with the linear axes. Such methods are well described in ISO standard 230-1 [2], and are frequently used for calibrating 5-axis machine tools. Other methods use indirect measurements of the error through measurements of the tooltip and a fitting process to identify several errors simultaneously and, thus, are an improvement over direct methods. Common indirect measurement methods for rotary axes include the ball bar [3, 4], R-test [5, 6], touch trigger probes [7, 8, 9], and machining tests [10]. These methods are summarized in [11]. Nearly all of the previously described tools calibrate only a portion of machine tool geometric errors and must be combined with other tools and methods to capture all 41 basic geometric errors. This piecemeal approach means that calibration becomes a time-consuming and expensive process. Furthermore, a complete picture of the machine tool behavior throughout the workspace is not obtained; therefore, some errors, especially complicated or unexpected geometric errors, are not measured, leading to erroneous confidence in the compensation.

As an alternative to some of the measurement tools described above, another indirect measurement instrument, the laser tracker, can be used to measure machine tool geometric errors more rapidly as it only requires one set up. The laser tracker is less

accurate than some conventional measurement instruments due to the inaccuracy of the angular positioning. For example, the accuracy of a typical laser interferometer is 0.5 ppm, while the angular accuracy of a typical laser tracker is 3.5 ppm. To mitigate this, multiple laser trackers [12, 13] or multiple set up locations [14, 15] have been used. Since the geometric errors are not being directly measured, more measurement points and a fitting algorithm that accounts for measurement variances can also mitigate less accurate individual measurements. Both Freeman [16] and Nubiola and Bonev [17] reported measuring hundreds of points in a few hours on a small 5-axis machine tool and a 6-axis industrial robot, respectively, demonstrating the speed of this instrument. Both used a single laser tracker for calibration and reported good improvement over the workspace, suggesting this instrument is not only quick, but has the accuracy needed to measure the geometric errors present in these types of machines.

In order to use indirect measurements for compensation, a model of the geometric errors must be constructed. It is desirable for a geometric error model to be 1) complete, in that it models each machine tool error, 2) continuous, in that small changes in the axis positions do not cause large changes in the compensation values, and 3) minimal, in that the model does not include redundant parameters. Several conventions are used to describe the rigid body kinematics of machines and their geometric errors. The Denavit-Hartenberg (D-H) convention based models, originally described by Denavit and Hartenberg [18], have been used for the kinematic calibration of robots and machine tools. However, the D-H convention lacks continuity when two axes are parallel and the model is not complete. Modifications have been proposed by Hayati [19] and Veitschegger and Wu [20]. Alternative kinematic models that attempt to address these issues include modeling shape and joint transformations separately [21, 22, 23], the Complete and Parametrically Continuous (CPC) model proposed by Zhuang et al. [24], the multi-body system model [25], screw theory [26], product-of-exponentials model [27, 28] for robot calibration, and the matrix summation method proposed by Lin and Shen [29]. The work in this paper makes use of the Zero Reference Model [30] to describe the nominal kinematics and describes geometric errors as three small translations and rotations between each machine tool axis, which is a common way to represent these types of errors [31, 32]. This method has been shown to be complete, continuous, and

minimal [16], making it an appropriate model to use for machine tool geometric error calibration.

The overall goal of calibration is to improve a machine tool's accuracy, which is typically achieved through compensation. Geometric error compensation is achieved by adjusting the machine tool's commanded axis positions to account for the modeled geometric errors. Typically this compensation is implemented using options available on machine tool controllers such as table-based compensation. Alternatively, offline compensation is implemented through the alteration of pre-task trajectories or the alteration of the part program for each part, as was done in [33].

Compensation tables, available on most machine tool controllers, may be a more practical option since they are calculated offline and are well integrated with other controller features. Each table contains a set of compensation values that correspond to a set of axis positions. The compensation values are the amounts a compensation axis will move when the input axis is at the corresponding axis position. When the input axis is at a position not found in the set of axis positions, interpolation is utilized. Different machine tool controllers have varying numbers of compensation tables, table resolution, and limitations on the combinations of tables that can be utilized. Most compensation tables use the measurement from an input axis to adjust the position of an output axis to correct for the geometric errors. For 3-axis machine tools, determining how to fill the compensation tables is relatively straight forward; however, this is not always the case for 5-axis machine tools. Therefore, a method to quickly and accurately calibrate 5-axis machine tools using table-based compensation is needed.

The primary contribution of this chapter is the development of a novel modeling framework for capturing complicated geometric errors and generating the corresponding table-based compensation for those geometric errors. Specifically, two models capable of describing complicated geometric error models are proposed. The first describes each machine tool axis with a six degree-of-freedom kinematic error that changes continuously along the range of the axis, while the second describes the machine tool with axis command-based geometric errors that lack the physical intuition of the former model, but are more amenable to the generation of compensation tables. A compensation-table generating algorithm for each model is presented and experimental evaluation of both

methods are obtained and compared. The remainder of the paper is organized as follows. Section 2.2 develops the kinematics for two geometric error models. Model identification is discussed in Section 2.3 and the compensation methods are presented in Section 2.4. The experimental setup is described in Section 2.5, Section 2.6 presents experimental results, and Section 2.7 summarizes this chapter and presents conclusions.

2. KINEMATIC MODELING

This section presents nominal machine tool kinematics, as well as two different kinematic models that describe position-dependent machine tool geometric errors.

2.1. Nominal Kinematics. Nominal kinematic equations describe the ideal position and orientation of a machine tool. Given a set of axis commands, the expected tooltip position is determined by transforming the machine tool base frame through a series of coordinate frames associate with each axis to the tooltip. Such transformations can be described using Linear Homogeneous Transformation (LHT) matrices [18],

$$\mathbf{T} = \begin{bmatrix} n_x & o_x & a_x & p_x \\ n_y & o_y & a_y & p_y \\ n_z & o_z & a_z & p_z \\ 0 & 0 & 0 & 1 \end{bmatrix}, \tag{1}$$

where the unit vectors, $\mathbf{n} = [n_x\ n_y\ n_z]^T$, $\mathbf{o} = [o_x\ o_y\ o_z]^T$, and $\mathbf{a} = [a_x\ a_y\ a_z]^T$ are the orientations of the x, y, and z-axes, respectively, of a frame with respect to the previous frame and $\mathbf{p} = [p_x\ p_y\ p_z]^T$ is a vector from the origin to the origin of the current frame. The nominal kinematics for an n-axis machine tool is

$$\mathbf{F}_n(\mathbf{q}) = \mathbf{T}_1(q_1)\mathbf{T}_2(q_2)\cdots\mathbf{T}_{n-1}(q_{n-1})\mathbf{T}_n(q_n), \tag{2}$$

where $\mathbf{q} = [q_1\ q_2\ \ldots\ q_n]^T$ is the axis command vector and $\mathbf{T}_1(q_1),\ldots,\mathbf{T}_n(q_n)$ are LHTs for axes 1,…,n, respectively.

The Zero Reference model [34] is a convenient way to define the LHT between two axes for machine tools. Using the Zero Reference model, the orientation of the machine tool reference coordinate frame can be chosen arbitrarily; however, it is convenient to select an orientation that aligns the positive coordinate directions with the positive direction of travel of the linear axes. The location of the reference coordinate frame is also arbitrary; however, depending on the machine tool configuration, some locations can simplify the kinematics. For 5-axis machine tools with both rotary axes at the spindle, it is convenient to place the reference coordinate frame at the intersection of the axes of rotation of the rotary axes.

Because of inaccuracies in machine tool component fabrication and assembly, the actual machine tool kinematics are never equivalent to those of the nominal kinematics. In the following two subsections, two models are proposed to describe the actual machine tool kinematics.

2.2. Six Degree of Freedom (6-DoF) Model. The Six Degree of Freedom (6-DoF) model assumes the actual machine tool kinematics can be described by the nominal kinematic model with three small position-dependent error rotations and three small position-dependent error translations included in each axis transformation. This idea is illustrated in Figure 1 where an error transformation appended to the nominal transformation is used to describe the location of the actual transformation.

For an *n*-axis machine tool, the 6-DoF model takes the form,

$$\mathbf{F}_{6DoF}(\mathbf{q}) = \mathbf{T}_1(q_1)\mathbf{E}_1(q_1)\mathbf{T}_2(q_2)\mathbf{E}_2(q_2)\cdots\mathbf{T}_n(q_n)\mathbf{E}_n(q_n), \tag{3}$$

where $\mathbf{E}_k(q_k)$ is the axis position-dependent 6-DoF kinematic error transformation from axis *k* to axis *k*'. Assuming the kinematic errors are small, the kinematic error transformation can be modeled by the linear approximation,

$$\mathbf{E}_k(q_k) = \begin{bmatrix} 1 & -\varepsilon_{kz}(q_k) & \varepsilon_{ky}(q_k) & \delta_{kx}(q_k) \\ \varepsilon_{kz}(q_k) & 1 & -\varepsilon_{kx}(q_k) & \delta_{ky}(q_k) \\ -\varepsilon_{ky}(q_k) & \varepsilon_{kx}(q_k) & 1 & \delta_{kz}(q_k) \\ 0 & 0 & 0 & 1 \end{bmatrix}, \tag{4}$$

where ε_{kx}, ε_{ky}, and ε_{kz} are position-dependent rotational errors in the k^{th} axis's local coordinate frame about the X, Y, and Z axes, respectively, and δ_{kx}, δ_{ky}, and δ_{kz} are position-dependent translational errors in the k^{th} axis's local coordinate frame along the X, Y, and Z axes, respectively.

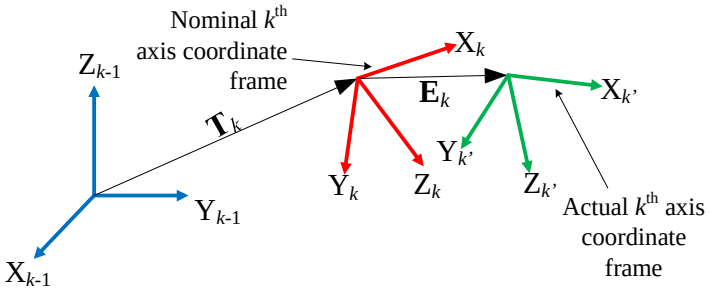

Figure 1: Illustration of nominal and actual axis coordinate frames where E_k describes transformation from nominal frame *k* to actual frame *k'*.

In order to capture complicated geometric errors, the 6-DoF errors are permitted to change along the range of the axis. To facilitate this position dependency, each of the error functions (e.g., ε_{kx}, ε_{ky}, ε_k, δ_{kx}, δ_{ky}, and δ_{kz}) are described by a function basis. In practice, a finite set of the basis functions are selected such that the number of basis functions is used as a tuning variable to select between model complexity and error modeling fidelity. To be a good candidate, basis functions need to be orthogonal over an interval and have similar scaling over the same interval. In the authors' experience, Chebyshev polynomials provide a particularly efficient basis for modeling machine tool geometric errors and, thus, are used throughout this paper. The Chebyshev polynomial basis functions are described recursively such that an m^{th} order Chebyshev polynomial normalized to the range $-1 < x < 1$ is

$$f(x) = a_0 c_0(x) + a_1 c_1(x) + a_2 c_2(x) + \cdots + a_m c_m(x), \tag{5}$$

where

$$c_0(x)=1, c_1(x)=x, c_2(x)=2x^2-1, \ldots, c_m(x)=2xc_{m-1}(x)-c_{m-2}(x) \quad (6)$$

and a_0, a_1,…, a_m are model parameters that need to be identified.

This type of model has been commonly used to evaluate the errors of machine tools [16, 32]. The 6-DoF model is complete [16], continuous if the function basis is continuous, and, depending on the machine tool configuration, minimal. For machine tool configurations where the 6-DoF model is not minimal, it can be made minimal by identifying and removing redundant terms, i.e., multiple terms describing the same position and orientation change at the tool tip. These redundant terms can cause model fitting issues such as slow fitting and poor estimates, so removing them from the model is preferable. Typically, the redundant terms for a specific axis depend on the axis which directly follows it. More detailed derivations of the redundant terms are available in [35]. For the XYZCB machine tool used in Section 4, the only redundant terms are the first order terms in $\delta_k(q_k)$ that are orthogonal to the direction of travel for the translational axes. Proof that the model can be made minimal is contained in [16] based on the work in [35].

2.3. Axis Perturbation (AP) Model. A new machine tool geometric error model is presented here for the purpose of efficiently calculating machine tool compensation tables. Compensation tables typically are look-up tables which depend on a single axis position (i.e., input axis) and contain a small adjustment to a single axis (i.e., output axis). The geometric error model that corresponds to this type of compensation space is one that represents the machine tool's geometric errors as small position-dependent perturbations to the nominal axis commands. This model is referred to in this paper as the Axis Perturbation (AP) model, and is

$$\mathbf{F}_{AP}(\mathbf{q})=\mathbf{F}_n\left(\mathbf{q}+\hat{\mathbf{q}}(\mathbf{q})\right), \quad (7)$$

where $\hat{\mathbf{q}}(\mathbf{q}) = [\hat{q}_1(\mathbf{q}) \quad \hat{q}_2(\mathbf{q}) \quad \cdots \quad \hat{q}_n(\mathbf{q})]^T$ is a vector of functions that perturb the nominal axis commands and $\mathbf{F}_n$ is the nominal kinematic model as described in (2). ***Remark:*** The reader may note that while the 6-DoF model introduces error kinematics, $\mathbf{E}_i$, with a direct connection to the underlying geometric errors, the explicit relationship between the perturbation functions in the AP model and specific geometric errors may not be apparent. Indeed, the AP model is not explicitly motivated by specific geometric errors, but rather by the structure of the compensation tables that will be generated by the model. Thus, while the 6-DoF model can be said to be motivated by kinematics, the AP model is motivated by compensation. As will be shown and discussed in Section 5, both models demonstrate good capability for describing and compensating complicated kinematic errors.

Unlike the 6-DoF model, the AP model is not necessarily a complete model of the basic geometric errors. An example is the translational offset between the axes of rotation in successive rotational axes, which is illustrated in the experimental system in Section 4. In some cases, the offset corrections for such errors, referred to here as mechanical offsets, can be corrected as parameters in the machine tool controller, which is different from the compensation tables. As demonstrated in Section 4, the AP model can be easily extended to include additional parameters corresponding to these additional compensation parameters.

The axis command perturbation functions in the AP model are described as an uncoupled sum of perturbations of each axis command (q_1, q_2,…, q_n) as,

$$\begin{aligned} \hat{q}_1(\mathbf{q}) &= f_{11}(q_1) + f_{21}(q_2) + \cdots + f_{n1}(q_n) \\ \hat{q}_2(\mathbf{q}) &= f_{12}(q_1) + f_{22}(q_2) + \cdots + f_{n2}(q_n) \\ &\vdots \\ \hat{q}_n(\mathbf{q}) &= f_{1n}(q_1) + f_{2n}(q_2) + \cdots + f_{nn}(q_n) \end{aligned}, \tag{8}$$

where $f_{ij}(q_i)$ is a scalar function mapping the axis command, q_i, on axis i onto a perturbation to the command for axis j. As in the 6-DoF model, the unknown error-describing functions, $f_{ij}(q_i)$, are modeled with a Chebyshev polynomial basis, (5) and (6)

in this paper. Although the AP model is not complete, as discussed above, the axis perturbation structure ensures that it is continuous when the basis functions are continuous.

3. MODEL PARAMETER IDENTIFICATION

The first step in the model parameter identification process is to measure a variety of machine tool positions and orientations. In Section 4.1, the measurement technique used in this paper is described. Once measurements are collected, a maximum likelihood estimator is used to identify the model parameters. This algorithm is described in Section 4.2. The geometric error model is then used to find an optimal set of table compensation functions, as described in Section 4.3.

3.1. Measurement. The proposed method uses a laser tracker to acquire position measurements of a tool located in the spindle. The position measured by the laser tracker is described by,

$$\mathbf{p}_m = \mathbf{T}_m \mathbf{E}_0 \mathbf{F}_* \left(\mathbf{q} + \boldsymbol{\nu} \right) \mathbf{p}_{Tl} + \boldsymbol{\xi} , \tag{9}$$

where $\mathbf{p}_m = [x_m \; y_m \; z_m \; 1]^T$ is the (x_m, y_m, z_m) measurement in the laser tracker measurement frame, $\mathbf{T}_m$ is the nominal transformation from the machine tool base frame to the measurement frame, $\mathbf{E}_0$ is the (unknown) 6-DoF error kinematic in the transformation $\mathbf{T}_m$,

$$\mathbf{E}_0 = \begin{bmatrix} 1 & -\varepsilon_{0z} & \varepsilon_{0y} & \delta_{0x} \\ \varepsilon_{0z} & 1 & -\varepsilon_{0x} & \delta_{0y} \\ -\varepsilon_{0y} & \varepsilon_{0x} & 1 & \delta_{0z} \\ 0 & 0 & 0 & 1 \end{bmatrix}, \tag{10}$$

$\mathbf{F}_*$ is the 6-DoF model, (3), or the AP model, (7), $\boldsymbol{\nu}$ is the positioning error of the axes, $\boldsymbol{\xi}$ is the measurement noise, and $\mathbf{p}_{Tl} = [u_x L_T \; u_y L_T \; u_z L_T \; 1]^T$, where L_T is the length of the measurement tool mounted in the machine spindle and $[u_x \; u_y \; u_z]^T$ is the unit vector defining the tool direction with respect to the last axis frame. Note that here, the

positioning error, **v**, represents the random positioning error of the machine tool, typically measured as repeatability. The measurement noise and the positioning error are assumed to be Gaussian.

3.2. Parameter Identification. The model parameter identification method chosen for this problem is the Implicit Loop Method (ILM) as described in [36]. The ILM treats the machine tool as having a closed kinematic chain from the reference coordinate frame to the tooltip, with the measurement instrument included in the chain in order to close the loop. The unknown machine parameters are estimated to maximize the likelihood, while satisfying the constraint. A key advantage of this method is that measurement errors and machine tool repeatability errors can be treated independently, using separate statistical models for each.

Let $\mathbf{\Sigma}_{\xi}$ be the covariance of the measurement noise, $\boldsymbol{\xi}$, and $\mathbf{\Sigma}_{\nu}$ be the covariance of the positioning error (repeatability) of the machine tool axes, **v** reflecting that the machine tool axes do not always achieve exactly the commanded position. Let **b** be a vector containing the $\mathbf{E}_0$ parameters in (10), all mechanical offsets to be modified in the machine tool controller, and the model parameters. The model parameters are the Chebyshev polynomial coefficients for the 6-DoF parameters in (5) in the case of the 6-DoF model, and the Chebyshev polynomial coefficients for the perturbation functions in (8) in the case of the AP model. Now, consider the parameters in **b** as random variables with normal distributions and assign a standard deviation, σ, to each parameter in **b**. Then, the covariance matrix for **b** is, $\mathbf{\Sigma}_b = diag\left(\sigma_1^2, \sigma_1^2, \ldots, \sigma_{N_b}^2\right)$, where σ_i is the standard deviation for the i^{th} parameter in **b** and the vector **b** contains N_b parameters. Then, the most likely parameter description of the system is obtained by minimizing,

$$\underset{\mathbf{v}_1, \boldsymbol{\xi}_1, \ldots, \mathbf{v}_N, \boldsymbol{\xi}_N, \mathbf{b}}{\arg\min} \sum_{i=1}^{N} \left(\mathbf{v}_i^T \mathbf{\Sigma}_{\nu}^{-1} \mathbf{v}_i + \boldsymbol{\xi}_i^T \mathbf{\Sigma}_{\xi}^{-1} \boldsymbol{\xi}_i \right) + \mathbf{b}^T \mathbf{\Sigma}_b^{-1} \mathbf{b}, \tag{11}$$

subject to the implicit loop constraints from (9), given by,

$$\mathbf{p}_{m,i} - \mathbf{T}_m \mathbf{E}_0 \mathbf{F}_* \left(\mathbf{q}_i + \mathbf{v}_i \right) \mathbf{p}_{Tl} + \boldsymbol{\xi}_i = \mathbf{0} \qquad i = 1, 2, \ldots, N \,, \tag{12}$$

where the index *i* represents the measurement number and *N* measurements are acquired.

In practice, determining appropriate standard deviations, σ_i, $i = 1,\ldots,N_b$, *a priori* for the parameters **b** is challenging. Therefore, here these standard deviations are treated as tuning variables that can be used to control the relative magnitude of each of the parameters to be identified. Larger values for the standard deviations will encourage a tighter model fit, but can cause challenges in the convergence of (11), (12) due to numerical sensitivity. Based on experience, the best models are obtained by starting with small variances and iteratively tuning the variances until desirable model performance is achieved. Model performance can be judged based on the residual volumetric errors and the value of the objective function, χ^2, given in (11). The expected value of χ^2 based on [36] is $5N$ with a standard deviation of $\sigma = \sqrt{10N}$. For large enough values of *N*, the distribution of χ^2 is approximately Gaussian, and χ^2 will value within three standard deviations of the expected value 99.7% of the time When χ^2 is above this range, the parameter or measurement variances may not be large enough, and when it falls below, they may be too large. The residual volumetric errors for the geometric error models of most machine tools measured with a laser tracker will typically fall below 0.125 mm, and when the residual error is larger than this, model fit may be improved by identifying errors outside of the typical range and increasing those parameter variances (ie comparing the size of parameters to their variances individually).

3.3. Compensation. The identified kinematic models provide the foundation for constructing optimal machine tool compensation tables. Compensation tables are lookup tables whose input is the measurement of one axis and output is a value to be added to (or subtracted from) an axis command. For example, a table whose input is a measurement of axis *i* and output is a correction to axis *o* may be represented as,

$$\begin{array}{ccc} \text{Entry} & \text{Input} & \text{Output} \\ 1 & q_{i,1}^{t} & t_{oi,1} \\ \vdots & \vdots & \vdots \\ j-1 & q_{i,j-1}^{t} & t_{oi,j-1} \\ j & q_{i,j}^{t} & t_{oi,j} \\ j+1 & q_{i,j+1}^{t} & t_{oi,j+1} \\ \vdots & \vdots & \vdots \\ N_t & q_{i,N_t}^{t} & t_{oi,N_t} \end{array} \tag{13}$$

where $q_{i,j}^{t}$ is the j^{th} table listing of the input axis, $t_{oi,j}$ is the corresponding compensation value to be added to the axis command for the output axis, and N_t is the number of table entries. Then, the compensated command to axis *o*, q_o^c, is linearly interpolated from table entries as,

$$q_o^c = q_o + t_{oi,j-1} + \left(t_{oi,j} - t_{oi,j-1}\right)\frac{q_i - q_{i,j-1}^{t}}{q_{i,j}^{t} - q_{i,j-1}^{t}} \tag{14}$$

where *j* is selected such that the measured input axis position q_i satisfies $q_{i,j-1}^{t} \le q_i \le q_{i,j}^{t}$ and q_o is the nominal command of the output axis.

To reduce the computational cost of generating optimal tables from the identified machine tool models (6-DoF or AP), the compensation functions, t_{oi}, are treated as smooth during optimization. After optimal smooth compensation functions are identified, they are discretized for lookup table entry. Consider a complete set of compensation tables, that is, a table for each combination of measurement axis inputs to compensation axis outputs. Then, the compensated axis commands are,

$$\mathbf{q}^{c} = \mathbf{q} + \mathbf{t}\left(\mathbf{q}\right) \tag{15}$$

where, $\mathbf{q}^{c} = \begin{bmatrix} q_1^c & q_2^c & \cdots & q_n^c \end{bmatrix}^T$, and,

$$\mathbf{t}(\mathbf{q}) = \begin{bmatrix} t_{11}(q_1) + t_{12}(q_2) + \cdots + t_{1n}(q_n) \\ t_{21}(q_1) + t_{22}(q_2) + \cdots + t_{2n}(q_n) \\ \vdots \\ t_{n1}(q_1) + t_{n2}(q_2) + \cdots + t_{nn}(q_n) \end{bmatrix}. \tag{16}$$

The table functions should be selected so that the kinematics of the actual system, with compensated commands, are close to the nominal kinematics. That is, it is desirable to have $\mathbf{F}_*(\mathbf{q}^c) \approx \mathbf{F}_n(\mathbf{q})$. For the AP model, the table optimization problem is solved from (7) and (15) by selecting compensation tables as the negative of axis perturbations, or

$$\mathbf{t}_{AP}(\mathbf{q}) = -\hat{\mathbf{q}}(\mathbf{q}), \tag{17}$$

for which $\mathbf{F}_{AP}(\mathbf{q}+\mathbf{t}_{AP}(\mathbf{q})) = \mathbf{F}_n(\mathbf{q})$. For the 6-DoF problem equality is not guaranteed and some tradeoff must be determined between accuracy in the position versus orientation of the compensated machine. The approach used here leverages the numerical tools developed for parameter identification in Section 4.2 to solve the table optimization problem. Two tool lengths, $\mathbf{p}_{Tl}$, are selected to span the length of cutting tools for the machine tool, one short tool length and one long tool length. A sequence of joint commands spanning the axis workspace are generated and pseudo-measurements of the 6-DoF model and nominal model are obtained numerically at each tool length and joint command, yielding the implicit loop constraint equation,

$$\mathbf{F}_{6DoF}(\mathbf{q}_i + \mathbf{t}_{6DoF}(\mathbf{q}_i))\mathbf{p}_{Tl} - \mathbf{F}_n(\mathbf{q}_i)\mathbf{p}_{Tl} - \mathbf{e}_i = \mathbf{0} \qquad i = 1, \ldots, N_{pm}, \tag{18}$$

where $\mathbf{e}_i$ is the position error of the compensated system and N_{pm} is the number of pseudo-measurements. The tables $\mathbf{t}_{6DoF}$ are approximated with a basis of Chebyshev polynomials whose coefficients are collected in the vector $\mathbf{b}_t$ optimized through the minimization of,

$$\underset{\mathbf{e}_1,\ldots,\mathbf{e}_{N_{pm}},\mathbf{b}_t}{\arg\min} \sum_{i=1}^{N_{pm}} \mathbf{e}_i^T \mathbf{e}_i + \mathbf{b}_t^T \boldsymbol{\Sigma}_{b_t}^{-1} \mathbf{b}_t \,, \tag{19}$$

with constraint (18), where $\boldsymbol{\Sigma}_{b_t}$ is a diagonal matrix of weighting parameters to aid in the optimization.

4. EXPERIMENTAL SETUP

An industrial 5-axis machine tool with a Siemens 840D controller, shown in Figure 2, was used to evaluate and compare the 6-DoF and AP models and their respective methods of generating compensation tables. The axis ordering for this machine tool is XYZCB, with both rotary axes at the spindle.

The machine tool axis limits are listed in Table 1. The nominal distance between the center of the B axis and the spindle face is T_{offset} = 98.0 mm. This is the only mechanical offset necessary for this machine tool configuration due to the choice of the fixed reference coordinate frame, which is shown in Figure 3. The fixed reference frame for the Zero Reference model is placed at the center of the B axis when all of the axes are in their zero positions. The unit vectors that describe the machine tool axes are with respect to this frame.

Table 1: Axis limits for industrial 5-axis machine tool.

Axis	Minimum	Maximum
X (mm)	-8.1	6101.0
Y (mm)	-2.5	2557.3
Z (mm)	0	1001.8
C	-272°	272°
B	-111°	111°

The nominal kinematics for an XYZCB 5-axis machine tool are

$$\mathbf{F}_n(\mathbf{q}) = \mathbf{T}_1(q_X)\mathbf{T}_2(q_Y)\mathbf{T}_3(q_Z)\mathbf{T}_4(q_C)\mathbf{T}_5(q_B), \tag{20}$$

where

$$\mathbf{T}_X(q_X) = \begin{bmatrix} 1 & 0 & 0 & q_X \\ 0 & 1 & 0 & 0 \\ 0 & 0 & 1 & 0 \\ 0 & 0 & 0 & 1 \end{bmatrix}, \mathbf{T}_Y(q_Y) = \begin{bmatrix} 1 & 0 & 0 & 0 \\ 0 & 1 & 0 & q_Y \\ 0 & 0 & 1 & 0 \\ 0 & 0 & 0 & 1 \end{bmatrix},$$
$$\mathbf{T}_Z(q_Z) = \begin{bmatrix} 1 & 0 & 0 & 0 \\ 0 & 1 & 0 & 0 \\ 0 & 0 & 1 & q_Z \\ 0 & 0 & 0 & 1 \end{bmatrix}, \mathbf{T}_C(q_C) = \begin{bmatrix} \cos(q_C) & -\sin(q_C) & 0 & 0 \\ \sin(q_C) & \cos(q_C) & 0 & 0 \\ 0 & 0 & 1 & 0 \\ 0 & 0 & 0 & 1 \end{bmatrix}, \tag{21}$$
$$\mathbf{T}_B(q_B) = \begin{bmatrix} \cos(q_B) & 0 & \sin(q_B) & -L_T\sin(q_B) \\ 0 & 1 & 0 & 0 \\ -\sin(q_B) & 0 & \cos(q_B) & -L_T\cos(q_B) \\ 0 & 0 & 0 & 1 \end{bmatrix}$$

and q_X, q_Y, q_Z, q_C, and q_B are the commands for the X, Y, Z, C, and B axes, respectively. The parameter T_{offset} is a modifiable mechanical offset in the machine tool controller; therefore, a correction to it is included in the model parameter vector, **b**, for both error models.

The machine tool tip position is measured using an Automated Precision Inc. T3 laser tracker and Active Target (AT). This instrument has a reported volumetric accuracy of ±15 μm or 5ppm, whichever is greater. Over the length of the experimental machine, the volumetric accuracy is at least 30 μm. The repeatability of the laser tracker to a static target was also measured at three locations measured over distances between 1-8 m, and the standard deviation is shown in Figure 4. The repeatability of the tracker should lie within three standard deviations 99.7% of the time if the noise is Gaussian, so considering this and that the experimental machine has average volumetric errors in

excess of 0.5 mm (Table 2), the laser tracker is accurate enough to measure these errors given enough measurement points.

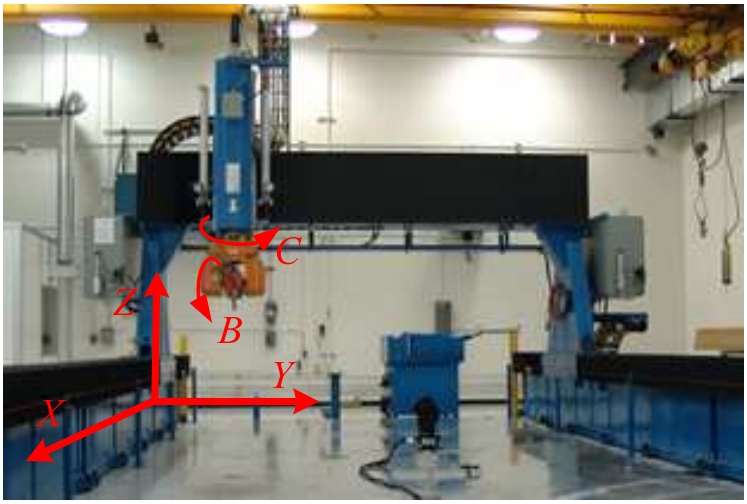

Figure 2: Industrial 5-axis machine tool used for experimental studies conducted in this paper.

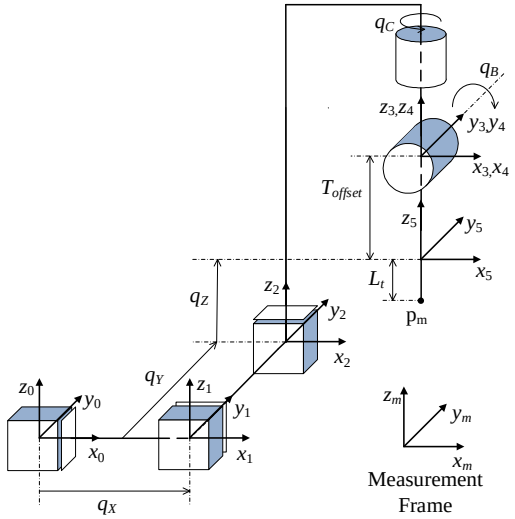

Figure 3: Diagram of axis kinematics for industrial 5-axis machine tool.

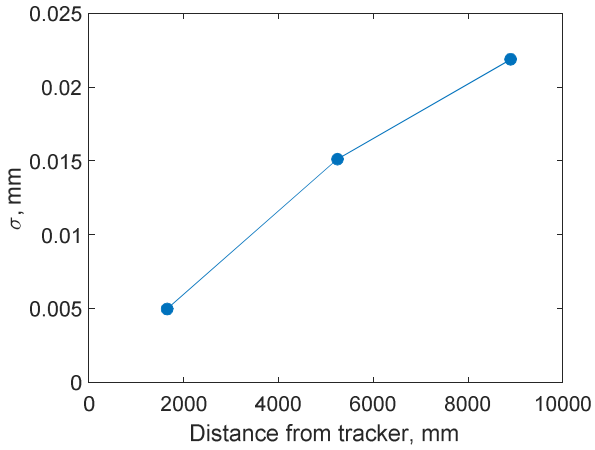

Figure 4: Standard deviation for laser tracker repeatability.

The machine tool repeatability, a measure of its ability to return to the same commanded position, is meaningful in the context of calibration in that it provides a lower bound to the measureable accuracy of the calibrated machine tool. To determine machine tool repeatability, a sequence of N_p random positions throughout the machine tool axis space are measured N_t times each. The order in which the positions are measured is random for each sequence. The repeatability of the i^{th} position for the j^{th} measurement, $\mathbf{p}_{i,j} = [p_{i,jx}\ p_{i,jy}\ p_{i,jz}]^T$, is

$$r_{i,j} = \left\| \left(\frac{1}{N_t} \sum_{k=1}^{N_t} \mathbf{p}_{i,k} \right) - \mathbf{p}_{i,j} \right\| \tag{22}$$

For $N_p = 12$ and $N_t = 4$, the repeatability of the machine tool used in this paper has a mean of 18 μm, and a standard deviation of 8 μm, which is within the same range as the instrument's repeatability, meaning that the machine is likely more repeatable than can be measured with this instrument.

A set of 295 commanded positions are measured twice, each set with a different tool length, giving a total of 590 three dimensional position measurements. The two measurement sets, referred to as the short tool measurement set and the long tool

measurement set, ensure that the complete measurement data is rich enough to contain spindle position and orientation. The length of each tool is calculated using measurements of a tool of known length, a Spherically Mounted Retrotreflector (SMR), and the laser tracker. The known tool is inserted into the spindle and its position is measured with the laser tracker. Then, without moving the machine tool, this tool is replaced with the AT, and the AT is aligned to the center of the spindle axis. The AT position is measured and compared against the measurement from the fixed length tool to obtain the AT tool length. This is illustrated in Figure 5. For this experiment, the short and long tool lengths are 214.88 and 312.86 mm, respectively.

The measurement points are distributed throughout the axis space using a random number generator. However, some points are removed to satisfy line-of-sight and collision-avoidance constraints. Figure 6 shows the axis space distribution of the measurement points with the areas labeled “LOS” and “CA” where points were removed due to Line-Of-Sight and Collision-Avoidance constraints, respectively. These measurements are then used to identify the 6-DoF and AP model parameters. Section 5 describes the performance of these models, as well as the experimental results when compensation based on these models is implemented on the industrial 5-axis machine tool.

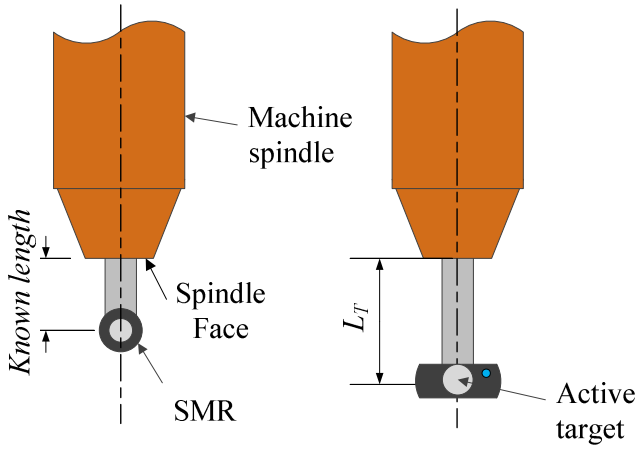

Figure 5: Illustration of tool length measurement.

5. EXPERIMENTAL RESULTS AND DISCUSSION

The accuracies of the 6-DoF and AP models are measured by the distance between the measured points and the corresponding points predicted by the model. In addition to the 590 points used to identify the models, 35 additional measurement points distributed throughout the axis space are selected using a quasi-random sequence to serve as validation points. Both models are constructed using a variety of Chebyshev polynomial orders for the basis functions. Both models include $\mathbf{E}_0$, the correction to the laser tracker and machine frame, and the nominal (uncompensated) model includes a nominal transformation from the instrument to the base frame of the machine tool. As seen in Table 2, the performance of both models improves with increasing basis order up to a point, after which the validation residual errors begin to increase, an indication of over fitting. For the 6-DoF model, 80% of the mean volumetric error in the identification data set can be accounted for using a zero order model, unlike the AP model, which only accounts for between 43-60% of the mean volumetric error, based on either the validation or identification set, respectively. The 6-DoF type of description has more complexity at low order than the AP model. The AP model can offset each axis (5 parameters) and correct the base frame (6 parameters), while the 6-DoF model has 6 zero order parameters per axis and 6 for the base frame, giving a total of 36. Additionally, as will be shown later, this machine has a significant rotary axis offset which can be described as a single parameter in the 6-DoF model, but requires a high order position-dependent description in the AP model. Beyond zero order, the models perform similarly. Expanding on this, the effect of using less data to construct both models was explored. A 50 and 150 point subset was randomly selected from the identification set and used to fit models of different polynomial orders. The results are shown in Figure 7 and Figure 8. The 6-DoF model fits the identification and validation data better than the AP model when fewer points are used, with a more pronounced effect when only 50 points are used. This could be because the 6-DoF model is able to describe some errors using a lower order polynomial, as discussed previously.

The best validation results for the 6-DoF model are obtained with 6^{th} order polynomials, while the best results for the AP model are 5^{th} order, with only minor performance loss at 6^{th} and 7^{th} order. For consistency, 6^{th} order polynomials are used for

both models in the subsequent analysis in this paper. A histogram of the identification measurements for the 6th order models is shown in Figure 9.

Comparing the selected models, the 6-DoF model shows a slightly larger mean error at 62 μm versus 49 μm for the AP model, while the AP model has a larger maximum error at 132 μm versus 92 μm for the 6-DoF model. Recalling that the machine tool repeatability was measured at 18 μm, both models achieve a mean accuracy over the entire workspace of approximately three times the machine tool repeatability. Noting that both models achieve approximately 90% improvement compared to the nominal model, it is clear that significant improvement is obtained.

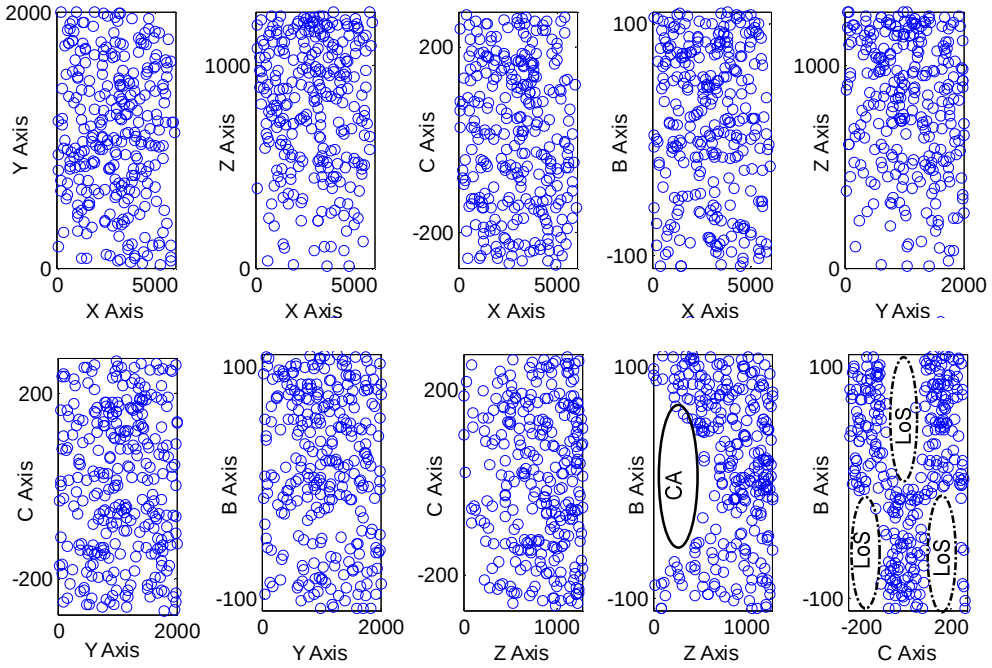

Figure 6: Distribution of measurement points used for model identification. Large circles show where points were removed due to Collision Avoidance (CA) and Line Of Sight (LOS) constraints.

A set of 25 machine tool compensation tables (five tables for each axis) and the correction to the mechanical offset T_{offset} are generated for each model using the

procedures outlined previously. The correction to T_{offset} was 68 μm for the AP tables and 72 μm for the 6-DoF tables. Figure 10 shows the generated 6-DoF and AP table compensation functions. The horizontal axis on the graphs is the traveling, or input, machine tool axis and the vertical axis on the graphs is the compensating, or output, machine tool axis. As seen in Figure 10, the table compensation functions generated from both models are similar. The function with the greatest difference, f_{bz}, is on average 8 μm different and at the maximum 64 μm different. The slight differences may be due to the additional fitting step required to generate the 6-DoF compensation tables.

Table 2: Polynomial order selection via identification and validation residual errors for 6-DoF and AP models.

			Identification Points			**Validation Points**		
Model	Order	Calculation time (min)	Mean (mm)	Max (mm)	Reduction in mean	Mean (mm)	Max (mm)	Reduction in mean
Uncompensated	--		0.602	1.417	-	0.568	1.110	-
6-DoF	0	23.70	0.124	0.323	80.0%	0.143	0.357	75.4%
6-DoF	1	267.10	0.109	0.334	81.7%	0.134	0.349	77.2%
6-DoF	2	110.50	0.081	0.242	86.7%	0.141	0.344	75.4%
6-DoF	3	136.20	0.054	0.206	91.7%	0.114	0.208	80.7%
6-DoF	4	75.10	0.029	0.124	95.0%	0.103	0.183	82.5%
6-DoF	5	214.20	0.031	0.113	95.0%	0.074	0.112	87.7%
6-DoF	6	144.20	0.027	0.071	96.7%	0.062	0.092	89.5%
6-DoF	7	118.70	0.025	0.072	96.7%	0.092	0.143	84.2%
AP	0	27.30	0.242	0.544	60.0%	0.323	0.552	43.9%
AP	1	26.70	0.081	0.353	86.7%	0.109	0.314	80.7%
AP	2	30.60	0.074	0.307	88.3%	0.103	0.316	82.5%
AP	3	27.40	0.053	0.173	91.7%	0.092	0.273	84.2%
AP	4	28.80	0.039	0.108	93.3%	0.074	0.157	87.7%
AP	5	27.40	0.034	0.102	95.0%	0.053	0.124	91.2%
AP	6	27.05	0.029	0.091	95.0%	0.049	0.132	91.2%
AP	7	38.30	0.027	0.084	95.0%	0.051	0.133	91.2%

The compensation functions shown in Figure 10 include traditional pitch and linear straightness errors, as well as some less common geometric errors. Pitch compensation functions are along the diagonal (a correction to an axis based on the position of that axis).

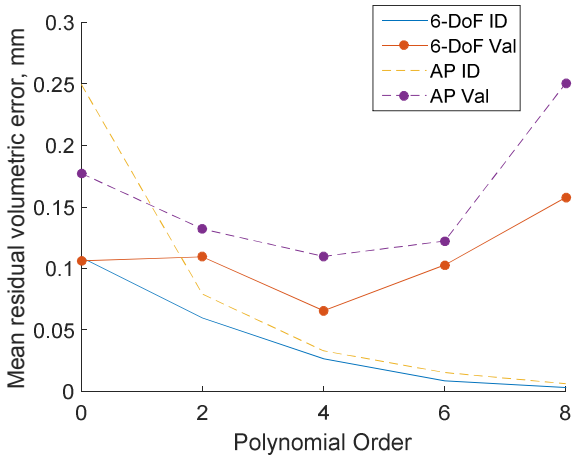

Figure 7: Mean residual volumetric error for different polynomial orders using 50 randomly selected points.

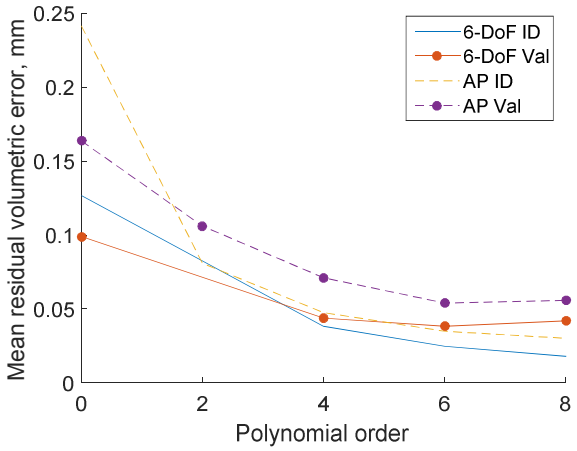

Figure 8: Mean residual volumetric error for different polynomial orders using 50 randomly selected points.

The linear straightness errors are located in the off-diagonal of the upper 3x3 graphs. The dominating linear component of these graphs can be attributed to squareness errors in the axis. However, the higher-order components of these graphs, especially notable in the f_{xz} graph, can be attributed to the non-straightness of the axes. The largest linear compensations to the X and Y axes arise from the rotary C axis position (f_{cx} and f_{cy}). The sinusoidal shape and 90° offset in f_{cx} and f_{cy} can be attributed to an offset

between the spindle axis and the C axis, resulting in a circular path in the X-Y plane for C rotations. The amplitude and phase of the sinusoids provides the magnitude and direction, respectively, of the offset. The C axis contains another large error in its pitch compensation f_{cc}, where the sinusoidal shape indicates that there is an eccentricity in the transmission between the C axis and the motor or the encoder mounting and the axis average line. The sinusoidal shape has more than one full rotation because the C axis has more than 360° of travel, returning the axis to the same physical location more than once during its full travel. Notably lacking in the tables are any significant coupling from the linear axes to the rotary axes, which would arise from a position-dependent angular error in the linear axes.

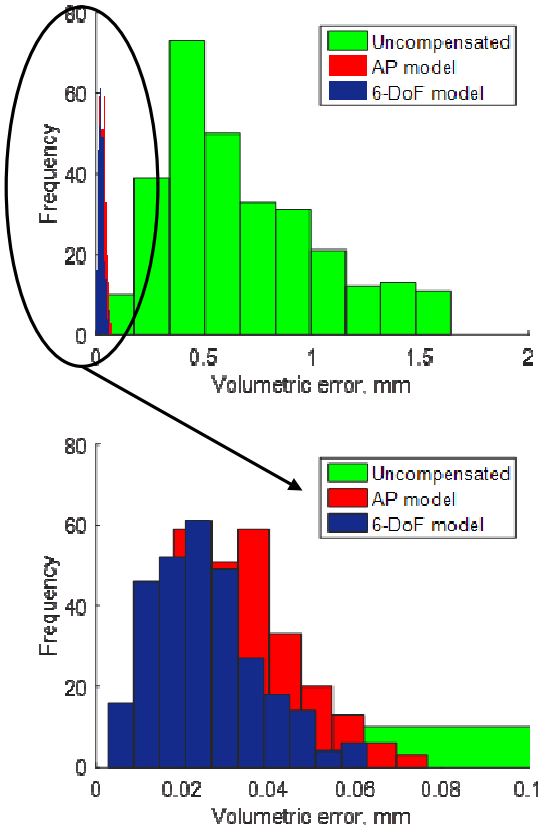

Figure 9: Histogram of identification measurements for nominal, 6-DoF, and AP models.

The complexity of the identified errors highlights a particular strength of the proposed method of populating compensation tables; no prior knowledge of the important machine tool errors is required. While some errors were not expected, other errors that may have been expected were not seen or were very small. Therefore, good performance over the entire workspace was achieved without *a priori* knowledge of the significant error sources. Likewise, time was not wasted in measuring errors that ultimately were insignificant. Furthermore, the complete set of compensation tables was generated in one step without recursively editing compensation tables with each measurement, as is typically done in classical methods.

The identified compensation functions were discretized into 1024 points along each axis and the resulting values were loaded onto the machine tool controller compensation tables. Then, the controller value for T_{offset} is modified by the amount identified. The compensation tables for both methods were activated in separate experiments and a new set of machine positions were measured at each of these points using the short tool length and the laser tracker. The measurements are compared to the uncompensated machine measurements in Table 3, and a histogram of the measurement accuracy is shown in Figure 11. The compensated accuracy in Table 3 is comparable with the model accuracy results in Figure 9. The differences between the model identification set and compensation results, in this case within approximately twice the repeatability, are expected since these points are not the same as those used to identify or validate the models.

As seen in Figure 11, both sets of compensation tables reduce the mean machine geometric error of the uncompensated system by approximately 90%. However, the performance difference between the two compensation solutions is a fraction of the machine tool repeatability, and therefore negligible. Thus, it can be concluded that both methods provide comparable performance improvement. This conclusion is notable because 6-DoF solutions originate from a complete model, whose foundations are well rooted in classical kinematics (a 6-DoF kinematic correction to each axis), whereas the AP model is incomplete and lacks a clear connection to foundational kinematics. The comparable performance may be attributable to the fact that both methods are constrained to the same solution space, compensation tables. While the AP model maps identically

onto the compensation space, there is a loss of information in the incomplete mapping of the 6-DoF model to the table-based compensation.

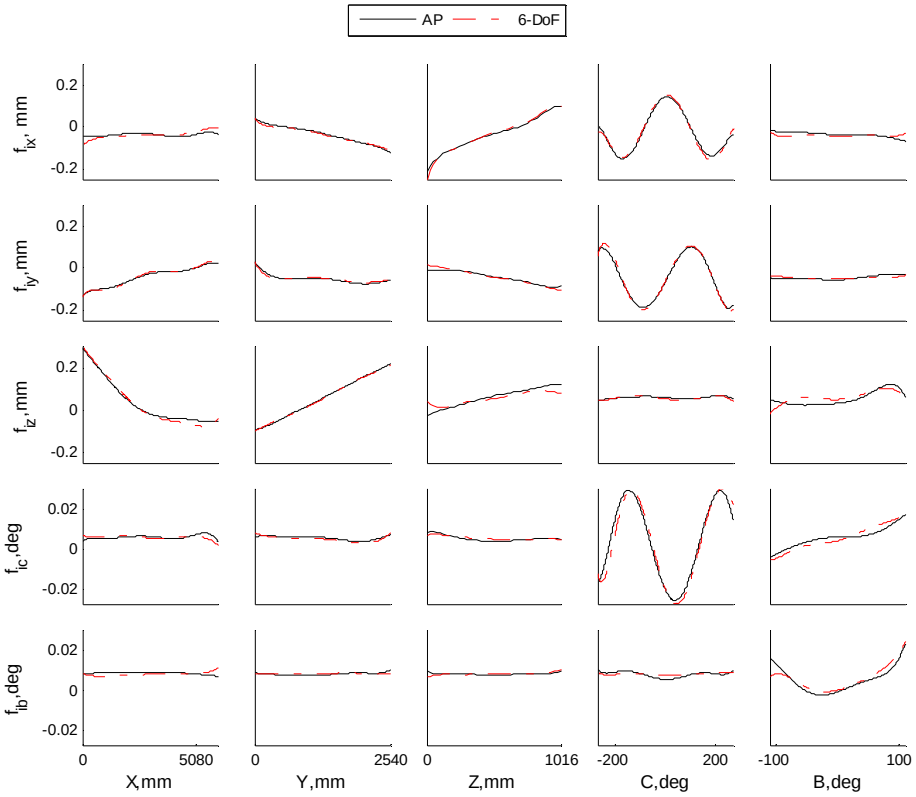

Figure 10: Compensation table functions generated from AP and 6-DoF models.

Table 3: Mean and maximum residuals between measured compensated positions and commanded positions and error reduction for each compensation type.

Model	Mean (mm)	Error Reduction	Maximum (mm)	Error Reduction
Uncompensated	0.551	--	0.940	--
6-DoF Tables	0.038	93.1%	0.099	89.5%
AP Tables	0.043	92.2%	0.094	90.0%

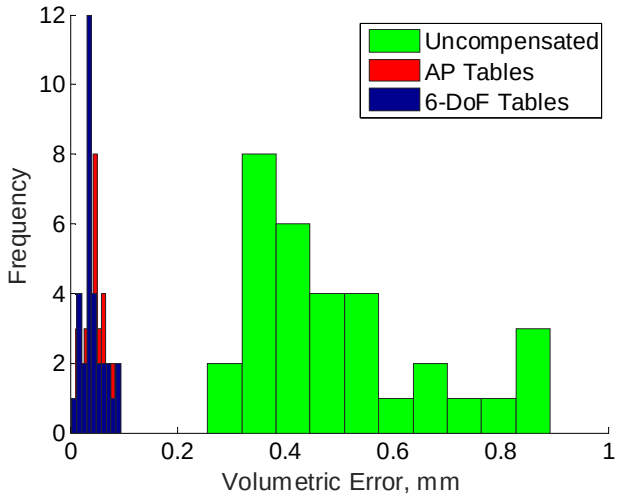

Figure 11: Histogram of validation measurements for compensated performance of AP and 6-DoF models.

A final compensation test, referred to as the rotation test, is performed to illustrate the performance improvements in the two methods. This test involves placing the tool tip at a location and rotating the orientation through a 180° arc, requiring a coordinated motion (and compensation) of at least three axes. The experimental results are shown in Figure 12. The uncompensated points are 377 µm from the average location at the worst point, while the compensated points are 53 µm from the average location at the worst point for the AP tables and 58 µm from the average location at the worst point for the 6-DoF tables. Both experiments further demonstrate that the compensation methods are effective in reducing machine tool geometric errors, which are particularly useful for complex 5-axis motions.

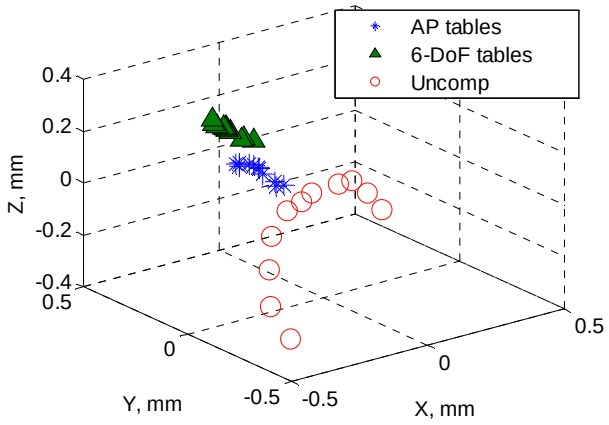

Figure 12: Experimental results for rotation test.

6. SUMMARY AND CONCLUSIONS

A method to generate table-based compensation for machine tool geometric errors using tool tip measurements distributed throughout the axis space is presented. Two models for the geometric errors of a machine tool are presented, and methods for identifying optimal table compensation from each are developed. Measurements are taken using a laser tracker with two tool lengths to capture both position and orientation errors. An industrial 5-axis machine tool was used for the experimental tests conducted in this paper. The machine tool was measured in 295 positions with two tool lengths, giving 590 total measurements, and was found to have volumetric errors of up to 1.417 mm, with a mean volumetric error of 0.602 mm. The machine tool repeatability was found experimentally as 18 μm. Both methods compensate the machine tool well, with average volumetric errors over the entire workspace of 0.038 mm and 0.043 mm for the 6-DoF and AP solutions, respectively. Both solutions are within 2.5 times the machine tool repeatability, demonstrating good accuracy, and the difference between the two is a fraction of the repeatability, demonstrating negligible difference between the solutions.

Analysis of the effect of increasing polynomial basis order on the model accuracy, as well as analysis of the compensating table solutions, demonstrates that significant and unexpected complicated kinematic behavior of the machine tool is present. The novel

methodology presented in this paper, a one-time measurement sequence using simultaneous motion of all axes over the entire workspace and simultaneous generation of all compensating tables, is particularly effective in efficiently capturing the unexpected complicated kinematics of the machine tool.

ACKNOWLEDGEMENTS

This work was supported by Boeing and the Center for Aerospace Manufacturing Technologies at the Missouri University of Science and Technology. Funding was provided by the National Science Foundation (NSF, grant CMMI-1335340), and the Department of Education (DOE, grant P200A120062).

REFERENCES

[1] B. Bringmann, J. P. Besuchet and L. Rohr, "Systematic Evaluation of Calibration Methods," CIRP Annals - Manufacturing Technology, vol. 57, no. 1, pp. 529-532, 2008.

[2] ISO 230-1, Test Code for Machine Tools Part I: Geometric Accuracy of Machine Tools Operating Under No-Load or Quasi-Static Conditions, Geneva, Switzerland: ISO, 2012.

[3] M. Tsutsumi and A. Saito, "Identification and Compensation of Systematic Deviations Particular to 5-Axis Machining Centers," International Journal of Machine Tools and Manufacture, vol. 43, pp. 771-780, 2003.

[4] S. H. H. Zargarbashi and J. R. R. Mayer, "Assessment of Machine Tool Trunnion Axis Motion Error, Using Magnetic Double Ball Bar," International Journal of Machine Tools and Manufacture, vol. 46, pp. 1823-1834, 2006.

[5] S. Weikert, "R-Test, a New Device for Accuracy Measurements on Five-Axis Machine Tools," CIRP Annals-- Manufacturing Technology, vol. 53, no. 1, pp. 429-432, 2004.

[6] S. Ibaraki, C. Oyama and H. Otsubo, "Construction of an Error Map of Rotary Axes on a Five-Axis Machining Center by Static R-Test," International Journal of Machine Tools and Manufacture, vol. 51, no. 3, pp. 190-200, 2011.

[7] T. Erkan and J. R. R. Mayer, "A Cluster Analysis Applied to Volumetric Errors of Five-Axis Machine Tools Obtained by Probing an Uncalibrated Artifact," CIRP Annals – Manufacturing Technology, vol. 59, pp. 539-542, 2010.

[8] S. Ibaraki, T. Iritani and T. Matsushita, "Calibration of Location Errors of Rotary Axes on Five-Axis Machine Tools by on-the-Machine Measurement Using a Touch-Trigger Probe," International Journal of Machine Tools and Manufacture, vol. 58, pp. 44-53, 2012.

[9] J. Jung, J. Choi and S. Lee, "Machining Accuracy Enhancement by Compensating for Volumetric Errors of a Machine Tool and on-Machine Measurement," Journal of Materials Processing Technology, vol. 174, pp. 56-66, 2006.

[10] C. Hong, S. Ibaraki and A. Matsubara, "Influence of Position Dependent Error of Rotary Axes on a Machining Test of Cone Frustram by Five-Axis Machine Tools," Precision Engineering, vol. 35, no. 1, pp. 1-11, 2001.

[11] S. Ibaraki and W. Knapp, "Indirect Measurement of Volumetric Accuracy for Three-axis and Five Axis Machine Tools: A Review," International Journal of Automation Technology, vol. 6, no. 2, 2012.

[12] K. Umetsu, R. Furutnani, S. Osawa, T. Takatsuji and T. Kurosawa, "Geometric Calibration of a Coordinate Measuring Machine Using a Laser Tracking System," Measurement Science and Technology, vol. 16, pp. 2466-2472, 2005.

[13] S. Ibaraki, T. Hata, T. Yano, T. Takatsuji, S. Osawa and O. Sata, "Esimation of the Three-dimensional Volumetric Errors of Machine Tools by a Laser Tracker," in Asian Symposium for Precision Engineering and Nanotechnology, Kitakyushu, Japan], 2009.

[14] H. Schwenke, M. Franke and J. Hannaford, "Error Mapping of CMMs and Machine Tools by a Single Tracking Interferometer," CIRP Annals – Manufacturing Technology, vol. 54, no. 1, pp. 475-478, 2005.

[15] H. Schwenke, R. Schmitt, P. Jatzkowskib and P. Warmanna, "On-the-fly Calibration of Linear and Rotary Axes of Machine Tools and CMMs Using a Tracking Interferometer," CIRP Annals--Manufacturing Technology, vol. 58, pp. 477-480, 2009.

[16] P. Freeman, "A Novel Means of Software Compensation for Robots and Machine Tools," in Aerospace Manufacturing and Automated Fastening Conference and Exhibition, Toulouse, France, September, 2006.

[17] Nubiola and I. Bonev, "Absolute Calibration of an ABB IRB1600 Robot Using a Laser Tracker," Robots and Computer Integrated Manufacturing, vol. 29, no. 1, p. 236–245, 2012.

[18] J. Denavit and R. Hartenberg, "A Kinematic Notation for Lower Pair Mechanisms Based on Matrices," Transactions of ASME-Journal of Applied Mechanics, vol. 22, pp. 215-221, 1955.

[19] S. Hayati, "Robot Arm Geometric Parameter Estimation," in Proceedings of the 22nd IEEE International Conference on Decision Control, San Antonio, TX, USA, 1983.

[20] W. K. Veitschegger and C. Wu, "Robot Calibration and Compensation," IEEE Journal of Robotics and Automation, vol. 4, no. 6, pp. 643-656, 1988.

[21] C. Sheth and J. Uicker, "IMP (Integrated Mechanism Program), a Computer-Aided Design Analysis System for Mechanisms and Linkages," ASME Journal of Engineering Industry, vol. 94, pp. 454-464, 1972.

[22] J. Soons, F. Theuws and P. Schellekens, "Modeling the Errors of Multi-Axis Machines: a General Methodology," Precision Engineering, vol. 14, no. 1, pp. 5-19, 1992.

[23] V. Kiridena and P. Ferreira, "Kinematic Modeling of Quasistatic Errors of Three-Axis Machining Centers," International Journal of Machine Tools and Manufacture, vol. 34, no. 1, pp. 85-100, 1994.

[24] H. Zhuang, Z. S. Roth and F. Hamano, "A Complete and Parametrically Continuous Kinematic Model for Robot Manipulators," IEEE Transactions on Robots and Automation, vol. 8, no. 4, pp. 451-463, 1992.

[25] J. W. Fan, J. L. Guan, W. C. Wang, Q. Z. Luo, X. L. and L. Y. Wang, "A Universal Modeling Method for the Enhancement the Volumetric Accuracy of CNC Machine Tools," Journal of Materials Processing Technology, vol. 129, pp. 624-628, 2002.

[26] Z. Yu, L. Tiemin and T. and Xiaoqiang, "Geometric Error Modeling of Machine Tools Based on Screw Theory," in International Conference on Advances in Engineering, Beijing, China, 2011.

[27] I.-M. Chen, G. Yang, C. T. Tan and S. H. Yeo, "Local POE Model for Robot Kinematic Calibration," Mechanism and Machine Theory, vol. 36, no. 1, pp. 1215-1239, 2001.

[28] R. He, S. Zhao and S. Yang, "Kinematic-Parameter Identification for Serial-Robot Calibration Based on POE Formula,"," IEEE Transactions on Robotics, vol. 26, no. 3, pp. 411-423, 2010.

[29] Y. Lin and Y. Shen, "Modelling of Five-Axis Machine Tool Metrology Models Using the Matrix Summation Approach," International Journal of Machine Tools and Manufacture, vol. 21, pp. 243-248, 2003.

[30] B. Mooring, Z. S. Roth and M. R. Driels, Fundamentals of Manipulator Calibration, John Wiley & Sons, Inc. , 1991.

[31] S. Sartori and G. X. Zhang, "Geometric Error Measurement and Compensation of Machines," CIRP Annals -- Manufacturing Technology, vol. 44, no. 2, pp. 599-609, 1995.

[32] Y. A. Mir, J. R. R. Mayer and C. Fortin, "Tool path error prediction of a five axis machine tool with geometric errors," Proceeding of the Institution of Mechanical Engineers, Part B: Journal of Engineering Manufacture, vol. 216, no. 5, pp. 697-712, 2002.

[33] M. Nojedeh, M. Habibi and B. Arezoo, "Tool Path Accuracy Enhancement Through Geometrical Error Compensation," International Journal of Machine Tools and Manufacture, vol. 51, pp. 471-482, 2011.

[34] K. Gupta, "Kinematic Analysis of Manipulators Using the Zero Refernce Position Description," International Journal of Robotics Research, vol. 5, no. 2, pp. 5-13, 1986.

[35] M. A. Meggiolaro and S. Dubowsky, "An Analytical Method to Eliminate the Redundant Parameters in Robot Calibration," in Proceedings of the 2000 IEEE International Conference on Robotics and Automation, San Francisco, CA, 2000.

[36] C. Hollerbach, J. Wampler and T. Arai, "An Implicit Loop Method for Kinematic Calibration and Its

II. SELECTION OF LIMITED AND CONSTRAINED COMPENSATION TABLES FOR 5-AXIS MACHINE TOOLS

J. Creamer[1], D.A. Bristow[2], R.G. Landers[2]

[1]Boeing Research and Technology, St. Louis, MO

[2]Department of Mechanical and Aerospace Engineering,

Missouri University of Science and Technology, Rolla, MO

ABSTRACT

Machine tool geometric inaccuracies are frequently corrected through the use of compensation tables available in machine tool controllers. Each compensation table contains a set of values that determine the incremental change in the commanded position of an axis given the current positions of the axes. While a five-axis machine tool, for example, can have at most 25 compensation tables, most machine tool controllers limit the number of compensation tables that can be implemented and provide constraints on the combinations of compensation tables that can be utilized. This work presents an artificial intelligence-based methodology to select and populate the optimal set of machine tool compensation tables when these limitations and constraints exist. Using data from an industrial 5-axis machine tool to construct a kinematic error model, simulation results for the proposed methodology and a heuristic based on the impact of individual compensation tables when selecting six compensation tables are compared, and the proposed methodology is found to outperform the heuristic. The proposed methodology and a solution based on a full set of compensation tables are experimentally implemented on the machine tool and the mean volumetric error resulting from the proposed methodology is found to be only 25 μm less than the volumetric error resulting from the full set of tables. The proposed methodology is then implemented in two more simulation studies where constraints are imposed on which combination of compensation tables could be used and which type of compensation tables could not be utilized. The resulting mean volumetric error was 7.0 and 28.3 μm greater, respectively, than the unconstrained solution.

Keywords: volumetric error, geometric error compensation, 5-axis machine tools

1. INTRODUCTION

Changes in the way parts are manufactured in the aerospace industry are driving a need for more accurate 5-axis machine tools. More parts are designed as monolithic structures, requiring a machine tool capable of manufacturing a large part with small, geometrically complex features, while maintaining tight tolerances over large distances. Machine tools inherently have errors arising from a variety of sources, such as geometric errors due to manufacturing and assembly tolerance errors and wear of machine tool components, thermal expansion, and structural deformation. No machine tool design changes can eliminate all geometric errors, and higher accuracy machine tools are much more expensive to manufacture and maintain. However, a large fraction of machine tool errors are repeatable and, as a result, machine tool calibration can be a cost effective means to substantially increase accuracy. In general, machine tool geometric errors change slowly over time due to wear of the moving parts; however, they can change quickly in the event the cutting tool collides with the part or machine tool table. As a result, a machine tool should be recalibrated at regular intervals or after a collision. Machine tool down time is costly and, therefore, methods for quickly calibrating machine tools are in demand.

Conventional approaches to machine tool calibration often attempt to isolate and measure individual geometric errors, which is time consuming and often makes the complete calibration of a machine tool prohibitive. These traditional methods are described in the ISO 230-1 standard [1]. Sartori and Zhang [2] and Schwenke, et al. [3] provided thorough overviews of direct measurement methods, and indirect measurement methods are summarized in Ibaraki, et al. [4]. Direct measurement methods measure machine tool errors individually [5], while indirect measurements attempt to identify several errors simultaneously. However, indirect methods typically require that the linear and rotary axes be calibrated separately, or make assumptions about being able to isolate the rotary axis errors from other geometric errors. Therefore, these methods typically involve multiple measurement instrument set ups and skilled personnel, leading to long calibration times (i.e., several days), and may not result in an accurate description of the machine tool geometric errors. Further, most geometric error modeling techniques employ low order models. Cheng et al. [6] used static geometric error models to conduct

an analysis based on multibody system theory to determine critical geometric errors. Matrix summation modeling using linear geometric errors was conducted in [7] such that the errors had physical meaning. Given the low order error modeling employed in these studies, they cannot account for the complexity of some geometric errors, such as sagging and twisting.

A method for machine tool geometric error compensation addressing the issues of long calibration times and the inability to describe complex machine tool errors was proposed in [8]. Unlike many calibration techniques [e.g., 6,7], the method in [8] uses high-order error descriptions to capture complex geometric errors. This method also uses a laser tracker, a metrology tool being used in more and more industrial applications [9], and was shown to work very well for the volumetric compensation of a subset of machine tool controllers that allow for the use of a complete set of compensation tables [10]. Many common machine tool controllers limit the number of compensation tables available due to memory or computational constraints, as well as cost, often with limitations on the possible combinations of compensation tables that can be implemented. Therefore, a method to select and populate the best possible set of compensation tables when limitations exist is needed. Selecting and populating a subset of compensation tables from all possible sets of compensation tables, while satisfying existing constraints, is a computationally intensive combinatorial optimization problem. A brute force approach that analyzes all possible combinations of compensation tables is impractical for this type of problem. Further, this class of problem cannot be solved with traditional gradient search techniques. An artificial intelligence method capable of incorporating constraints is needed. A genetic algorithm is a common technique for combinatorial optimization and can easily be tailored to constraints common in machine tool controllers.

The rest of the paper is organized as follows. Section 2 briefly describes the general method to populate an unconstrained set of machine tool compensation tables. Section 3 presents a method of selecting and populating the optimal set of compensation tables when constraints exist. Section 4 presents results using data from an industrial 5-axis machine tool and Section 5 presents the implementation and experimental validation of compensation tables selected with the methodology and additional simulations for

several classes of constraints. Section 6 summarizes the paper and draws conclusions from the work.

2. BACKGROUND

A novel method for machine tool calibration using machine tool compensation tables was developed in [10]. Compensation tables are lookup tables on the machine tool controller whose input is the measurement of an axis and whose output is an incremental value to be added to (or subtracted from) an axis position command. Note these axes may or may not be the same. A table whose input is a measurement of axis *i* and whose output is a correction to axis *o* may be represented as,

$$\begin{array}{ccc} \text{Entry} & \text{Input} & \text{Output} \\ 1 & q^t_{i,1} & t_{oi,1} \\ \vdots & \vdots & \vdots \\ j-1 & q^t_{i,j-1} & t_{oi,j-1} \\ j & q^t_{i,j} & t_{oi,j} \\ j+1 & q^t_{i,j+1} & t_{oi,j+1} \\ \vdots & \vdots & \vdots \\ N_t & q^t_{i,N_t} & t_{oi,N_t} \end{array}, \tag{1}$$

where $q^t_{i,j}$ is the j^{th} table listing of the i^{th} input axis, $t_{oi,j}$ is the corresponding compensation value to be added to (or subtracted from) the axis command of the o^{th} output axis, and N_t is the number of table entries. Then, the compensated command to axis *o* is linearly interpolated from the table entries as,

$$q^c_o = q_o + t_{oi,j-1} + \left(t_{oi,j} - t_{oi,j-1}\right)\frac{q_i - q^t_{i,j-1}}{q^t_{i,j} - q^t_{i,j-1}}, \tag{2}$$

where *j* is selected such that the measured input axis position q_i satisfies $q^t_{i,j-1} \le q_i \le q^t_{i,j}$ and q_o is the nominal position command of the output axis.

This method takes tool tip error measurements distributed throughout the axis space with a laser tracker using two different tool lengths, i.e., distances between the spindle face and measurement device, allowing both position and orientation errors to be measured. In order to relate the position and orientation measurements of the machine tool with the commanded axis positions, a model of the relationships between the nominal axes is developed by assuming the machine tool can be treated as a kinematic chain of rigid axes, with the relationships between the axes described by Linear Homogeneous Transformation (LHT) matrices [4],

$$\mathbf{T} = \begin{bmatrix} n_x & o_x & a_x & l_x \\ n_y & o_y & a_y & l_y \\ n_z & o_z & a_z & l_z \\ 0 & 0 & 0 & 1 \end{bmatrix}, \tag{3}$$

where the unit vectors, $\mathbf{n} = [n_x\, n_y\, n_z]^T$, $\mathbf{o} = [o_x\, o_y\, o_z]^T$, and $\mathbf{a} = [a_x\, a_y\, a_z]^T$ are the orientations of the x, y, and z-axes, respectively, of an axis coordinate frame with respect to the coordinate frame of the previous axis in the kinematic chain and $\mathbf{l} = [l_x\, l_y\, l_z]^T$ is a vector from the origin of an axis coordinate frame to the origin of the coordinate frame of the previous axis in the kinematic chain. The nominal kinematic model for an *n*-axis machine tool is,

$$\mathbf{F}_n(\mathbf{q}, L_T) = \mathbf{T}_1(q_1)\mathbf{T}_2(q_2)\cdots\mathbf{T}_{n-1}(q_{n-1})\mathbf{T}_n(q_n)\mathbf{T}_{T_l}(L_T), \tag{4}$$

where $\mathbf{q} = [q_1\, q_2\, \ldots\, q_n]^T$ is the axis command vector, $\mathbf{T}_1(q_1),\ldots,\mathbf{T}_n(q_n)$ are LHTs for axes 1,…,*n*, respectively, $\mathbf{T}_{Tl}$ is the transformation from the last axis to the tool tip, and L_T is the tool length. The conventions described in the Zero Reference Model [11], a model commonly applied in robotics [12], are used to define the vectors **n**, **o**, **a**, and **l** for each transformation matrix.

Machine tools are never perfectly described by the nominal kinematics due to manufacturing tolerances, errors in assembly, and wear over time. Consider a model of the actual kinematics as $\mathbf{F}_a(\mathbf{q},L_T)$, which may be generated by any kinematic modeling method. One method accounts for complex kinematic errors by introducing an error

transformation, $\mathbf{E}_k(q_k)$, between each axis transformation in the nominal kinematic model, as in Freeman [8]. For an *n*-axis machine tool, the actual kinematics are modeled as,

$$\mathbf{F}_a(\mathbf{q}, L_T) = \mathbf{T}_1(q_1)\mathbf{E}_1(q_1)\mathbf{T}_2(q_2)\mathbf{E}_2(q_2)\cdots\mathbf{T}_n(q_n)\mathbf{E}_n(q_n)\mathbf{T}_{T_l}(L_T), \qquad (5)$$

The kinematic error transformation at machine tool axis *k*, $\mathbf{E}_k$, is described by three rotational errors and three translational errors that depend on the commanded axis position q_k. For small errors, the kinematic error transformation of the k^{th} axis can be approximated by

$$\mathbf{E}_k(q_k) = \begin{bmatrix} 1 & -\varepsilon_{kZ}(q_k) & \varepsilon_{kY}(q_k) & \delta_{kX}(q_k) \\ \varepsilon_{kZ}(q_k) & 1 & -\varepsilon_{kX}(q_k) & \delta_{kY}(q_k) \\ -\varepsilon_{kY}(q_k) & \varepsilon_{kX}(q_k) & 1 & \delta_{kZ}(q_k) \\ 0 & 0 & 0 & 1 \end{bmatrix}, \qquad (6)$$

where ε_{kX}, ε_{kY}, and ε_{kZ} are rotational errors in the k^{th} axis' local coordinate frame about the x, y, and z axes, respectively, and δ_{kX}, δ_{kY}, and δ_{kZ} are translational errors in the k^{th} axis' local coordinate frame along the x, y, and z axes, respectively. The error transformations are identified from the machine tooltip error measurements using a maximum likelihood estimator [13].

The kinematic error model can be used to generate corrections to the nominal machine tool commands to improve the machine tool's accuracy via machine tool compensation tables. These tables are modeled as continuous, position-dependent corrections to the axis commands and populated such that the difference between the nominal machine tool position and orientation and the compensated actual machine tool position and orientation is minimized. That is, $\mathbf{F}_a(\mathbf{q} + \mathbf{t}(\mathbf{q}), L_T) \approx \mathbf{F}_n(\mathbf{q}, L_T)$, where**,**

$$\mathbf{t}(\mathbf{q}) = \begin{bmatrix} t_{11}(q_1) + t_{12}(q_2) + \cdots + t_{1n}(q_n) \\ t_{21}(q_1) + t_{22}(q_2) + \cdots + t_{2n}(q_n) \\ \vdots \\ t_{n1}(q_1) + t_{n2}(q_2) + \cdots + t_{nn}(q_n) \end{bmatrix}, \tag{7}$$

is the update to the axis commands based on the values contained in the individual compensation tables, $t_{ij}(q_j)$, where i is the output axis and j is the input axis. For ease of optimizing compensation tables from the identified machine tool model, $\mathbf{F}_a$, the discrete data in each compensation table will be modeled by smooth functions. After these functions, referred to here as compensation functions, are determined, they are sampled discretely to populate the compensation tables. Further information regarding the kinematic error models can be found in [10]. As discussed in [10], the kinematic error model is not a complete geometric error model of the machine tool. Rather, the kinematic error model is based on the compensation tables available in the machine tool controller.

The next step in the calibration process is to identify the parameters of the compensation functions. The approach used here leverages the numerical tools developed for parameter identification [13] to identify the parameters of the basis functions used to represent the compensation functions. Two measurement tool lengths are selected to span a considerable portion of the length of cutting tools typically used in the machine tool: one short measurement tool length and one long measurement tool length, denoted $\alpha = 1$ and 2, respectively. A sequence of axis commands spanning the axis workspace are generated over which the cost function,

$$\chi^2 = \sum_{i=1}^{N_{pm}} \mathbf{e}_i^T \mathbf{e}_i + \mathbf{b}_t^T \boldsymbol{\Sigma}_{\mathbf{b}_t}^{-1} \mathbf{b}_t, \tag{8}$$

is minimized for all axis commands. This cost function minimizes the positional errors, $\mathbf{e}$, with the most likely values of geometric error model parameters, $\mathbf{b}_t$. The i^{th} position error of the compensated system for tool α, $\mathbf{e}_i$, is,

$$\mathbf{e}_i = \begin{bmatrix} 1 & 0 & 0 & 0 \\ 0 & 1 & 0 & 0 \\ 0 & 0 & 1 & 0 \end{bmatrix} \left(\mathbf{F}_a \left(\mathbf{q}_i + \mathbf{t}\left(\mathbf{q}_i\right), L_{T,\alpha} \right) - \mathbf{F}_n \left(\mathbf{q}_i, L_{T,\alpha} \right) \right) \begin{bmatrix} 0 \\ 0 \\ 0 \\ 1 \end{bmatrix}, \quad i = 1, \ldots, N_{pm}, \quad (9)$$

where N_{pm} is the number of pseudo-measurements, which are tool tip positions discretely sampled from the machine tool geometric error model, $\mathbf{F}_a$. The compensation tables $\mathbf{t}(\mathbf{q})$ are approximated by Chebyshev polynomials whose coefficients are collected in the vector $\mathbf{b}_t$. The matrix $\mathbf{\Sigma}_{\mathbf{b}t}$ is a diagonal matrix of weighting parameters that are set based on experience to appropriately scale the problem, leading to easier optimization. Poor scaling, due to the finite precision of any solver, can cause numerical instability. After optimal, smooth compensation functions are identified, they are discretized into compensation tables and loaded onto a machine tool controller.

However, the full set of compensation tables can only be implemented on relatively few models of machine tool controllers. When there are a limited set of compensation tables available and constraints on compensation table combinations exist, it is not clear how to best select and populate the compensation tables. A method that can select the optimal set of compensation tables satisfying constraints imposed by a specific machine tool controller is needed to extend this calibration method to machine tool controllers with limited compensation options. A method based on artificial intelligence optimization, in this case a genetic algorithm, is described in the next section.

3. REDUCED TABLE SELECTION METHODOLOGY

The problem of selecting the best set of machine tool compensation tables from the full set of compensation tables is a combinatorial optimization problem. These types of problems tend to be very computationally intensive. For a five-axis machine tool, assuming the five pitch compensation tables are always included, there are 20 compensation tables to choose from. Figure 1 shows an example of a full set of compensation tables for a 5-axis machine tool. These tables are divided into four sections. The upper left section contains six straightness tables (on the off diagonals) and three pitch tables (on the diagonals) that compensate the linear axes by incrementing

linear axis positions. The bottom left section consists of tables that compensate rotary axes by incrementing linear axis positions. These tables, in combination with other tables, can be used to correct some of the linear axis angular errors. The top right section contains six tables that compensate linear axes by incrementing rotary axis positions, and compensate geometric errors such as an offset of a rotary axis. The bottom right section contains four tables that compensate rotary axes by incrementing rotary axis positions. The two tables on the diagonals are the rotary pitch tables. **Remark 1**: A 5-axis machine tool does not have enough degrees of freedom to compensate all possible geometric errors; therefore, even the full set of compensation tables do not describe all of the machine tool geometric errors.

When there are 20 total compensation tables from which k tables are selected, where $k < 20$, the number of table combinations is,

$$N_s(k) = \frac{20!}{k!(20-k)!}, \tag{10}$$

The identification of a single solution requires approximately 10 min using a 2.6 GHz Intel Xeon processor with 12 parallel cores. For $k = 6$, $N_s = 38{,}760$, which would require approximately 550 hr using the same computer. Brute force methods (i.e., exhaustive searches) are, therefore, impractical for all but the simplest problems. One way to efficiently determine the optimum set of compensation tables is to apply artificial intelligence. One such technique is a Genetic Algorithm (GA), which is based on biological principles and is widely used for complex and intensive search and optimization problems. This technique is particularly useful for optimization problems with large discrete decision spaces since it does not require the evaluation of all possible solutions, while still sampling from the solution space effectively [14].

Genetic Algorithms find the solution to search and optimization problems by mimicking the biological natural selection process to iteratively improve the solutions. Each iteration is referred to as a *generation*. Genetic algorithms operate on a set of individual solutions, which is referred to as a *population*. Individual solutions are referred to as *chromosomes*, and the variables that compose each chromosome are referred to as

genes. For the compensation table selection problem considered here, each gene is a specific compensation table, and a chromosome is a complete set of compensation tables. Genes are denoted here by the pair *ij*, where *i* is the output axis and *j* is the input axis. For example, if six compensation tables are to be chosen for a machine tool with three linear axes (denoted x, y, and z) and two rotational axes (denoted b and c), a potential chromosome would be ‘cx cy xy cb zx yz’, where the six genes are ‘cx,’‘cy,’‘xy,’‘cb,’‘zx,’ and ‘yz.’

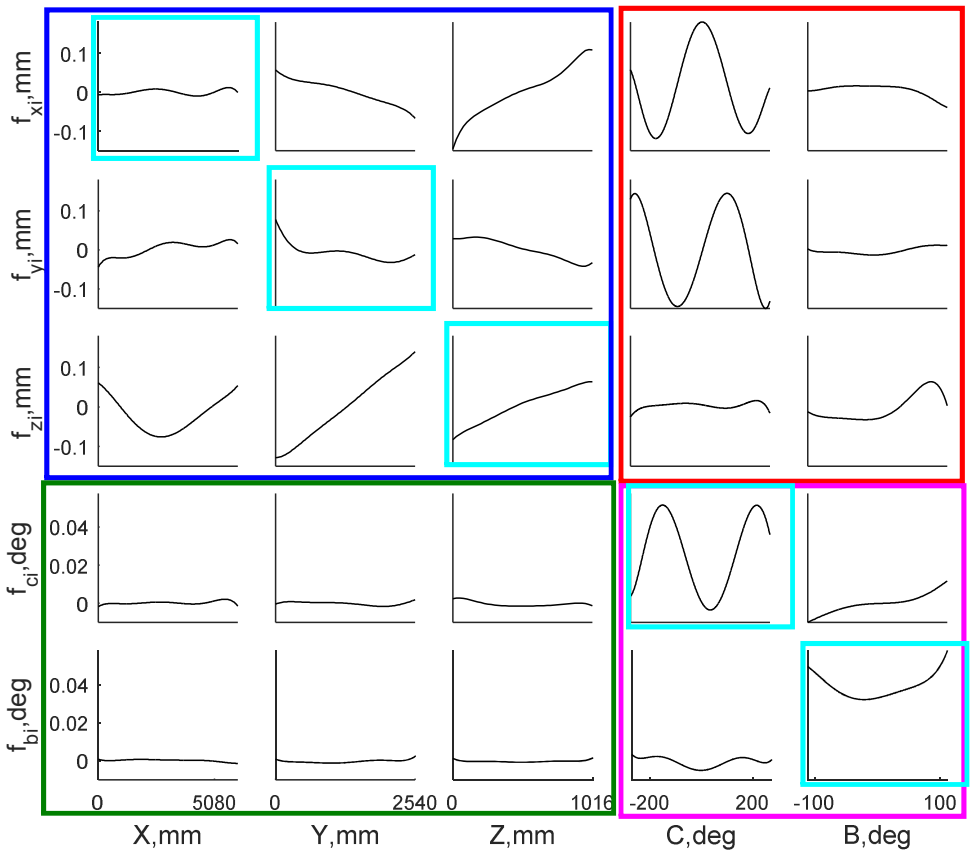

Figure 1: Example of full set of compensation tables. Horizontal axis is ranges of machine tool axes to be compensated (i.e., input axes) and vertical axis is compensation functions of axes to be incremented (i.e., output axes).

The performance of a particular chromosome is referred to as its *fitness.* Here, the mean volumetric error, e_m, which is the distance between the actual tool tip position at a given set of position commands and the nominal tool tip position, is used as the fitness. It is calculated using the geometric error model and identified compensation tables,

$$e_m = \frac{1}{AN}\sum_{\alpha=1}^{A}\sum_{i=1}^{N}\left\| \begin{bmatrix} 1 & 0 & 0 & 0 \\ 0 & 1 & 0 & 0 \\ 0 & 0 & 1 & 0 \end{bmatrix} \mathbf{F}_a\left(\mathbf{q}_i + \mathbf{t}(\mathbf{q}_i), L_{T,\alpha}\right) \begin{bmatrix} 0 \\ 0 \\ 0 \\ 1 \end{bmatrix} - \begin{bmatrix} 1 & 0 & 0 & 0 \\ 0 & 1 & 0 & 0 \\ 0 & 0 & 1 & 0 \end{bmatrix} \mathbf{F}_n\left(\mathbf{q}_i, L_{T,\alpha}\right) \begin{bmatrix} 0 \\ 0 \\ 0 \\ 1 \end{bmatrix} \right\|, \qquad (11)$$

where N is the total number of measurements and A is the total number of tool lengths. Solutions with smaller mean volumetric errors over a large set of commanded positions are more fit (i.e., they are better solutions).

Once a fitness value is assigned to each chromosome, a new generation of chromosomes is created. New chromosomes are introduced into the population in two ways: reproduction and mutation. A percentage, 50% in this study, of the fittest chromosomes of the previous population (i.e., the *parents*) is retained and new chromosomes are added through reproduction. Reproduction is the process of splicing together genes from two parents to produce new chromosomes. In order to ensure more fit chromosomes are chosen as parents, weighted random selection is used. A standard weighted random selection algorithm [15] is used to select parents based on a set of weights calculated below. Each chromosome is ranked based on its fitness from the most fit (i.e., $n = 1$) to the least fit, and this rank, n, is used to determine the weight for each chromosome,

$$W_n = \frac{N_{keep} - n + 1}{\sum_{j=1}^{N_{keep}} j}, \qquad (12)$$

where N_{keep} is the number of chromosomes to retain each iteration and n is the chromosome rank. Only the chromosomes ranked between 1 and N_{keep} are used for reproduction (i.e., the creation of new chromosomes). The chromosomes selected as parents are paired randomly. To create new chromosomes from the parents, several

different methods can be employed. The most common methods of reproduction employed in GAs are not well suited to this problem since the ordering of compensation tables in the chromosome does not matter. For this problem, a new method that does not consider the order of genes is introduced. A random number of genes from the parents are selected and swapped for the same number of genes in the other parent. The genes to be swapped are initially selected in the first parent. For each gene to be swapped in the first parent, the second parent is checked to determine if it contains a copy of this gene. If it does, then the duplicate genes are exchanged so that new chromosome will not have more than one copy of a specific gene (i.e., the set of compensation tables should not contain multiple instances of the same compensation table). Machine tool controllers may have constraints that create limitations when exchanging genes which must be integrated into the algorithm for gene exchange. These constraints and their resulting limitations on the exchange of genes during reproduction are discussed below. The entire reproduction process for the compensation table selection problem is illustrated in Figure 2. ***Remark* 2**: It is possible for both parents to be identical, which would result in all ν genes in parent #1 existing in parent #2. In this case, the resulting chromosome is the same as the parents before mutation. This can lead to saturation, or the presence of only very similar solutions, which can be mitigated by using mutation operations, as discussed below.

After reproduction occurs, random mutations alter a percentage of the genes in the population. For the compensation table selection problem, a percentage of the compensation tables are exchanged for other compensation tables selected at random from the set of all possible compensation tables, subject to machine tool controller constraints. If the randomly selected new gene violates a constraint, a new gene is selected at random until a gene is found that creates a valid solution. Mutations serve as a way to randomly introduce new solutions. A higher mutation rate creates an algorithm which acts more like a random search method, while a lower mutation rate limits the rate at which new genes are introduced into potential solutions. The GA reproduction method without mutation is prone to saturation, also called in-breeding. That is, the population will contain only very similar solutions and be unable to create different solutions via reproduction. Either extreme (i.e., high or low mutation rates) is slow and inefficient.

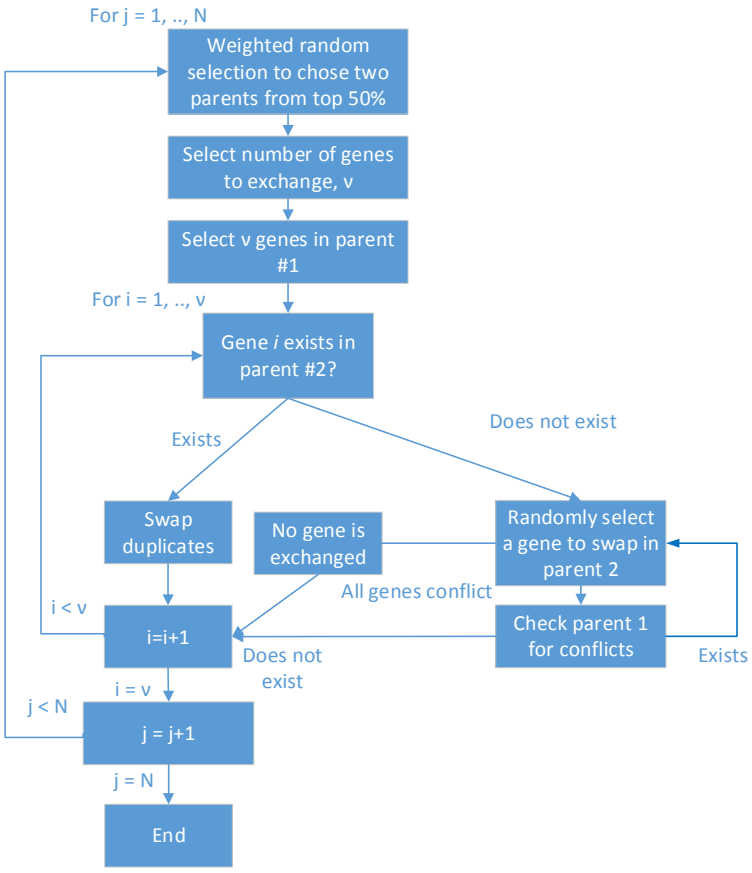

Figure 2: Illustration of reproduction.

The iterative process then starts over with the evaluation of the fitness for each chromosome in the new generation, and the process repeats until a specified convergence criterion is satisfied. An outline for the sequence of steps for the GA used in this work is shown in Figure 3.

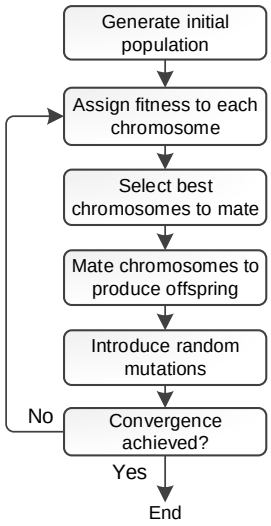

Figure 3: Outline of Genetic Algorithm steps.

3.1. Parameter Tuning. The GA has several tunable parameters, namely the mutation rate, population size, and convergence criterion. The effect these parameters have on the compensation table selection problem is now explored using data from the machine described in Section 4 for the selection of six compensation tables. Figure 4 shows the minimum cost at each generation averaged over five different GA runs for different mutation rates. The 0% mutation rate shows saturation in early iterations and does not perform as well as higher mutation rates even after 50 generations. Once the algorithm is completely saturated and without mutation to introduce new compensation tables, it will never perform better regardless of how many generations it is allowed to run. At the other extreme, a mutation rate of 85% causes the best solution to improve more slowly. By 50 generations, the best solution has a mean volumetric error of 0.046 mm, while lower mutation rates have a best solution less than 0.040 mm. High mutation rates cause the algorithm to rely mostly on random search, which is slow and does not take advantage of previous solutions with good performance. For this problem, a mutation rate of 20% produces the lowest minimum cost; therefore, this mutation rate provides enough of a random search element to prevent saturation without causing the algorithm to require significantly more iterations to converge. Figure 5 shows the

minimum cost at each generation averaged over five different GA runs for population sizes of 8, 16, and 24. Note that this study was conducted on a computer with 8 processor cores; therefore, population sizes with multiples of 8 were selected. Initially, larger population sizes perform better, but after 35 generations, all population sizes have approximately the same performance, although larger population sizes reach this performance level in fewer generations. Since the final performance between all population sizes is similar and a population size of 8 runs faster (though requires more generations), a population size of 8 is used in this study. The iteration limit is set to 50 for both the mutation rate and population size studies. The average minimum cost for both studies reaches their minimum value before 50 generations, with many occurring before 35 generations. The convergence criterion is selected to be a maximum of 50 generations for the rest of the experiments conducted in this study based on this fact since additional generations add significant time to experiments with little probability of increased performance. If the algorithm remains at the same minimum cost for more than 20 generations, it is assumed to have converged and terminates even if 50 generations have not yet been completed.

3.2. Constraint Inclusion. Three general classes of table compensation constraints exist. The first is a constraint on the overall number of compensation tables. The other two are 1) constraints on the specific axes that may be used and 2) constraints on the combinations of compensation tables that may appear together.

3.2.1. Constrained number. Many controllers limit the total number of compensation tables or the memory allocated for compensation tables. This is the most common constraint and has been discussed in detail earlier in this paper.

3.2.2. Constrained axes. This constraint can be caused by the way an axis is integrated into a machine tool controller. In some configurations, an axis encoder signal is available to the machine tool controller; however, the axis motion is controlled separately and, therefore, may not be able to accept compensation commands. Implementation of such a rule would involve reducing the number of compensation tables available to select from. For example, for a typical 5-axis machine tool, there are 25 compensation tables. If a specific axis cannot be set as an output axis, then there are five fewer compensation tables to choose from.

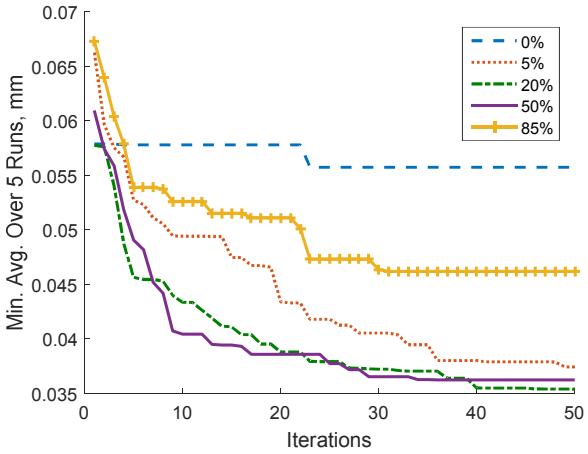

Figure 4: Minimum cost averaged over five runs for various mutation rates and population size of eight.

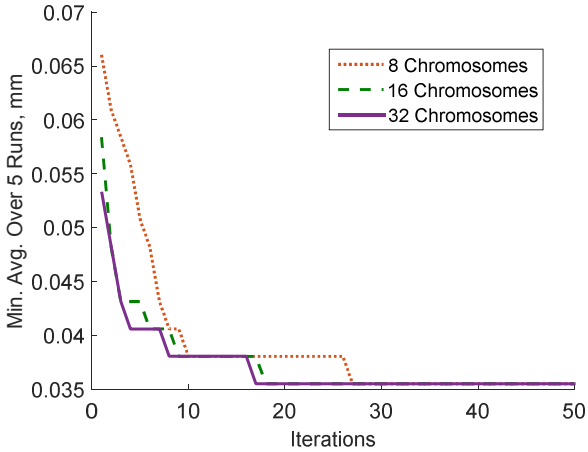

Figure 5: Minimum cost averaged over five runs for various population sizes and 20% mutation rate.

3.2.3. Constrained combinations. This type of constraint is often machine tool controller specific. An example of this type of constraint is circular compensation, i.e., when two compensation tables have swapped input and output axes, such as the two compensation tables ‘bc’ and ‘cb’. If a gene selected from parent 1 would combine with a

gene in parent 2 to form an illegal combination, then the selected gene is instead swapped with the gene in parent 2 which would cause the constraint violation, yielding new solutions that do not violate any constraints. This process is illustrated in Figure 6. Other machine tool controller constraints can be incorporated in a similar manner.

4. RESULTS AND DISCUSSION

Data collected from an industrial 5-axis machine tool located in a Boeing experimental laboratory is used in the following experiments. The machine tool configuration is illustrated in Figure 7 and the axis limits are listed in Table 1. The machine tool is measured at 295 unique random axis configurations using an API T3 laser tracker and active target (see Figure 8). Each position is measured twice, using long and short tool lengths of 317.15 mm and 218.44 mm, respectively, which are the distances from the active target to the spindle face. The tool length is obtained using laser tracker measurements and a comparison to a tool with known length. A parameter is included in the geometric error model to correct for inaccuracies in the tool length measurements. Using two tool lengths allows both position and orientation errors to be captured.

This data is used to fit the error model described in Section 2. The volumetric errors between the model outputs and measured data are shown in Table 2. The error model fits its identification data well, with the mean distance between the measured tool tip position and the modeled position being only 25 μm, which is within twice the machine tool repeatability. A set of compensation tables is then identified as described in Section 2 and, to analyze their ability to compensate the machine tool, the performance in simulation for the set of identification points is evaluated. The identified set of compensation tables is predicted to be able to account for 94.0% of the mean volumetric error and 93.9% of the maximum volumetric error, which is the largest volumetric error over the entire set of measured volumetric errors.

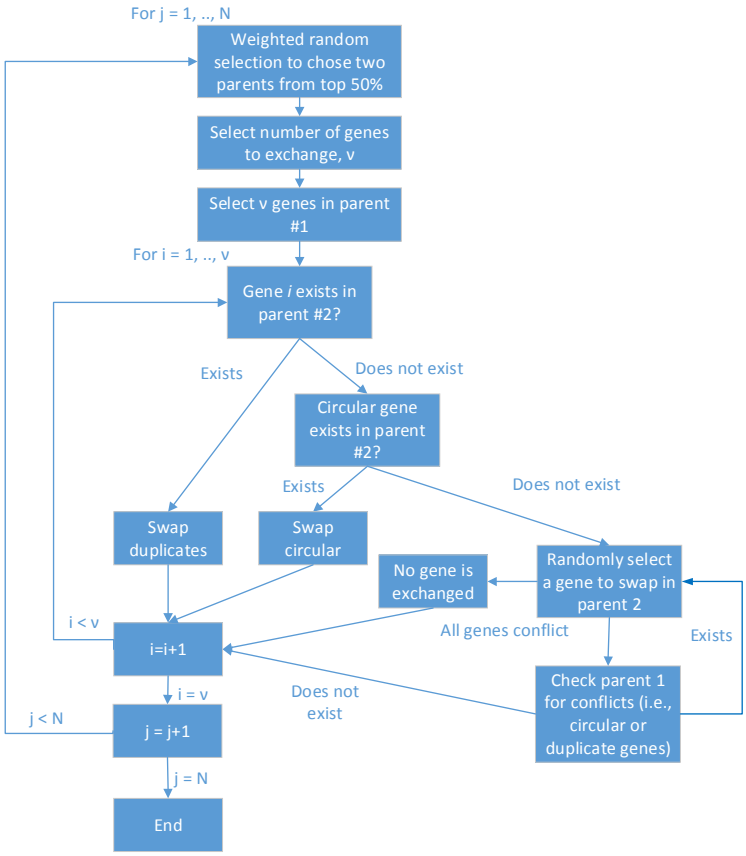

Figure 6: Illustration of reproduction when circular compensation is prohibited.

Table 1: Axis limits of industrial 5-axis machine tool used in experimental studies.

Axis	Minimum	Maximum
X (mm)	-8.1	6101.0
Y (mm)	-2.5	2557.3
Z (mm)	0	1001.8
B	-111°	111°
C	-272°	272°

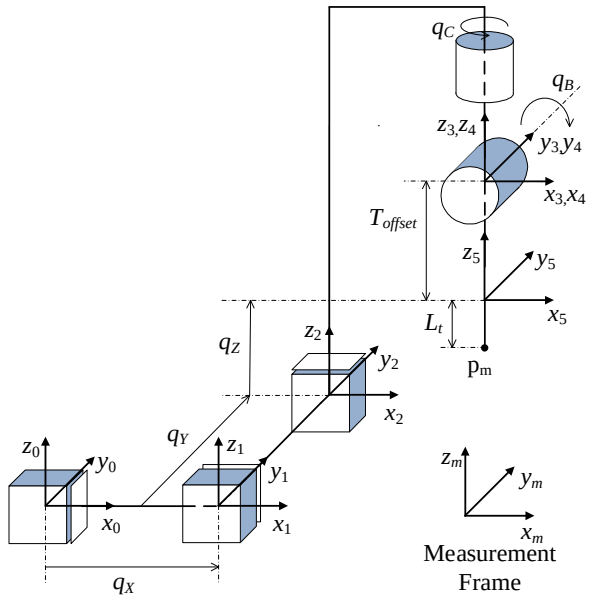

Figure 7: Industrial 5-axis machine tool kinematic diagram.

The most basic set of compensation tables only accounts for individual axis positioning. These compensation tables are known as pitch compensation tables and are included on virtually every machine tool controller. This set of compensation tables serves as a performance baseline, i.e., any set of compensation tables that includes more than this basic set should perform better. The pitch compensation tables are applied to the identification points in simulation and are able to account for 76.2% of the mean volumetric error and 75.5% of the maximum volumetric error. These sets of compensation tables (i.e., full and pitch) form bounds for other sets of compensation tables. The volumetric errors for any set of compensation tables should be less than when using pitch compensation tables alone and more than when using the full set of compensation tables.

The compensation table selection methodology is now applied to the problem of selecting the best six compensation tables out of 20 possible compensation tables, assuming the pitch compensation tables are always utilized. Note the 20 possible compensation tables are the non-diagonal tables in Figure 1. The problem of selecting six

compensation tables is considered here as many machine tool controllers only allow six compensation tables to be implemented.

Figure 8: Illustration of laser tracker and active target.

Table 2: Volumetric errors for error model and table-based compensation.

Model	Mean error (mm)	Maximum error (mm)
Uncalibrated	0.597	1.420
Error model	0.025	0.071
Full set of tables	0.031	0.071
Pitch tables only	0.142	0.348

The algorithm is run on a computer with 12 Intel Xeon 2.60 GHz processing cores. Solution evaluations for each generation are run in parallel. The population size and mutation rate are 12 and 20%, respectively, and the convergence criterion is that the GA produces the same solution for 20 generations or 50 generations have been produced,

whichever occurs first. The results are shown in Table 3. The average calculation time for the GA solutions is 5.2 hr, which is significantly faster than 550 hr (i.e., the time required for an exhaustive search to calculate all 38,640 possible solutions). The solutions share the compensation tables ‘yc xz zx’ and all but one solution has the compensation table ‘xc’. The full set of compensation tables are plotted in Figure 9. The shared compensation tables ‘yc xz zx’ and the compensation table ‘xc’ are all large when compared to the machine volumetric error, with ‘xz’ and ‘zx’ spanning 0.25 mm and 0.14 mm, respectively, which is 42.3% and 23.7% of the volumetric error; however, other compensation tables such as ‘yb’ and ‘cy’ span 0.025 mm and 0.004 mm. Compensation tables correcting the rotary axes are not as obvious since they cannot be directly compared to the volumetric error. Additionally, the pitch errors on the rotary axes of this machine tool clearly dominate, with compensation tables such as ‘bc’ and ‘cy’, having maximum values of 5.8% and 3.1% of the maximum of the pitch compensation function, $f_{cc.}$

Another solution to the problem of selecting compensation tables may be to develop a heuristic to select compensation tables based on the relative size of each compensation function. Many metrics can be used to compare the significance of each compensation table. One possible heuristic is based on the impact an individual compensation table has on the overall compensation performance, as measured by the mean volumetric error for the identification set.

Table 3: Performance for each GA run.

Run	Computation Time (hrs)	Mean error (mm)	Solution
1	6.1	0.0493	xz zx yc xc yb cy
2	4.7	0.0493	xz zx yc xc cb bc
3	5.8	0.0445	xz zx yc xc yx bc
4	5.8	0.0460	xz zx yc xy cb zc
5	3.8	0.0460	xz zx yc xc yb zy
Average	**5.2**	**0.0470**	--

Table 4 shows the mean volumetric errors for models including all compensation tables except the one listed in the first column. The larger the mean volumetric error is without a compensation table, the greater the impact of that compensation table on the compensation performance. The six compensation tables with the most impact are then selected to form the heuristic solution. Using the identification measurement set collected above, the heuristic solution is ‘yz zx xc yc zy bx’ with a mean volumetric error of 0.0625 mm, 15.3 μm worse than the GA solution and 31.3 μm worse than the full set of compensation tables. Referring to the GA solutions, some of the selected compensation tables, such as ‘yb’, ‘zc’, and ‘cy,’ are ranked as having low impact in Table 4. These compensation tables are ranked 15th, 16th, and 19th, respectively. Therefore, examining the impact of the mean volumetric error of an individual compensation table is not always an adequate indicator of whether the compensation table should be included in the solution. The compensation functions using the full set of compensation tables are plotted alongside the GA solution and the heuristic solution in Figure 9. Where the heuristic or GA solutions share tables with the solution that utilizes all of the tables, the shape and magnitude for some of those compensation functions can be very different, for example, the compensation functions ‘xx’, ‘yx’, and ‘zx’. This method of identifying table-based compensation finds the best set of functions to reduce the machine tool kinematic errors so that the tool tip position and orientation most closely match the desired position and orientation described by $\mathbf{F}_n$. As a result, some errors are being approximated by compensation functions that do not necessarily describe the physical source of the measured error, which will be particularly true with a reduced number of compensation tables. Evaluating the impact of a single compensation table on the mean or maximum volumetric error of the full set does not measure how well an error might be approximated using other terms, only its size in a complete solution. For this reason, evaluating the entire solution together is more effective than evaluating the impact of a single compensation table. The heuristic solution is compared to the average GA solution in Table 5.

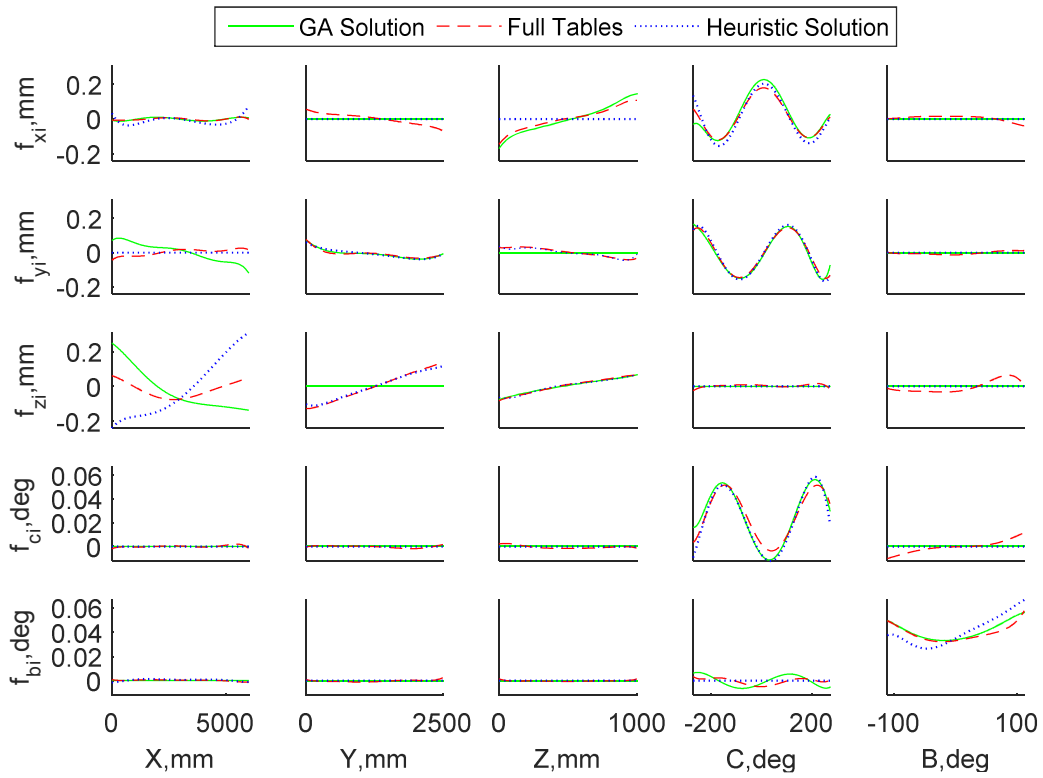

Figure 9: Compensation table functions generated from error model for full set of compensation tables, best GA solution, and heuristic solution.

4.1. Experimental Compensation Results. The previously described machine tool was measured at 295 unique measurement locations using two tool lengths, and the new set of data was used to identify a set of compensation tables using the GA. The GA compensation tables are compared in simulation first, then implemented on the machine tool controller. The predicted mean volumetric error for the GA compensation tables is the same as for the full set of compensation tables, while the maximum mean volumetric error is 11 μm larger. However, the repeatability of the machine tool and measurement instrument is 17 μm, so there is unlikely to be a measureable difference between the two. The set of compensation tables identified using the GA was implemented on the machine tool and compared to the full set of compensation tables experimentally. Both sets of compensation tables are discretized into 1024 points per table. The compensated mean volumetric errors are evaluated over a validation set of 35 quasi-random points, which are

different from those used to generate the compensation tables. The results are shown in Table 6. The GA compensation tables have a mean volumetric error 8 µm larger than the full set of compensation tables for the validation set. The maximum error is similarly close, with the GA compensation tables being 10 µm larger than the full set of compensation tables. Good performance over the validation set indicates that the low mean volumetric error for the GA compensation tables is not due to overfitting, and translates to verifiable performance improvement on the machine tool. The GA compensation tables perform nearly as well as the full compensation tables when implemented on the machine tool, demonstrating the GA is able to find near optimal solutions even when the number of compensation tables is restricted.

Table 4: Model mean volumetric error excluding compensation table listed in column 1.

Table	Rank	Mean error (mm)
zx	**1**	**0.1169**
yc	**2**	**0.1126**
xc	**3**	**0.1000**
zy	**4**	**0.0924**
yz	**5**	**0.0792**
bx	**6**	**0.0751**
by	7	0.0725
bc	8	0.0724
bz	9	0.0701
.	.	.
.	.	.
.	.	.
xb	17	0.0530
cx	18	0.0489
cy	19	0.0474
cz	20	0.0463

Table 5: Performance of heuristic and average GA solutions.

Solution	Computational Time (hr)	Mean error (mm)	Solution
Full tables	--	0.0310	--
Heuristic	1.0	0.0625	yz zx xc yc zy bx
Average GA	5.2	0.0470	--

Table 6: Volumetric errors for validation experiments on 5-axis industrial machine tool, mm.

		Model errors		Comp. errors	
Model	Tables	Mean	Maximum	Mean	Maximum
Full tables	--	0.036	0.086	.043	0.122
GA	xc zx yc yx yz cz	0.036	0.097	.051	0.132

4.2. Constraint Inclusion. Data from the previously described machine tool is used to test two specific controller constraints, which were described in Section 3.2. The first constraint is largely seen in older machine tool controllers and prevents what is termed circular compensation, i.e., the situation where the compensation table *ij* is populated and, thus, the compensation table *ji* may not be used. The GA is run five times for each constraint and the mean volumetric errors over the identification set are compared to the unrestricted GA in Table 7. The GA with the constraint on circular compensation is slightly worse than the average GA, with one solution 5.6 μm worse and the other solution 10.1 μm worse. The difference between the GA solutions with constraints on circular compensation and the unconstrained GA solutions is statistically significant based on a paired t-test of the mean volumetric error using a significance level of 0.05. This is expected since added constraints reduce the number of possible solutions and, for this particular machine tool, there are several circular combinations of compensation tables that are large. For example, the machine tool has a significant error described by the compensation table function ‘zx’, which represents sagging of the long axis, X, as well as an error described by the compensation table function ‘xz’ that

represents the Z axis ram not travelling straight. There also is significant coupling between the rotary axes, described by the compensation table functions ‘cb’ and ‘bc’.

Table 7: Mean volumetric error for ga solutions with no constraints, no circular compensation, and no x axis compensation.

Model	Mean error (mm)	Solution
Full tables	0.0310	--
Average GA	0.0470	--
Best GA	0.0445	xz yc xc yx zx bc
Circular compensation		
Result 1	0.0571	zx yc xc zy cb xb
Result 2	0.0526	zx yc xc xy yb xb
Result 3	0.0526	xz yc xc yx cb yb
Result 4	0.0540	xz yc xc yx cb zy
Result 5	0.0535	xz yc xc yx yb xb
Restricted axis (X)		
Result 1	0.0753	zx yx yc zb cb bc
Result 2	0.0753	zx yx yc zb cb bc
Result 3	0.0753	zx yx yc zb cb bc
Result 4	0.0753	zx yx yc zb cb bc
Result 5	0.0753	zx yx yc zb cb bc

The second constraint considered here does not allow compensation for a specific axis, in this case the X axis. Three runs of the GA found the same solution for the second constraint, and this solution performs worse than the unrestricted GA solution, with the mean volumetric error being 28.3 μm worse than the average unrestricted GA solution. This is not unexpected based on the size of the X axis compensations in the full set of compensation table functions shown in Figure 9 and the unrestricted GA solutions, the best of which contains the tables ‘xz’ and ‘xc’.

The proposed volumetric error compensation methodology differs from the methodologies reported in the literature, summarized in [3,4], in two ways. First, nearly every machine tool calibration methodology measures only a few geometric errors in one

set up, e.g., interferometers for linear axes and ball bars and R test for rotational axes, and, thus, populates only a few compensation tables with each set up. The proposed methodology measures geometric errors over the entire axis space and is able to populate the entire set of compensation tables, if no limitations or constraints exists, in just one set up. Second, if there is a limitation on the number of compensation tables that can be implemented or there are constraints on the combination of compensation tables that can be utilized, the proposed methodology is able to optimally select the best combination of compensation tables. To the authors' knowledge, this issue has not been previously addressed in the literature.

5. SUMMARY AND CONCLUSIONS

A quick machine tool geometric error calibration method that generates compensation tables from tooltip measurements was extended in this paper to situations where the number of machine tool controller compensation tables is limited and constraints exist on the possible combinations of tables that can be utilized. The reduced table selection methodology is based on artificial intelligence that utilizes a Generic Algorithm (GA) to find the optimal set of compensation tables without having to evaluate all possible combinations of tables. Data from an industrial 5-axis machine tool was used in a simulation study to compare the GA methodology to the selection of compensation tables using a heuristic. The heuristic uses a logical metric based on the impact of individual compensation tables to select a set of compensation tables. When selecting six compensation tables, the mean volumetric error for tables selected by the GA methodology was 44.7% smaller than the mean volumetric error for the tables selected by the heuristic. The heuristic and GA methodology required 1 and 5.2 hr, respectively, to find solutions, while 550 hr were required for an exhaustive search, which is impractical for most applications. The GA methodology was then experimentally implemented on an industrial 5-axis machine tool using a validation data set and the resulting mean and maximum volumetric errors were 8.0 and 10.1 μm, respectively, greater than the mean and maximum volumetric errors when the full set of compensation tables were implemented. In a second simulation study, the GA methodology was used to select six compensation tables for the industrial machine tool assuming that circular compensation

could not be utilized. The GA methodology was implemented and the resulting mean volumetric error was 7.0 μm greater than the mean volumetric error for the compensation tables found by the unconstrained GA methodology. This demonstrates the importance of using circular compensation for this machine tool, as the compensation tables xz and zx were present in the unconstrained solution. In a third simulation study, the GA methodology was used to select six compensation tables for the industrial machine tool assuming that compensation could not be implemented for the x axis. The GA methodology was implemented and the resulting mean volumetric error was 28.3 μm greater than the mean volumetric error for the compensation tables found by the unconstrained GA methodology. This demonstrates the importance of compensating the x axis for this machine tool, as the compensation tables xz and xc were present in the unconstrained solution. The GA methodology presented here is able to efficiently select compensation tables for a variety of machine tool controllers, even when their existing compensation options limit the number of tables that can be implemented or the combination of tables that can be utilized.

ACKNOWLEDGEMENTS

The work presented here was supported by the Boeing Company, the Center for Aerospace Manufacturing Technologies at the Missouri University of Science and Technology, the National Science Foundation (grant CMMI-1335340), and the Department of Education (grant P200A120062).

REFERENCES

[1] ISO 230-1, "Test Code for Machine Tools Part I: Geometric Accuracy of Machine Tools Operating Under No-Load or Quasi-Static Conditions," ISO, Geneva, Switzerland, 2012.

[2] S. Sartori and G. X. Zhang, "Geometric Error Measurement and Compensation of Machines," CIRP Annals -- Manufacturing Technology, vol. 44, no. 2, pp. 599-609, 1995.

[3] H. Schwenke, W. Knapp, H. Haitjema, A. Weckermann, R. Schmitt and F. Delbessine, "Geometric Error Measurement and Compensation of Machines-An Update," CIRP Annals - Manufacturing Technology, vol. 57, no. 2, pp. 660-675, 2008.

[4] S. Ibaraki and W. Knapp, "Indirect Measurement of Volumetric Accuracy for Three-axis and Five Axis Machine Tools: A Review," International Journal of Automation Technology, vol. 6, no. 2, pp. 110-124, 2012.

[5] Khan, A.W. and Chen, W., "A Methodology for Systematic Geometric Error Compensation in Five-Axis Machine Tools," International Journal of Advanced Manufacturing Technology, vol. 53, pp. 615-628, 2011.

[6] Cheng, Q., Zhao, H., Zhang, G., Gu, P., and Cai, L., "An Analytical Approach for Crucial Geometric Errors Identification of Multi-Axis Machine Tool Based on Global Sensitiity Analysis," International Journal of Advanced Manufacturing Technology, vol. 75, pp. 107-121, 2014.

[7] Lin, Y. and Shen, Y., "Modelling of Five-Axis Machine Tool Metrology Models using the Matrix Summation Approach," International Journal of Advanced Manufacturing Technology, vol. 21, pp. 243-248, 2003.

[8] P. Freeman, "A Novel Means of Software Compensation for Robots and Machine Tools," in Aerospace Manufacturing and Automated Fastening Conference and Exhibition, Toulouse, France, September, 2006.

[9] Wang, Z., Mastrogiacomo, L., Franceschini, F., and Maropoulos, P., "Experimental Comparison of Dynamic Tracking Performance of iGPS and Laser Tracker," International Journal of Advanced Manufacturing Technology, vol. 56, pp. 205-213, 201.

[10] Creamer, J., Sammons, P.M., Bristow, D.A., and Landers, R.G., 2017, “Table–Based Volumetric Error Compensation of Large 5–Axis Machine Tools,” ASME Journal of Manufacturing Science and Engineering, Vol. 139, No. 1, pp. 021011-1:11.

[11] B. Mooring, "The Effect of Joint Axis Misalignment on Robot Positioning Accuracy," in Proccedings of the 1983 ASME Computers in Engineering Conference, Chicago, Illinois, August 1983.

[12] B. Mooring, Z. S. Roth and M. R. Driels, Fundamentals of Manipulator Calibration, John Wiley and Sons, Inc., 1991.

[13] C. Hollerbach, J. Wampler and T. Arai, "An Implicit Loop Method for Kinematic Calibration and Its Application to Closed-Chain Mechanisms," IEEE Trans. Robotics and Automation, vol. 11, no. 5, pp. 710- 724, 1995.

[14] D. E. Goldberg, Genetic Algorithms in Search, Optimization, and Machine Learning, Reading, MA: Addison-Wesley Publishing Company, Inc., 1989.

[15] P. S. Efraimidis and P. Spirakis, "Weighted Random Sampling," in Encyclopedia of Algorithms, Springer Science and Business Media, 2008, pp. 1-99.

SECTION

2. TABLE-BASED VOLUMETRIC ERROR COMPENSATION IMPLEMENTATIONS

In addition to the laboratory machine presented in the previous papers, table-based volumetric error compensation has been implemented or evaluated for implementation on a variety of other machine tools. For each machine tool was evaluated, a set of tool tip measurements were collected using a laser tracker and a table-based model was identified In the following sections, each machine is described and some results from measurement and modeling are presented.

2.1. CINCINNATI 20V, BOEING RESEARCH AND TECH ST. LOUIS

The Cincinnati 20V, shown in Figure 2.1, is also located in a laboratory environment. It is a small 5-axis hard metals machining center with an XYZAB configuration with axis travel shown in Table 2.1. The machine has a Siemens 840D controller.

Table 2.1:Axis limits for Cincinnati 20V

Axis	Minimum	Maximum
X	-.14 in	80 in
Y	-30.16 in	.23 in
Z	-24 in	0 in
B	-25 deg	25 deg
A	-25 deg	25 deg

Model performance is shown in Table 2.2. The mean volumetric error for the JP model is $0.7x10^{-3}$ in, which is a 96.5% reduction in error. The model accuracy over its identification set is nearing the accuracy of the measurement instrument, (repeatability of $0.7x10^{-3}$ in, as detailed in Paper I), indicating that much of the residual error could be attributed to measurement noise. The gage line offset correction was found to be $0.5x10^{-3}$ in, which is near the accuracy of the tool length measurement, so this is small enough to be noise. The axis perturbation functions are plotted in Figure 2.2.

Figure 2.1: Cincinnati machine

Table 2.2: Machine volumetric error, new data

Model	Mean (in $x10^{-3}$)	Max (in $x10^{-3}$)
Uncalibrated	20.1	37.4
JP	0.7	2.1

Some high order effects are present at Z axis positions close to the table, but this is likely due to poor measurement coverage in this area due to the length of the active target mounted in the spindle. This area is considered to be outside the work volume for most standard tools. The largest translational compensations are to the Z axis. One is dependent on Y position, representing that this axis is slanted. The other is the Z positioning error. The largest X compensation depends on the B axis position. The largest angular compensation is the angular positioning error of the A axis, but a close second is the Z dependent B compensation, which has a large peak near the top of the Z axis. This machine has significantly less travel in the rotary axes than the previous experimental machine (Flow 5-axis, C travel [-272, 272] and B travel [-11,111]) and has a smaller work volume. It was expected that this type of calibration would provide less benefit to small machines with less complexity, however, this machine, despite small travels for the rotary axes, has non-trivial errors that depend on the rotary axis location (f_{bx}, f_{bz}). The model accuracy on this machine also predicts significant error reduction, demonstrating that VEC is of benefit to even small 5-axis machines.

2.2. SNK 120V BOEING DEFENSE AND SPACE, ST. LOUIS

The SNK 120V is a production 5-axis machining center with XYZAB configuration and axis travels shown in Table 2.3. This machine has a Fanuc 30i controller. Results for this machine are shown in Table 2.4. This machine presents a new challenge compared to most others in this section. A majority of the machines evaluated have Siemens 840D controllers, which allow a large number of compensation tables (64). However, the Fanuc 30i allows 5 pitch compensation tables and 6 straightness tables of some description. There are 20 straightness tables that are possible, so a new method to select the best tables is needed. A method using artificial intelligence is presented in Paper II.

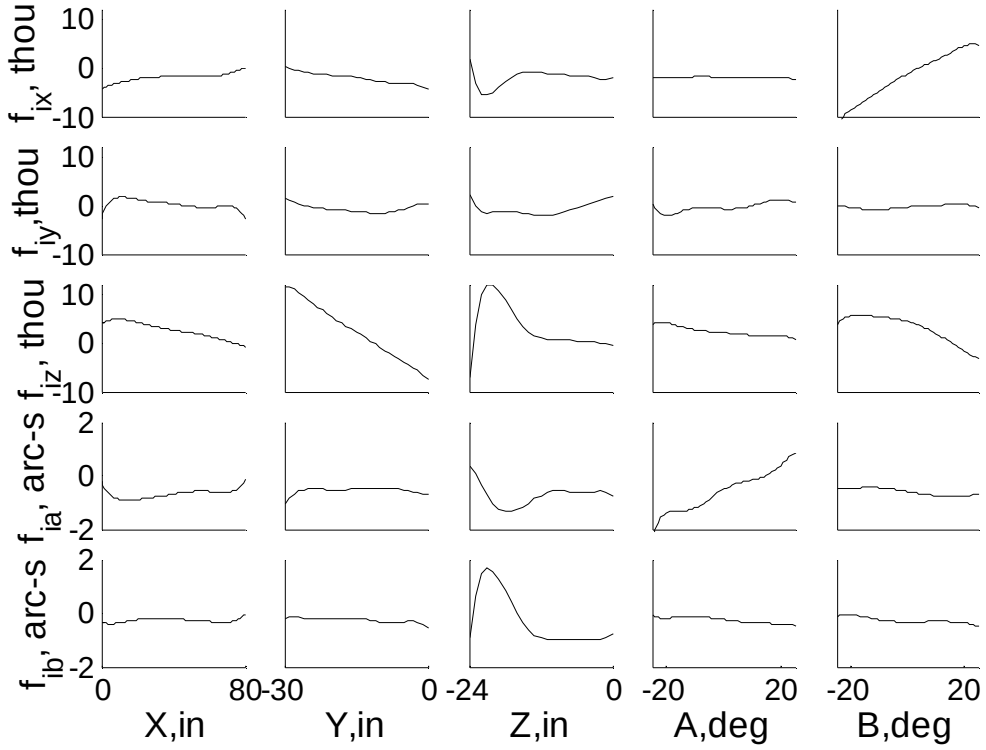

Figure 2.2: Axis perturbation functions.

Table 2.3: Axis limits for SNK.

Axis	Minimum	Maximum
X	-.4 in	120 in
Y	-48 in	0 in
Z	-27 in	0 in
A	-25 deg	25 deg
B	-25 deg	25 deg

Table 2.4: Results for the SNK machine tool.

	Mean (inx10^{-3})	Max (inx10^{-3})
Uncalibrated	8.4	19.1
AP Model	0.8	2.5

2.3. INGERSOLL HORIZONTAL MACHINING CENTER, NASA

The NASA Ingersoll is a large 5-axis gantry horizontal machining center with and additional rotary table and tail stock. It has an XYZCA configuration with axis travels shown in Table 2.5 (without considering the rotary table). The machine is pictured in Figure 2.3. This machine was measured as a part of a joint effort with Automated Precision, Inc.

Table 2.5: NASA Ingersoll axis limits.

Axis	**Min**	**Max**
X (in)	-196.89	276.22
Y (in)	-0.04	157.52
Z (in)	-1.97	137.83
C	-400^o	400^o
A	-110^o	110^o

The machine was measured using a set of pseudo-random points and an axis perturbation model was fit. The initial results are shown in Table 2.6. The performance of the compensation degrades as a function of Y axis position on the grid of validation

points, indicating that some error on the machine is not well described by the model, as shown in Figure 2.4.

Figure 2.3: Photo of machine tool during calibration.

The Y gantry of this machine is known to have significant skewing based on the original compensation and the mismatched current of the two motors, so it may be that these errors are hard to model using the AP model. Terms representing possible skewing between the gantry axes are introduced and a new set of model parameters are identified. For the Y gantry, a small rotation about the X axis, θ_{Yg}, is inserted, and for the X gantry, a similar small rotation, θ_{Xg}, is introduced as

$$\mathbf{F}_{AP}(\mathbf{q}+\hat{\mathbf{q}}) = \mathbf{T}_X(q_X+\hat{q}_X)\mathbf{T}_{\theta_{X_g}}\left(\theta_{X_g}\right)\mathbf{T}_Y(q_Y+\hat{q}_Y)\mathbf{T}_{\theta_{Y_g}}\left(\theta_{Y_g}\right)\mathbf{T}_Z(q_Z+\hat{q}_Z)\mathbf{T}_C(q_C+\hat{q}_C)\mathbf{T}_A(q_A+\hat{q}_A)\mathbf{T}_{Tt} \quad (23)$$

where θ_{Yg} is modeled as a function of each axis position,

$$\theta_{Y_g} = f(q_X) + f(q_Y) + f(q_Z) + f(q_C) + f(q_A) \tag{24}$$

and θ_{Xg}, is modeled in much the same way.. In this model, the maximum residual error is reduced to 3.21×10^{-3} from 5.5×10^{-3}, which is a 42% decrease. The identified functions are plotted in Figure 2.5.

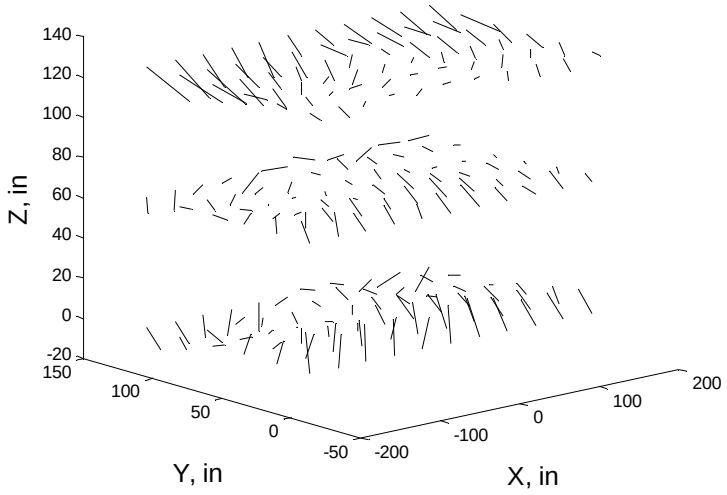

Figure 2.4: Vector plot of grid point errors with compensation active.

Table 2.6: Residual error for uncompensated machine and AP model.

Model	Mean (in)	Max (in)
Uncompensated	10.5×10^{-3}	25.0×10^{-3}
AP model	1.57×10^{-3}	5.50×10^{-3}
AP+θ_{Yg}, θ_{Xg} model	1.34×10^{-3}	3.21×10^{-3}
AP tables (validation)	2.6×10^{-3}	4.8×10^{-3}
Original tables	5×10^{-3}	10×10^{-3}

2.4. SPAR MILL 23, BOEING COMMERCIAL (BCA), SEATTLE, WA

Spar mill 23 is a 110ft long four-axis mill with two spindles that run mirrored, meaning that their movements are synchronized but opposite. The controller is a Fanuc 33i. This machine is older, but had undergone a recent retrofit. The repeatability of the machine is shown in Figure 2.7, and is found to degrade somewhat over several hours between the two data sets shown. The volumetric error on the uncompensated machine is shown in Figure 2.6. Data is shown ordered by point number to check for any time dependence in the measurements. Based on a long term repeatability of 3.4 thou and a mean volumetric error of 3.6 thou with an observed maximum of 8.2 thou, it was determined that the machine was unlikely to benefit from VEC and no tables were implemented.

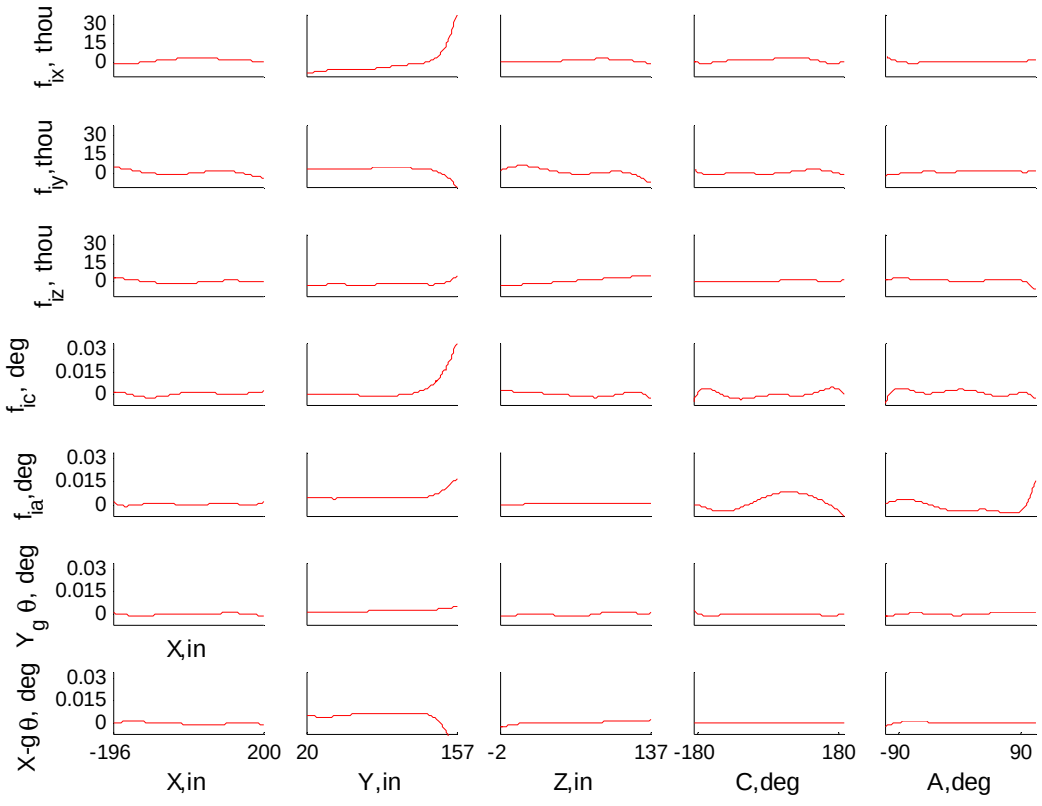

Figure 2.5: Functions for the model including both θ_{Yg} and θ_{Xg}.

Repeatability of this machine was established by measuring nine points four times using the SMR over 19 minutes, and again by comparing the two sets of identification measurements, taken over 5 hours and 50 minutes. The distributions of the repeatability over long and short measurement times are shown in Figure 2.10 and Figure 2.11. The results are in Table 2.8.

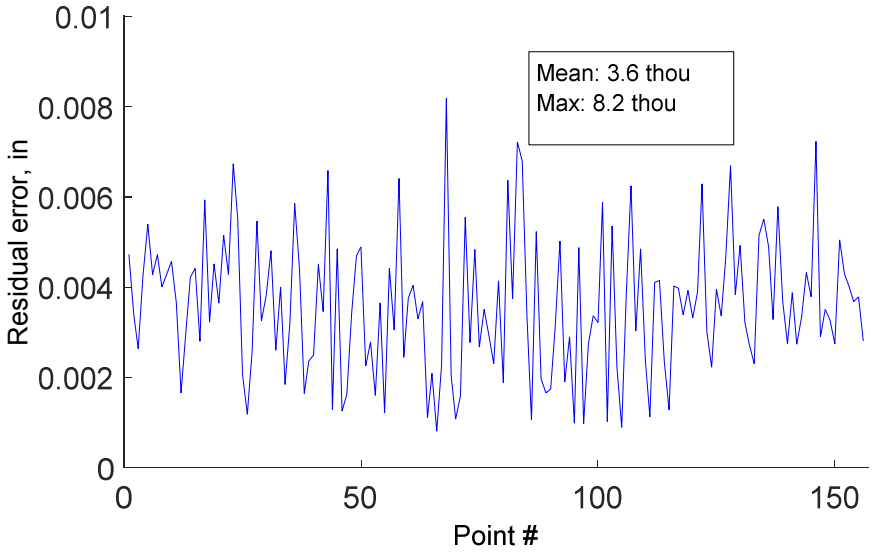

Figure 2.6: Volumetric error before compensation on Spar Mill 23.

The average repeatability over the short measurement period is on average 0.7 thou, which is approximately equivalent to the repeatability of the instrument, meaning the machine is more repeatable than a laser tracker can measure when time dependent effects (such as thermal changes) are minimized. However, when the repeatability was calculated using 287 points over 5.8 hours, the mean increases to 2.1 thou and the maximum to 9.0 thou. During this time, 4^{o} F of temperature change was recorded at the machine table, and this temperature change may be partially responsible for the degradation of the repeatability.

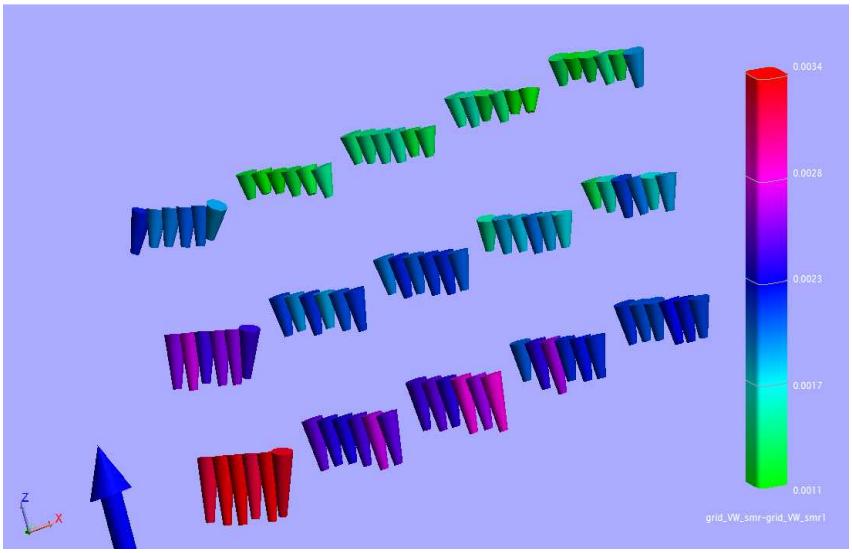

Figure 2.7: Grid of repeated points evaluating repeatability of Spar Mill 23 over time.

Table 2.7: Master Mill axis limits.

Axis	Min	Max	Naming
X (in)	-325	325	AX1, AX8
Y (in)	-80	80	AX2
Z (in)	30	110	AX3
C	-200°	200°	AX4
A	-110°	110°	AX5

These measurements were then used to fit a joint perturbation model using the implicit loop method. This model used a base frame with orientation fixed to the machine table. Table 2.9 shows the mean and maximum volumetric error between the model and identification points. The functions are shown in Figure 2.12.

Figure 2.8: Master Mill machining a complex part.

Figure 2.9: View down the long axis (X) of the Master Mill.

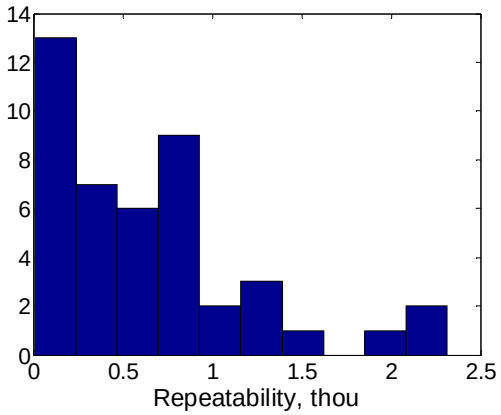

Figure 2.10: Distribution of short term repeatability.

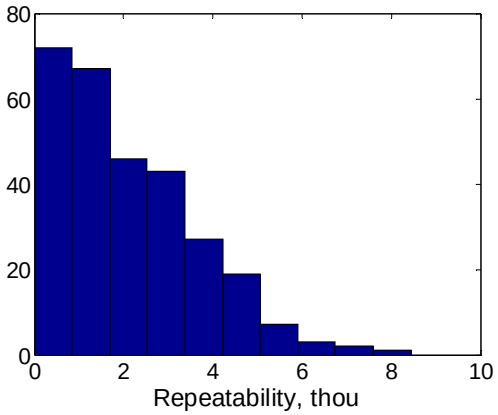

Figure 2.11: Distribution of long term repeatability.

Table 2.8: Mean and maximum repeatability.

Repeatability type	Mean (thou)	Max (thou)	Std. (thou)	Time (hr)
Short term	0.7	2.3	0.1	0.3
Long term	2.1	9.0	1.6	5.8

Table 2.9: Model residual errors, thousandths of an inch.

	Identification		Validation	
Model	**Mean**	**Max**	**Mean**	**Max**
Uncompensated	11.6	30.4	11.6	20.4
Joint perturbation	2.2	5.8	3.7	8.7

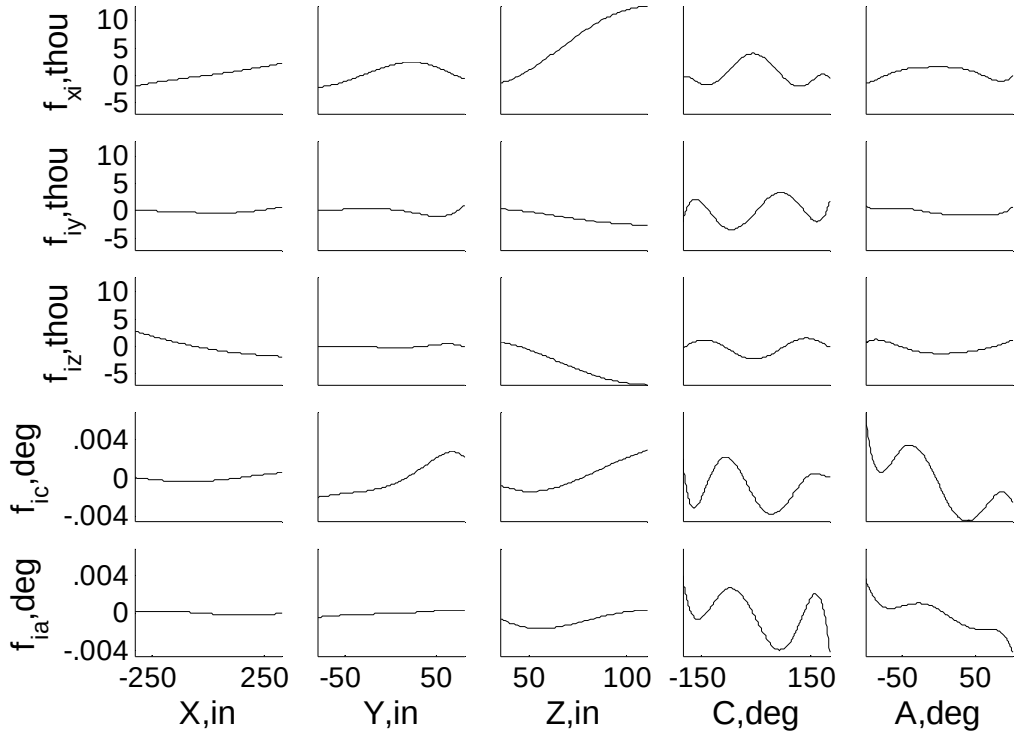

Figure 2.12: Axis perturbation functions, thousandths of an inch (thou) and degrees.

In Figure 2.12, the horizontal axis for each function is the input axis, and the vertical axis is the compensated machine axis. The functions f_{cx} and f_{cy} are sinusoidal in C position, representing an unaccounted for offset between the C and A axes. The function f_{yx} indicates that the Y axis bows out in the X direction. In addition to the compensation

tables, the nominal lengths of any links are corrected. The correction to the gage line offset was 0.3 thou.

The AP model functions, shown in the previous section in Figure 2.12, were each discretized into 1024 points and loaded into 30 compensation tables. Normally there are 5x5=25 tables possible for a 5-axis machine, but this machine has a gantry system and needs to have X compensation tables for both the leading and following axes. The functions in the top row of Figure 2.11 were placed in two tables, one for the leading and one for the following axis.

Both new and old compensation tables were evaluated over this validation set, and the mean and maximum residual errors after compensation are shown in Table 2.10. Figure 2.13 shows the distribution of residual volumetric error for both sets of compensation tables and the uncompensated machine.

Table 2.10: Compensated residual error, thousandths of an inch.

Compensation	Mean	Max
Uncompensated	11.6	20.4
Original	14.2	23.2
Volumetric	6.7	13.6

2.6. UNDISCLOSED PRODUCTION MACHINE, ST. LOUIS, MO

The undisclosed production machine is a large gantry that has an XYZBAW configuration, where W is the translational axis mounted after the B and A rotary axes that moves in the tool Z direction. The axis limits are shown Table 2.11. This machine has a Siemens 840D controller and is a production implementation of table-based VEC. The machine is calibrated in small zones to get better compensation performance, which is a strategy unique to this machine in terms of VEC implementations. The performance

overall and in these zones is shown in Table 2.12. The residual volumetric error after compensation is marginally higher than on other machines presented here, but may partially be attributed to the longer X-axis and single tracker setup. This distance causes the laser tracker to have more error in its measurements, affecting both the model quality and the ability to measure the true residual error over a small set of points. Future implementations on this machine should consider two laser tracker locations to mitigate the distance related measurement error.

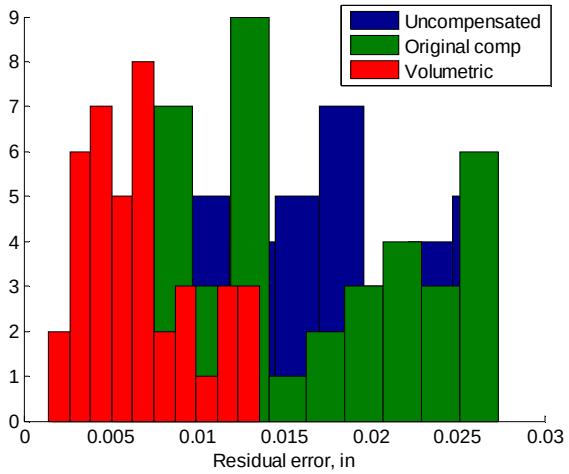

Figure 2.13: VEC performance over old validation set

2.7. MACHINE TOOL EVALUATION SUMMARY

This section has presented results from measurement or implementation on a variety of machines in different settings. Two machines were Boeing Defense production machines (SNK 120V and the undisclosed production machine), two were Boeing Commercial production machines (Master mill and the Spar mill), one was a Boeing lab machine, and one was a NASA production machine. Each machine had its unique challenges, with some being very long, some having odd configurations, and some having errors not

encountered in the lab setting such as temperature fluctuations and skewing between multiple gantry axes. Despite this, table-based VEC was able to reduce errors on all of these machines with the exception of a single machine whose accuracy was already as good as typical VEC accuracies.

Table 2.11: Axis limits of production machine.

Axis	Min	Max
X	450 in	1000 in
Y	0 in	30 in
Z	0 in	130 in
B	-5°	5 °
A	-200 °	17 °
W	-15 in	0 in

Table 2.12: Compensation performance in selected zones.

Model	**Overall**		**East**		**West**	
	Mean	Max	Mean	Max	Mean	Max
Uncalibrated	16.4	33.9	18.6	46.6	13.6	34.3
AP Model	2.2	6.0	1.8	4.2	1.8	4.1
Compensated	5.6	9.4	4.3	7.1	4.2	8.4

3. INSTRUMENT INTEGRATION

3.1 INTRODUCTION

The cost of machine down time and the speed with which laser trackers can collect measurements of a machine tool has driven their use as a calibration tool for machine tools. Due to the lower accuracy of the angular positioning of a laser tracker, multiple laser trackers [17, 18]or multiple positions [43, 19] are sometimes used so that the three-dimensional position of the tool tip may be found by triangulation. Ibaraki et al [18] found that even using this method, the laser tracker error in identifying the position of a corner cube could be as large as typical positioning errors. In [20], Nubiola and Bonev used a single laser tracker and multiple reflectors to calibrate an ABB IRB1600 robot and achieved good improvement in the volumetric error in simulation. A laser tracker is also used for measurements by Aguado et al [44]. Most of the measurement methods reviewed here require several different set ups to acquire enough measurements to build a complete model. Some require additional measurement methods. Laser trackers have the potential to be very fast, and are the only instrument required to build a complete model. Nubiola and Bonev [20] reports taking 1000 measurements in 1-2 hours. However as of 2009, even using multilateration, laser trackers were reported in [18] not to be accurate enough for this purpose. The commercial laser tracker used in [20] has a volumetric accuracy at 10m of 49 µm, and an error of 23 µm when measuring a 2.3 m scale bar from 2 m away.

The use of large numbers of measurements (200-500) and a maximum likelihood estimator can mitigate the issue of laser tracker accuracy. Measurements of the tooltip are typically recorded in Cartesian coordinates since this is how the machine tool kinematics are described. However, it is known that the angular measurements are much less accurate than the range measurements for the laser tracker, and that the accuracy depends on the distance away from the laser tracker. This information can be incorporated into the maximum likelihood estimator to improve the model accuracy by converting the kinematic equations to spherical coordinates.

3.2. BACKGROUND

The relationship between a set of axis commands $\mathbf{q}_i = [q_1\ q_2 \ldots q_n]$ and the tooltip position and orientation can be described by treating the machine tool as a kinematic chain of rigid links. The relationship between these links can be described using Linear Homogeneous Transformation (LHT) matrices, as described in Paper I.

The machine tool kinematics are modeled using the Zero Reference Model [45], a method commonly applied in robotics [33]. The nominal kinematics for an *n*-link machine tool are then given by

$$\mathbf{F_n}\left(\mathbf{q}, L_{T,\alpha}\right) = \mathbf{T}_1\left(q_1\right)\mathbf{T}_2\left(q_2\right)\cdots\mathbf{T}_{n-1}\left(q_{n-1}\right)\mathbf{T}_n\left(q_n\right)\mathbf{T}_T\left(L_{T,\alpha}\right) \tag{25}$$

where and $\mathbf{T}_1(q_1),\ldots,\mathbf{T}_n(q_n)$ are LHTs for axes 1,…,*n* respectively and $\mathbf{T_T}(L_{T,\alpha})$ is the transformation from the last joint to the tool tip where $L_{T,\alpha}$ is the length of the tool. Because of inaccuracies in machine tool component fabrication and assembly, the actual kinematics of the machine tool are not equivalent to those of the nominal kinematic model. Errors are introduced as a small deviation from the nominal axis command. For an *n*-link machine tool, the actual kinematics are

$$\mathbf{F}_{AP}\left(\mathbf{p},\mathbf{q}, L_{T,\alpha}\right) = \mathbf{E}_0\left(\mathbf{p}\right)\mathbf{F_n}\left(\mathbf{q}+\hat{\mathbf{q}}\left(\mathbf{p},\mathbf{q}\right), L_{T,\alpha}\right) \tag{26}$$

where $\mathbf{p}$ is a vector of model parameters and $\hat{\mathbf{q}}(\mathbf{p},\mathbf{q}) = \left[\hat{q}_1(\mathbf{p},\mathbf{q}) \quad \hat{q}_2(\mathbf{p},\mathbf{q}) \quad \cdots \quad \hat{q}_n(\mathbf{p},\mathbf{q})\right]^T$ is a vector of axis perturbation functions that perturb the nominal joint variables. The base frame correction $\mathbf{E}_0$ is defined as three small constant rotary corrections and three small constant translational corrections,

$$\mathbf{E}_0\left(\mathbf{p}\right) = \begin{bmatrix} 1 & -\varepsilon_{0z} & \varepsilon_{0y} & \delta_{0x} \\ \varepsilon_{0z} & 1 & -\varepsilon_{0x} & \delta_{0y} \\ -\varepsilon_{0y} & \varepsilon_{0x} & 1 & \delta_{0z} \\ 0 & 0 & 0 & 1 \end{bmatrix}, \varepsilon_{0x} \ldots \delta_{0_x} \ldots \delta_{0_z} \in \mathbf{p} \tag{27}$$

Each perturbation is composed of a combination of basis functions depending on each joint position individually and is represented as an m^{th} order Chebychev polynomial,

$$\begin{aligned}
\hat{q}_1(\mathbf{q}) &= a_{10} + a_{111}C_1(q_1) + \ldots + a_{11m}C_m(q_1) \ldots + a_{1n1}C_1(q_n) + \ldots + a_{1nm}C_m(q_n) \\
\hat{q}_2(\mathbf{q}) &= a_{20} + a_{211}C_1(q_1) + \ldots + a_{21m}C_m(q_1) \ldots + a_{2n1}C_1(q_n) + \ldots + a_{2nm}C_m(q_n) \\
&\vdots \\
\hat{q}_n(\mathbf{q}) &= a_{n0} + a_{n11}C_1(q_1) + \ldots + a_{n1m}C_m(q_1) \ldots + a_{nn1}C_1(q_n) + \ldots + a_{nnm}C_m(q_n)
\end{aligned} \tag{28}$$

where $C_k(q_i)$ is the k^{th} order Chebychev polynomial. Then the parameter vector, **p**, is composed of the six terms from $\mathbf{E}_0$ and the a_{ijk} terms,

$$\mathbf{p} = \begin{bmatrix} \varepsilon_{0x} & \varepsilon_{0y} & \varepsilon_{0z} & \delta_{0_x} & \delta_{0_y} & \delta_{0_z} & a_{110} & \cdots & a_{11m} & \cdots & a_{nn0} & \cdots & a_{nnm} \end{bmatrix} \tag{29}$$

The position and orientation of the machine tool tip are measured at each of hundreds of axis positions $\mathbf{q}_i$. The position and orientation are captured by measuring the tool tip position with two tool lengths, $L_{T,1}$ and $L_{T,2}$.. The laser tracker measures three dimensional position for each tool length in spherical coordinates,

$$\mathbf{s}_{i,L_{T,\alpha}} = \begin{bmatrix} R_{i,\alpha} & \phi_{i,\alpha} & \theta_{i,\alpha} \end{bmatrix}^T \tag{30}$$

where i =1,.., N, N being the total number of measurements, α = 1, …, N_T is the number of tools, $R_{i,\alpha}$ is the range, $\varphi_{i,\alpha}$ is the elevation, and $\theta_{i,\alpha}$ is the azimuth. The kinematics for a machine tool expressed in Cartesian coordinates, so the laser tracker measurement is often converted to Cartesian coordinates for the identification of parameters. The tool tip measurement is then

$$\mathbf{x}_{i,L_{T,\alpha}} = \begin{bmatrix} x_{i,\alpha} & y_{i,\alpha} & z_{i,\alpha} \end{bmatrix}^T \tag{31}$$

where $x_{i,\alpha}$, $y_{i,\alpha}$, and $z_{i,\alpha}$ are the x, y, and z components of the tooltip measurement, respectively. Assume for some $\mathbf{p}$ that the machine motion is described by $\mathbf{F}_{AP}(\mathbf{p}, \mathbf{q}_i + \tilde{\mathbf{q}}_i, L_{T\alpha})$, then the measurement can be described as

$$\mathbf{x}_{i,L_{T\alpha}} = \begin{bmatrix} 1 & 0 & 0 & 0 \\ 0 & 1 & 0 & 0 \\ 0 & 0 & 1 & 0 \end{bmatrix} \mathbf{F}_{AP}\left(\mathbf{p}, \mathbf{q}_i + \tilde{\mathbf{q}}_i, L_{T,\alpha}\right) \begin{bmatrix} 0 \\ 0 \\ 0 \\ 1 \end{bmatrix} + \tilde{\mathbf{x}}_{i,L_{T\alpha}} \tag{32}$$

where $\tilde{\mathbf{q}}_i = \begin{bmatrix} \tilde{q}_1 & \cdots & \tilde{q}_n \end{bmatrix}^T$ is the error on the axis commands and $\tilde{\mathbf{x}}_{i,L_{T\alpha}} = \begin{bmatrix} \tilde{x}_{i,\alpha} & \tilde{y}_{i,\alpha} & \tilde{z}_{i,\alpha} \end{bmatrix}^T$ is the error on the measurement. The Cartesian tooltip measurement is related to the spherical one by the operator C_{rt}(-)

$$\mathbf{x}_{i,L_{T,\alpha}} = C_{rt}\left(\mathbf{s}_{i,L_{T,\alpha}}\right) = \begin{bmatrix} R_i \sin(\phi_i)\cos(\theta_i) \\ R_i \sin(\phi_i)\sin(\theta_i) \\ R_i \cos(\phi_i) \end{bmatrix} \tag{33}$$

Since the measurement is natively in spherical coordinates, the measurement error, $\tilde{\mathbf{s}}_{i,L_{T,\alpha}} = \begin{bmatrix} \tilde{R}_{i,\alpha} & \tilde{\phi}_{i,\alpha} & \tilde{\theta}_{i,\alpha} \end{bmatrix}^T$, is also. Then,

$$\mathbf{x}_{i,L_{T,\alpha}} + \tilde{\mathbf{x}}_{i,L_{T,\alpha}} = C_{rt}\left(\mathbf{s}_{i,L_{T,\alpha}} + \tilde{\mathbf{s}}_{i,L_{T,\alpha}}\right) \tag{34}$$

where C_{rt}(-) is the spherical to Cartesian conversion. However, since C_{rt}(-) is a nonlinear transformation, $C_{rt}\left(\mathbf{s}_{i,L_{T,\alpha}} + \tilde{\mathbf{s}}_{i,L_{T,\alpha}}\right) \neq C_{rt}\left(\mathbf{s}_{i,L_{T,\alpha}}\right) + C_{rt}\left(\tilde{\mathbf{s}}_{i,L_{T,\alpha}}\right)$, so the information about the measurement error cannot be directly used in Cartesian coordinates. To best utilize

information about measurement accuracy (i.e., that it depends on the range, R_i from the tracker), the kinematics are also expressed in spherical coordinates using the following conversion operator, S(-),

$$S\left(\begin{bmatrix} p_x \\ p_y \\ p_z \end{bmatrix}\right) = \begin{bmatrix} R \\ \phi \\ \theta \end{bmatrix} = \begin{bmatrix} \sqrt{p_x^2 + p_y^2 + p_z^2} \\ \tan^{-1}\left(p_y, p_x\right) \\ \tan^{-1}\left(\sqrt{p_x^2 + p_y^2}, p_z\right) \end{bmatrix} \tag{35}$$

where $\mathbf{x} = [p_x\, p_y\, p_z]^T$ is a position in Cartesian coordinates and $\tan^{-1}(\text{-})$ is the four quadrant inverse tangent. Figure 3.1 illustrates the relationship between Cartesian and spherical coordinate systems. The measurement can then be modeled as

$$\mathbf{s}_{i,L_{T,m}} = S\left(\begin{bmatrix} 1 & 0 & 0 & 0 \\ 0 & 1 & 0 & 0 \\ 0 & 0 & 1 & 0 \end{bmatrix} \mathbf{F}_{AP}\left(\mathbf{p}, \mathbf{q}_i + \tilde{\mathbf{q}}_i, L_{T,\alpha}\right) \begin{bmatrix} 0 \\ 0 \\ 0 \\ 1 \end{bmatrix}\right) + \tilde{\mathbf{s}}_{i,L_{T,\alpha}} \tag{36}$$

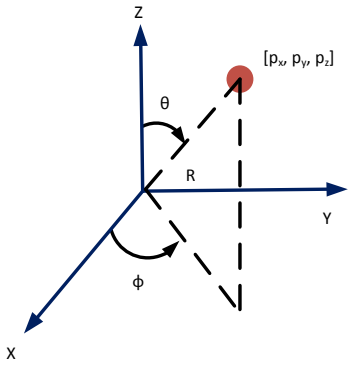

Figure 3.1: Illustration of the conversion between spherical and Cartesian coordinates.

Methods for identifying the model parameters, **p**, and the measurement errors $\tilde{\mathbf{s}}_i = \left[\tilde{\mathbf{s}}_{i,L_{T,1}} \cdots \tilde{\mathbf{s}}_{i,L_{T,N_T}} \quad \tilde{\mathbf{q}}_i \right]$ from the machine tooltip error measurements are described in Section 0. The constraint equations are developed based on the Implicit Loop Method [38], but can be adapted to other solution methods.

Rather than consider the measurements and their respective noise in spherical coordinates, sometimes multiple laser trackers are used and the noisy azimuth and elevation measurements are discarded in a process called multilateration. The next section compares the technique described in this section to multilateration.

3.3. TRIANGULATION AND MULTILATERATION

Triangulation or multilateration refers to the process of using three (or multiple) laser trackers or laser tracker locations to measure the position of a retroreflector more accurately. This is the common practice when laser trackers are used for metrology of tooling and parts and for machine tool calibration. This section will demonstrate that using a maximum likelihood estimator and a single laser tracker approaches the solution with multiple laser trackers.

Triangulation assumes the position of three laser trackers is exactly known. Both techniques use only the distance measurement, R_{ij}, where $i = 1, \ldots, N$ is the measurement number and $j = 1, \ldots, M$ is the tracker number, and R_{ij} is the distance between the ith tool position and the jth laser tracker. The tracker position for the j^{th} tracker is $U_j = [u_j \; v_j \; w_j]^{\text{T}}$. Then the i^{th} tool tip position $p_i = [x_i \; y_i \; z_i]^{\text{T}}$ is the solution to

$$R_{ij} = \left\| p_i - U_j \right\| \tag{37}$$

for $i = 1, \ldots, N$ and $j = 1, \ldots, M$. When $M = 3$, the positions of the laser trackers, U_j, must be exactly known in order to identify each p_i. When $M > 3$, the additional measurements can be used to identify the laser tracker locations. In literature, this system of equations is often solved with the Newton Method, or a similar method [18]. To formulate this problem in the same way as the use of one laser tracker, it is assumed that there is

Gaussian noise on the measurement R_{ij} and on the axis commands $\mathbf{q}_i$, giving a constraint equation similar to the ball bar for each of M trackers and N measurements,

$$0 = R_{ij} + \tilde{R}_{ij} - \left\| \begin{bmatrix} 1 & 0 & 0 & 0 \\ 0 & 1 & 0 & 0 \\ 0 & 0 & 1 & 0 \end{bmatrix} F_{AP}\left(\mathbf{p}, \mathbf{q}_i + \tilde{\mathbf{q}}_i, L_{T\alpha}\right) - U_j \right\| \tag{38}$$

This problem can also be formulated in the same way as a single laser tracker with minor modifications. The constraint equations are

$$f_{i,\alpha}\left(\mathbf{s}_i + \tilde{\mathbf{s}}_i, \mathbf{p}\right) = \mathbf{s}_{i,\alpha} - S\left(\begin{bmatrix} 1 & 0 & 0 & 0 \\ 0 & 1 & 0 & 0 \\ 0 & 0 & 1 & 0 \end{bmatrix} \mathbf{F}_{AP}\left(\mathbf{p}, \mathbf{q}_i + \tilde{\mathbf{q}}_i, L_{T,\alpha}\right) \begin{bmatrix} 0 \\ 0 \\ 0 \\ 1 \end{bmatrix} \right) + \tilde{\mathbf{s}}_{i,\alpha} = 0 \tag{39}$$

where $i = 1, \ldots, N$, N being the total number of measurement commands, $\alpha = 2M$ and $\mathbf{p}$ contains $6(M\text{-}1)$ additional parameters to define the location of each laser tracker. The model parameters, $\mathbf{p}$, and the measurement errors $\tilde{\mathbf{s}}_i = \begin{bmatrix} \tilde{\mathbf{s}}_{i,1} \cdots \tilde{\mathbf{s}}_{i,N_T} & \tilde{\mathbf{q}}_i \end{bmatrix}$ are identified from the machine tooltip error measurements using a constrained optimization routine. The error on the measurements and the model parameters, $\tilde{\mathbf{s}}_i, \mathbf{p}$, are assumed to be independent and Gaussian with the probability density function $e^{-\eta^T \Sigma^{-1} \eta / 2}$ where $\eta = \begin{bmatrix} \tilde{\mathbf{s}}_i^T & \mathbf{p} \end{bmatrix}$ and Σ is the covariance matrix for the measurement errors and the parameters. Based on these assumptions (independent, Gaussian), maximizing the likelihood is the same as minimizing $\eta^T \Sigma^{-1} \eta$ [46]. The maximum likelihood estimate is then

$$\left\{\mathbf{p}, \tilde{\mathbf{s}}\right\} = \arg\min_{\mathbf{p}, \tilde{\mathbf{s}}} \chi^2 = \arg\min_{\mathbf{p}, \tilde{\mathbf{s}}} \sum_{i=1}^{N} \tilde{\mathbf{s}}_i^T \Sigma_{s_i}^{-1} \tilde{\mathbf{s}}_i + \mathbf{p} \Sigma_p^{-1} \mathbf{p} \tag{40}$$

while satisfying (49) for all i and α. For a single laser tracker,

$$\Sigma_{x_i} = diag\left(\begin{bmatrix} \sigma_{q_x} & \sigma_{q_y} & \sigma_{q_z} & \sigma_{q_c} & \sigma_{q_b} & \sigma_R & \sigma_\theta & \sigma_\phi \end{bmatrix}\right) \tag{41}$$

where $\sigma_{qx},\ldots,\sigma_{qb}$ are the standard deviations for the machine axes, and σ_R, $\sigma_{\theta,}$ and σ_ϕ are the static standard deviations associated with each measurement component from the laser tracker. The multilateration solution can be approached assuming:

$$\begin{aligned} &\tilde{\mathbf{q}}_i \to 0 \\ &\sigma_\theta, \sigma_\phi \to \infty \\ &\sigma_R \to 0 \end{aligned} \tag{42}$$

Then, rewriting the objective function,

$$\{\mathbf{p}, \tilde{\mathbf{x}}\} = \arg\min_{\mathbf{p},\tilde{\mathbf{x}}} \chi^2 = \arg\min_{\mathbf{p},\tilde{\mathbf{x}}} \sum_{i=1}^{N_{meas}} \sum_{\alpha=1}^{N_T} \left(\frac{\tilde{R}_{i,\alpha}^2}{\sigma_R^2} + \frac{\tilde{\phi}_{i,\alpha}^2}{\sigma_\phi^2} + \frac{\tilde{\theta}_{i,\alpha}^2}{\sigma_\theta^2} + \tilde{\mathbf{q}}_i^T \Sigma_{q_i}^{-1} \tilde{\mathbf{q}}_i \right) + \mathbf{p}^T \Sigma_p^{-1} \mathbf{p} \tag{43}$$

and taking the limit

$$\begin{aligned} &\lim_{\substack{\sigma_\theta,\sigma_\phi \to \infty \\ \tilde{\mathbf{q}}_i,\sigma_R \to 0}} \arg\min_{\mathbf{p},\tilde{\mathbf{x}}} \sum_{i=1}^{N_{meas}} \sum_{\alpha=1}^{N_T} \left(\frac{\tilde{R}_{i,\alpha}^2}{\sigma_R^2} + \frac{\tilde{\phi}_{i,\alpha}^2}{\sigma_\phi^2} + \frac{\tilde{\theta}_{i,\alpha}^2}{\sigma_\theta^2} + \tilde{\mathbf{q}}_i^T \Sigma_{q_i}^{-1} \tilde{\mathbf{q}}_i \right) + \mathbf{p}^T \Sigma_p^{-1} \mathbf{p} = \\ &\lim_{\sigma_R \to 0} \arg\min_{\mathbf{p}} \sum_{i=1}^{N_{meas}} \sum_{\alpha=1}^{N_T} \left(\frac{\tilde{R}_{i,\alpha}^2}{\sigma_R^2} \right) + \mathbf{p}^T \Sigma_p^{-1} \mathbf{p} = \\ &\lim_{\sigma_R \to 0} \arg\min_{\mathbf{p}} \sigma_R^2 \left[\sum_{i=1}^{N_{meas}} \sum_{\alpha=1}^{N_T} \left(\frac{\tilde{R}_{i,\alpha}^2}{\sigma_R^2} \right) + \mathbf{p}^T \Sigma_p^{-1} \mathbf{p} \right] = \\ &\lim_{\sigma_R \to 0} \arg\min_{\mathbf{p}} \sum_{i=1}^{N_{meas}} \sum_{\alpha=1}^{N_T} \tilde{R}_{i,\alpha}^2 + \sigma_R^2 \mathbf{p}^T \Sigma_p^{-1} \mathbf{p} = \\ &\arg\min_{\mathbf{p}} \sum_{i=1}^{N_{meas}} \sum_{\alpha=1}^{N_T} \tilde{R}_{i,\alpha}^2 \end{aligned} \tag{44}$$

the solution reduces to a simple least squares minimization of the sum of the squared errors on the measurement $R_{i,\alpha}$. This shows that this methodology approaches the solution achieved using multilateration under certain circumstances, but is more flexible since the estimates include information on measurement noise.

3.4. RADIAL FRAMEWORK

On some machines, it may be desirable to integrate small or more accurate measurement tools into the calibration strategy presented in previous sections. One such instrument that might be integrated alongside the laser tracker is the telescoping ball bar, and this will be used as an example of how additional instruments can be integrated.

3.4.1. Ball Bar Description. The telescoping ball bar measures the deviation of the radius of a circle, as illustrated in Figure 3.2.

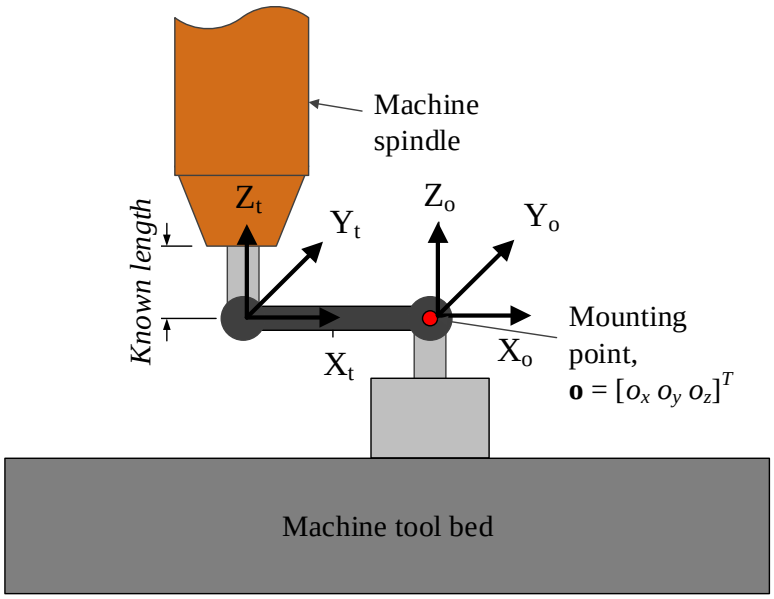

Figure 3.2: Diagram of ball bar measuring a machine.

The ball bar returns a single scalar value, a radius, at each measurement position. To predict this radius, the distance between the tooltip position as modeled and the mounting location of the ball bar, $\mathbf{o} = [o_x\ o_y\ o_z]^T$,

$$r_p(\mathbf{q}_i) = \left\| \begin{bmatrix} 1 & 0 & 0 & 0 \\ 0 & 1 & 0 & 0 \\ 0 & 0 & 1 & 0 \end{bmatrix} \mathbf{F}_{AP}(\mathbf{q}_i, \mathbf{p}, L_{T,\alpha}) \begin{bmatrix} 0 \\ 0 \\ 0 \\ 1 \end{bmatrix} - \mathbf{o} \right\|_2 \tag{45}$$

The measured radius can be represented as the distance between the actual machine with noise on the axis positions, $\tilde{\mathbf{q}}_\mathbf{i}$, and the mounting location, $\mathbf{o}$, with noise $\tilde{r}_i$ corrupting the measured radius,

$$r_i = \left\| \begin{bmatrix} 1 & 0 & 0 & 0 \\ 0 & 1 & 0 & 0 \\ 0 & 0 & 1 & 0 \end{bmatrix} \mathbf{F}_{AP}(\mathbf{p}, \mathbf{q}_i + \tilde{\mathbf{q}}, L_{T,\alpha}) \begin{bmatrix} 0 \\ 0 \\ 0 \\ 1 \end{bmatrix} - \mathbf{o} \right\|_2 + \tilde{r}_i \tag{46}$$

This instrument is incorporated as an additional loop equation (constraint equation) in the ILM or another solution method as

$$f_i(\tilde{\mathbf{x}}_i, \mathbf{p}) = r_i - \tilde{r}_i - \left\| \begin{bmatrix} 1 & 0 & 0 & 0 \\ 0 & 1 & 0 & 0 \\ 0 & 0 & 1 & 0 \end{bmatrix} \mathbf{F}_{AP}(\mathbf{p}, \mathbf{q}_i + \tilde{\mathbf{q}}_i, L_{T,\alpha}) \begin{bmatrix} 0 \\ 0 \\ 0 \\ 1 \end{bmatrix} - \mathbf{o} \right\|_2 \tag{47}$$

where $\tilde{\mathbf{x}}_\mathbf{i}$ is a vector of measurement noise on both the axis positions ($\tilde{\mathbf{q}}_\mathbf{i}$) and the tooltip measurement ($\tilde{r}_i$).

3.4.2. Parameter Identification. Throughout the majority of this work, the Implicit Loop Method has been used to identify parameters of the geometric errors models. This method is generally well suited to this task, but encounters some problems when integrating different types of measurements together. The following subsections discuss methods of solving the constrained optimization problem using the constraint (loop) equations and cost function presented in previous sections, beginning with one of the most common solvers, then discussing the ILM, and finally discussing the quasi-newton methods used by commercially available solver packages such as Matlab.

3.4.2.1. Newton method. The Newton method is a common optimization routine when an x that minimizes $g(a)$ is desired. Starting with some initial value, a^0, the new value of a, a^k, can be calculated based on the previous value, a^{k-1},

$$a^k = a^{k-1} - t\nabla^2 g\left(a^{k-1}\right)^{-1} \nabla g\left(a^{k-1}\right) \tag{48}$$

where t is the step size. This method requires the second derivatives of the objective function, which may be difficult to obtain. Several methods to avoid using second derivatives have been developed. For the problem of machine tool and robot calibration, an algorithm called the Implicit Loop Method (ILM) [38] has been developed and is presented below.

3.4.2.2. Implicit loop method. The model parameters, p, and the measurement errors $\tilde{\mathbf{s}}_i = \left[\tilde{\mathbf{s}}_{i,L_{T,1}} \cdots \tilde{\mathbf{s}}_{i,L_{T,N_T}} \quad \tilde{\mathbf{q}}_i\right]$ are identified from the machine tooltip error measurements using the Implicit Loop Method (ILM) [citation], which is a maximum likelihood estimator. The ILM uses constraint equations, called loop equations, which ensure that all deviation between the measured tool tip position and modeled one be assigned either to the model parameters, p, or the measurement and axis position errors, $\tilde{\mathbf{s}}_i$,

$$f_{i,\alpha}\left(\mathbf{s}_i + \tilde{\mathbf{s}}_i, \mathbf{p}\right) = \mathbf{s}_{i,L_{T,}\alpha} - S\left(\begin{bmatrix} 1 & 0 & 0 & 0 \\ 0 & 1 & 0 & 0 \\ 0 & 0 & 1 & 0 \end{bmatrix} \mathbf{F}_{AP}\left(\mathbf{p}, \mathbf{q}_i + \tilde{\mathbf{q}}_i, L_{T,\alpha}\right) \begin{bmatrix} 0 \\ 0 \\ 0 \\ 1 \end{bmatrix}\right) + \tilde{\mathbf{s}}_{i,L_{T,\alpha}} = 0 \tag{49}$$

where $i = 1, \ldots, N$ and $\alpha = 1, \ldots, A$. The implicit loop method then finds the most likely values for $\tilde{\mathbf{s}}_i$ and model parameters, $\mathbf{p}$, so that these loop equations are satisfied. The error on the measurements and the model parameters, $\tilde{\mathbf{s}}_i, \mathbf{p}$, are assumed to be independent and Gaussian with the probability density function $e^{-\eta^T \Sigma^{-1} \eta/2}$ where $\eta = \begin{bmatrix} \tilde{\mathbf{s}}_i^T & \mathbf{p} \end{bmatrix}$ and Σ is the covariance matrix for the measurement errors and the parameters. Based on these assumptions (independent, Gaussian), maximizing the likelihood is the same as minimizing $\eta^T \Sigma^{-1} \eta$ [46]. The maximum likelihood estimate is then

$$\{\mathbf{p}, \tilde{\mathbf{s}}\} = \arg\min_{\mathbf{p}, \tilde{\mathbf{s}}} \chi^2 = \arg\min_{\mathbf{p}, \tilde{\mathbf{s}}} \sum_{i=1}^{N} \tilde{\mathbf{s}}_i^T \Sigma_{s_i}^{-1} \tilde{\mathbf{s}}_i + \mathbf{p} \Sigma_p^{-1} \mathbf{p} \tag{50}$$

while satisfying (49) for all i and α. For each i, the loop equations are

$$f_i(\mathbf{s}_i + \tilde{\mathbf{s}}_i, \mathbf{p}) = \begin{bmatrix} f_{i,1}(\mathbf{s}_i + \tilde{\mathbf{s}}_i, \mathbf{p}) \\ \vdots \\ f_{i,A}(\mathbf{s}_i + \tilde{\mathbf{s}}_i, \mathbf{p}) \end{bmatrix} \tag{51}$$

In order to simplify the solution to the minimization, an iterative method that requires only the first derivatives of the loop equations, $f_{i,\alpha}$, is developed. First, the normalized variables $\boldsymbol{\xi}_i$ and $\boldsymbol{\psi}$ are introduced, each having a covariance matrix equal to identity. These are related to the measurement noise and parameters by

$$\boldsymbol{\xi}_i = \Sigma_{s_i}^{-1/2} \tilde{\mathbf{x}}_i, \boldsymbol{\psi} = \Sigma_p^{-1/2} \mathbf{p} \tag{52}$$

Rewriting the cost, χ^2 in (50),

$$\chi^2 = \sum_{i=1}^{N} \boldsymbol{\xi}_i^T \boldsymbol{\xi}_i + \boldsymbol{\psi}^T \boldsymbol{\psi} \tag{53}$$

The algorithm is initialized with a guess of zero for both $\boldsymbol{\xi}_i$ and $\boldsymbol{\psi}$. At each step a correction $\Delta\boldsymbol{\xi}_i$ and $\Delta\boldsymbol{\psi}$ is calculated to minimize

$$\chi^2 = \sum_{i=1}^{N} \left(\boldsymbol{\xi}_i + \Delta\boldsymbol{\xi}_i\right)^T \left(\boldsymbol{\xi}_i + \Delta\boldsymbol{\xi}_i\right) + \left(\boldsymbol{\psi} + \Delta\boldsymbol{\psi}\right)^T \left(\boldsymbol{\psi} + \Delta\boldsymbol{\psi}\right) \tag{54}$$

subject to the constraints

$$J_{\xi i}\Delta\boldsymbol{\xi}_i + J_{\psi i}\Delta\boldsymbol{\psi} = -f_i\left(\mathbf{s}_i + \Sigma_{x_i}^{1/2}\boldsymbol{\xi}_i, \Sigma_p^{1/2}\boldsymbol{\psi}\right) \tag{55}$$

where $J_{\psi i}$ and $J_{\xi i}$ are matrices of partial derivatives of f_i obtained using the chain rule. To simplify the solution, an orthogonal decomposition to remove $\Delta\boldsymbol{\psi}_i$ can be performed. First the QR-decomposition of the Jacobian matrix is calculated

$$\mathbf{Q}_i\mathbf{R}_i = J_{\xi\, i}^T \tag{56}$$

Then, the decomposition is used to define $\mathbf{E}_i$ and $\mathbf{D}_i$, which are used to pose the problem in the form of least squares,

$$\begin{aligned} \mathbf{D}_i &= \mathbf{R}_i^{-T} J_{\psi i} \\ \mathbf{E}_i &= \mathbf{Q}_i^T\boldsymbol{\xi}_i - \mathbf{R}_i^{-T} f_i\left(\overline{\mathbf{s}}_i + \Sigma_{x_i}^{1/2}\boldsymbol{\xi}_i, \overline{\mathbf{p}} + \Sigma_p^{1/2}\boldsymbol{\psi}\right) \end{aligned} \tag{57}$$

Then $\Delta\boldsymbol{\xi}_i$ is the least squares solution to

$$\begin{bmatrix} \mathbf{D}_1 \\ \vdots \\ \mathbf{D}_N \\ 1 \end{bmatrix} \Delta\boldsymbol{\xi}_i = \begin{bmatrix} \mathbf{E}_1 \\ \vdots \\ \mathbf{E}_N \\ -\boldsymbol{\xi}_i \end{bmatrix} \tag{58}$$

and $\Delta\boldsymbol{\psi}$ can be found using

$$\boldsymbol{\xi}_i + \Delta\boldsymbol{\xi}_i = \mathbf{Q}_i\left(\mathbf{E}_i - \mathbf{D}_i\Delta\boldsymbol{\psi}\right) \tag{59}$$

This is iterated upon until convergence, when $\Delta\boldsymbol{\psi}$ and $\Delta\boldsymbol{\xi}_i$ are smaller than a set tolerance (typically 10^{-4} has yielded good results).

3.4.2.3. Quasi-newton methods. These methods are similar to the Newton method described in 5.1.1.1, but use first derivatives to approximate the gradient, and are advantageous over the solution algorithm in the ILM because they do not use a least squares update to the parameters as in (58), which is problematic when using measurements with different numbers of constraints since the matrices in (52) would not be invertible. A general quasi-Newton method formulates the minimization of $g(a)$ so that starting with some initial value, a^0, the new value of a, a^k, can be calculated based on the previous value, a^{k-1},

$$a^k = a^{k-1} - tH_{k-1}^{-1}\nabla g\left(a^{k-1}\right) \tag{60}$$

where t is the step size and H_{k-1} is the Hessian at step k-1. One of several ways to update the Hessian, H_k, is to use the Broyden-Fletcher-Goldfarb-Shanno (BFGS) algorithm [47]. The inverse update equation based on BFGS is

$$H_k^{-1} = \left(I - \frac{sy^T}{y^T s}\right)H_{k-1}^{-1}\left(I - \frac{ys^T}{y^T s}\right) + \frac{ss^{-1}}{y^T s} \tag{61}$$

where $s = a^k - a^{k-1}$ and $y = \nabla g\left(a^k\right) - \nabla g\left(a^{k-1}\right)$. This algorithm can be applied with $g(a)$ as the previously defined objective function,

$$\chi^2\left(\mathbf{p},\tilde{\mathbf{s}}_i\right)=\sum_{i=1}^{N}\tilde{\mathbf{s}}_i^T\Sigma_{x_i}^{-1}\tilde{\mathbf{s}}_i+\mathbf{p}\Sigma_p^{-1}\mathbf{p} \tag{62}$$

with the constraints described in (49).

3.5. SIMULATION AND EXPERIMENTAL RESULTS

Below are selected results for a measurement event in spherical coordinates and simulations integrating a ball bar with laser tracker measurements.

3.5.1. Spherical Coordinate Experiments. The Flow machine, described previously, was measured at 262 locations using two tool lengths and a single laser tracker location. Of those measurement, 50 were reserved for validation purposes and 212 were used to fit an Axis Perturbation model of the machine geometric errors with the measurements described either in Cartesian coordinates with static variances, or with Spherical coordinates with variances depending on the distance from the tracker, *R*. Table 3.1 shows the mean and maximum residual volumetric error of each model over the validation set. The residual error in the *R* direction is also calculated. Using spherical coordinates improves the model by a small margin. The mean residual error is reduced by 0.28 thousandths of an inch (0.00028”) and the maximum is reduced by 0.13 thousandths. The residual in the *R* direction is significantly smaller when spherical coordinates are used, so the more accurate component of the measurement is being used more effectively. However, the Flow machine is only 240” long, so the benefit of using spherical coordinates is not as obvious since the laser tracker is reasonably accurate in this range (see accuracy/repeatability data for the API T3 in paper I). This improvement could be more significant on longer machines such as the Master Mill and the Spar Mill presented in Section 2. While very long machines still require multiple laser tracker locations, using distance-based accuracy information is expected to make the modeling process less sensitive to inevitable noisy measurements.

Table 3.1: Modeling results for spherical and Cartesian coordinates.

Measurement type	Mean error, thou	Max error, thou	Mean R resid., thou
Cartesian	1.70	4.00	1.23
Spherical	1.42	3.87	-0.02

3.5.2. Ball Bar Integration. The AP model from 5/2015 Flow data and the Flow machine configuration were used to test the integration of the ball bar. Laser tracker (LT) data was simulated for 300 quasi-random measurement locations and two tool lengths. Ball bar (BB) data was generated for a single location with 300 quasi-randomly selected machine orientations and locations on a sphere with a 10 in radius. Two angles, α_1 and α_2, are used to describe the position of the end of the ball bar, and therefore the tool tip. The tool tip position depends on the angles by

$$\mathbf{p} = \begin{bmatrix} p_x \\ p_y \\ p_z \end{bmatrix} = \begin{bmatrix} r\cos(\alpha_1)\sin(\alpha_2) \\ r\sin(\alpha_1)\sin(\alpha_2) \\ r\cos(\alpha_2) \end{bmatrix} \tag{63}$$

The tool orientation is specified by randomly selecting two of the three components of the tool unit vector <*i*, *j*, *k*>. Since random combinations do not necessarily make a unit vector, the vector is checked to ensure that for some value of the third component, the magnitude is 1. If not, the *i* and *k* components are re-selected until the criterion is met. Once the unit vector components *i* and *k* and the angles α_1 and α_2 are selected, the axis commands are

$$\mathbf{q}_i = \begin{bmatrix} q_b \\ q_c \\ q_x \\ q_y \\ q_z \end{bmatrix} = \begin{bmatrix} \cos^{-1}(k) \\ \cos^{-1}\left(i/\sin(q_b)\right) \\ p_x - \cos(q_c)\sin(q_b)L_T \\ p_y - \sin(q_c)\sin(q_b)L_T \\ p_z - \cos(q_b)L_T \end{bmatrix} \tag{64}$$

The radial measurements can be calculated from the true model parameters, $\mathbf{p}_a$,

$$r_{i,sim} = \left\| \begin{bmatrix} 1 & 0 & 0 & 0 \\ 0 & 1 & 0 & 0 \\ 0 & 0 & 1 & 0 \end{bmatrix} \mathbf{F}_{AP}\left(\mathbf{p}_a, \mathbf{q}_i + \tilde{\mathbf{q}}_{i,sim}, L_{T,\alpha}\right) \begin{bmatrix} 0 \\ 0 \\ 0 \\ 1 \end{bmatrix} - \mathbf{o} \right\|_2 + \tilde{r}_{i,sim} \tag{65}$$

where $\tilde{\mathbf{q}}_{i,sim}$ and $\tilde{r}_{i,sim}$ are randomly generated to be normally distributed with zero mean and variance as listed in Table 1. Similarly, the LT measurements at a position $\mathbf{q}_i$ are generated as

$$\mathbf{x}_{i,sim} = \begin{bmatrix} 1 & 0 & 0 & 0 \\ 0 & 1 & 0 & 0 \\ 0 & 0 & 1 & 0 \end{bmatrix} \mathbf{F}_{AP}\left(\mathbf{p}_a, \mathbf{q}_i + \tilde{\mathbf{q}}_{i,sim}, L_{T,\alpha}\right) \begin{bmatrix} 0 \\ 0 \\ 0 \\ 1 \end{bmatrix} + \tilde{\mathbf{x}}_{i,sim} \tag{66}$$

where $\tilde{\mathbf{q}}_{i,sim}$ and $\tilde{\mathbf{x}}_{i,sim}$ are randomly generated to be normally distributed with zero mean and variance as listed in Table 3.4.

A validation set of 3000 quasi-random points with no measurement noise was generated to evaluate all models. Each validation point, $\mathbf{x}_{v,i}$, is generated from the true model parameters, $\mathbf{p}_a$,

$$\mathbf{x}_{v,i} = \begin{bmatrix} 1 & 0 & 0 & 0 \\ 0 & 1 & 0 & 0 \\ 0 & 0 & 1 & 0 \end{bmatrix} \mathbf{F}_{AP}\left(\mathbf{q}_i, \mathbf{p}_a, L_{T,\alpha}\right) \begin{bmatrix} 0 \\ 0 \\ 0 \\ 1 \end{bmatrix} \tag{67}$$

The problem is initialized with all parameter values at zero and all deviation between measured and modeled position assigned to measurement noise so that the constraints are satisfied. The solver is set to automatically scale the problem based on the initial objective and constraint values since the problem as posed is poorly scaled. A sixth

order axis perturbation model is fit to the simulated LT measurement data, and the model is evaluated over 3000 quasi-random simulated validation points with no measurement noise to calculate the residual volumetric error (VE). Different combinations of laser tracker and ball bar measurements and different levels for the measurement variances are tested to determine the impact of integrating a more accurate instrument on the residual volumetric error. The results are shown in Table 3.3.

Table 3.2: Variance settings for simulated measurements (and algorithm).

Variance	**Setting**
$\sigma_x^2, \sigma_y^2, \sigma_z^2$ (linear axis positioning)	2.5×10^{-7}
σ_c^2, σ_b^2 (rotary axis positioning)	4.0×10^{-6}
σ_{LT}^2 (laser tracker measurements)	1.0×10^{-6}
σ_r^2 (ball bar measurements)	1.0×10^{-8}

Integration of ball bar measurements causes no significant change in the residual volumetric error with 300 or 100 LT measurements, with either one tool length or two (meaning either only position, or position and orientation data). However, when only 50 LT measurements are used, an additional 30 ball bar measurements reduce the mean residual VE from 13.5 thousandths of an inch to 3.9 with one tool length, and from 6.7 to 2.8 with two tool lengths. This demonstrates that the ball bar measurements can be successfully integrated into the model fitting process without negative effect. The ball bar, or a similar instrument could be of particular use where parts of the machine are not visible to the laser tracker, or where taking a large number of laser tracker measurements is not practical due to space or time constraints.

Table 3.3: Mean and maximum residual volumetric errors for models fit from indicated measurements.

Laser tracker	Ball Bar	Variances and notes	Mean (thou)	Max (thou)
300	0	Baseline	0.6	2.5
300	30	Baseline	0.7	2.4
100	0	Baseline	1.4	5.1
100	30	Baseline	1.3	5.0
100	0	1 tool length (baseline variances)	1.7	6.4
100	30	1 tool length (baseline variances)	1.7	7.1
50	0	1 tool length (baseline variances)	13.5	70.4
50	30	1 tool length (baseline variances)	3.9	17.2
50	0	Baseline	6.7	28.2
50	30	Baseline	2.8	13.1

3.6. CONCLUSIONS

This section introduced a modeling and parameter selection methodology that accounts for the accuracy of individual measurement components, which mitigates the lower accuracy of laser trackers. Measurements are used in spherical coordinates so that the dependence of the accuracy on the distance from the instrument can be included in the modeling process. Spherical and Cartesian measurements are compared experimentally on the Flow machine and spherical measurements are found to have an advantage even on a machine only 240” in length. Larger benefits are expected on longer machines due to the distance dependence of the laser tracker accuracy. This methodology was then compared to the industry standard method of handling laser tracker inaccuracy-multilateration. It is common to measure the same machine or part location from four different laser tracker locations and use only the distance measurement from each to solve for the three dimensional position. A proof was presented that the methodology presented here is equivalent under an assumption that the error variance on the azimuth and elevation is infinitely large and the error variance of the range measurement, R,

approaches zero. Since this is not practically true, the presented methodology better accounts for the real measurement errors and utilizes more available information, which will yield a more accurate model.

This method was then extended to instruments in addition to the laser tracker. The ball bar was selected as an example and a description for its measurements was developed. Algorithms for parameter identification were examined to allow each measurement to have a variable number of constraint equations (i.e. for measurements to come from different instruments). Simulations were then performed demonstrating the integration of the ball bar with laser tracker measurements. The ball bar was found not to significantly impact model accuracy as evaluated over a validation set when a sufficient number of laser tracker measurements were used (>100 in this case), but when too few laser tracker measurements were used (50), the ball bar measurements were able to drastically improve the model accuracy. This could be a particular significance for difficult to measure machines that are either very long or have areas of their work volume with poor visibility to the laser tracker, allowing a more accurate or compact instrument to be used to supplement measurements in that area.

4. SUMMARY AND CONCLUSIONS

This work presents a novel machine tool calibration methodology using a laser tracker to collect position and orientation of the tool tip, then examines models of the geometric errors and generates optimal compensation for a variety of machine tool controllers. Paper 1 presents the general methodology and compares two ways of modeling the machine tool geometric errors with the purpose of creating compensation that is implemented via look up tables on the machine tool controller. This compensation is then validated experimentally on a lab 5-axis machine tool. The table-based volumetric error compensation methodology is shown to be able to generate a model of the machine that accounts for the interaction between the different machine tool axes that significantly reduces the machine geometric errors.

Section 2 takes this methodology and implements it on a wide variety of machines in different settings. Previous work was conducted only on a laboratory machine in a well-controlled environment, but this section presents six different machine tools, five of which were in a production environment. Two machines each were Boeing Commercial and Boeing Defense, and the fifth machine was a NASA production machine. Each machine had its unique challenges, with some being very long (Boeing Commercial-Spar Mill), some having odd configurations (Boeing Defense), and some having errors not encountered in the lab setting such as temperature fluctuations (Boeing Commercial-Master Mill) and skewing between multiple gantry axes (NASA Ingersoll). Despite this, table-based VEC was able to reduce errors on all of these machines with the exception of a single machine whose accuracy was already as good as typical VEC accuracies.

Compensation was implemented on certain machines with a Siemens 840D, which allows a larger number of compensation look up tables. However, several of the machine tool controllers encountered had limitations to the number or combinations of look up tables that could be used. The method developed in Paper I assumes that all possible compensation tables can be implemented on the machine tool controller, and this is not the case. In Paper II, an artificial intelligence algorithm was proposed to solve the difficult combinatorial optimization problem of selecting an optimal subset of compensation tables from the set of possible tables. This method was compared to a simple heuristic in simulation and validated on a laboratory machine experimentally. The

artificial intelligence algorithm was able to produce a better performing solution than the heuristic in less time than a brute force solution.

Section 3 addresses the accuracy of the instrument used to collect tool tip data for the construction of the models used in previous sections. Measurements are modeled in spherical rather than Cartesian coordinates and distance dependent variances are used in a Maximum Likelihood Estimator to identify model parameters. This method is shown to improve model accuracy even on smaller machines, and may have an even larger impact on longer machines were laser tracker accuracy particularly suffers. This method was also compared to multilateration, which is a standard practice of measuring the same tool tip location from at least four different laser tracker locations and identifying the three dimensional position from only the more accurate interferometer measurement provided by each of the laser trackers. This is demonstrated to be equivalent to the proposed method under an assumption that the error variance on the encoder measurements (azimuth and elevation) is infinitely large and the error variance of the interferometer measurement, R, approaches zero. Since this is not practically true, the presented methodology better accounts for the real measurement errors and utilizes more available information, which will yield a more accurate model. The model fitting method was also adapted to include more accurate instruments, although the studied instrument only improved the model over a validation set in simulation when an inadequate number of laser tracker measurements were used. However, including an additional instrument could be of more benefit when parts of a machine workspace have poor visibility to the laser tracker or are not possible to reach with the laser tracker's active target mounted in the spindle. For example, the workspace very close to the table is difficult to measure particularly on small machines, and other machine may be very enclosed. In these cases a minimal number of laser tracker measurements combined with another instrument could allow a model to be made of errors in otherwise unmeasurable areas of the workspace.

Overall, this work presents a fast method of machine tool calibration that requires no foreknowledge of errors and builds whole model of geometric errors with one set of measurements. This method is able to create optimal compensation for a variety of machine tool controllers and has been proven on a variety of machine tools, bringing volumetric error compensation to both old and new machines, regardless of controller

capability or difficult to measure configurations. The proposed methodology benefits a wide variety of machine tools and can bring cost savings by causing less machine down time, producing better quality parts, and fewer rejected parts due to machine inaccuracy.

BIBLIOGRAPHY

[1] S. Sartori and G. X. Zhang, "Geometric Error Measurement and Compensation of Machines," *CIRP Annals -- Manufacturing Technology,* vol. 44, no. 2, pp. 599-609, 1995.

[2] H. Schwenke, M. Franke and J. Hannaford, "Error Mapping of CMMs and Machine Tools by a Single Tracking Interferometer," *CIRP Annals – Manufacturing Technology,* vol. 54, no. 1, pp. 475-478, 2005.

[3] ISO 230-1, *Test Code for Machine Tools Part I: Geometric Accuracy of Machine Tools Operating Under No-Load or Quasi-Static Conditions,* Geneva, Switzerland: ISO, 2012.

[4] S. Ibaraki and W. Knapp, "Indirect Measurement of Volumetric Accuracy for Three-axis and Five Axis Machine Tools: A Review," *International Journal of Automation Technology,* vol. 6, no. 2, 2012.

[5] M. Tsutsumi and A. Saito, "Identification and Compensation of Systematic Deviations Particular to 5-Axis Machining Centers," *International Journal of Machine Tools and Manufacture,* vol. 43, pp. 771-780, 2003.

[6] S. H. H. Zargarbashi and J. R. R. Mayer, "Assessment of Machine Tool Trunnion Axis Motion Error, Using Magnetic Double Ball Bar," *International Journal of Machine Tools and Manufacture,* vol. 46, pp. 1823-1834, 2006.

[7] S. Weikert, "R-Test, a New Device for Accuracy Measurements on Five-Axis Machine Tools," *CIRP Annals-- Manufacturing Technology,* vol. 53, no. 1, pp. 429-432, 2004.

[8] S. Ibaraki, C. Oyama and H. Otsubo, "Construction of an Error Map of Rotary Axes on a Five-Axis Machining Center by Static R-Test," *International Journal of Machine Tools and Manufacture,* vol. 51, no. 3, pp. 190-200, 2011.

[9] W. T. Lei, I. M. Paung and C.-C. Yu, "Total Ballbar Dynamic Tests for Five-Axis CNC Machine Tools," *International Journal of Machine Tools and Manufacture,* vol. 49, no. 1, pp. 488-499, 2009.

[10] W. Jywe, T. Hsu and C.-H. Liu, "Non-Bar, An Optical Calibration System for Five-Axis CNC Machine Tools," *International Journal of Machine Tools and Manufacture,* vol. 59, no. 1, pp. 16-23, 2012.

[11] P. Freeman, "A Novel Means of Software Compensation for Robots and Machine Tools," in *Aerospace Manufacturing and Automated Fastening Conference and Exhibition*, Toulouse, France, September, 2006.

[12] I.-M. Chen, G. Yang, C. T. Tan and S. H. Yeo, "Local POE Model for Robot Kinematic Calibration," *Mechanism and Machine Theory,* vol. 36, no. 1, pp. 1215-1239, 2001.

[13] R. He, S. Zhao and S. Yang, "Kinematic-Parameter Identification for Serial-Robot Calibration Based on POE Formula,"," *IEEE Transactions on Robotics,* vol. 26, no. 3, pp. 411-423, 2010.

[14] C. Hollerbach, J. Wampler and T. Arai, "An Implicit Loop Method for Kinematic Calibration and Its Application to Closed-Chain Mechanisms," *IEEE Trans. Robotics and Automation,* vol. 11, no. 5, pp. 710- 724, 1995.

[15] K. Umetsu, R. Furutnani, S. Osawa, T. Takatsuji and T. Kurosawa, "Geometric Calibration of a Coordinate Measuring Machine Using a Laser Tracking System," *Measurement Science and Technology,* vol. 16, pp. 2466-2472, 2005.

[16] S. Ibaraki, T. Hata, T. Yano, T. Takatsuji, S. Osawa and O. Sata, "Esimation of the Three-dimensional Volumetric Errors of Machine Tools by a Laser Tracker," in *Asian Symposium for Precision Engineering and Nanotechnology*, Kitakyushu, Japan], 2009.

[17] H. Schwenke, M. Franke and J. and Hannaford, "Error Mapping of CMMs and Machine Tools by a Single Tracking Interferometer," *CIRP Annals – Manufacturing Technology,* vol. 54, no. 1, pp. 475-478, 2005.

[18] H. Schwenke, R. Schmitt, P. Jatzkowskib and P. Warmanna, "On-the-fly Calibration of Linear and Rotary Axes of Machine Tools and CMMs Using a Tracking Interferometer," *CIRP Annals--Manufacturing Technology,* vol. 58, pp. 477-480, 2009.

[19] A. Nubiola and I. Bonev, "Absolute Calibration of an ABB IRB1600 Robot Using a Laser Tracker," *Robots and Computer Integrated Manufacturing*, vol. 29, no. 1, p. 236–245, 2012.

[20] S. Aguado, D. Samper, J. Santolaria and J. Aguilar, "Identification Strategy of Error Parameter in Volumetric Error Compensation of Machine Tool Based on Laser Tracker Measurements," *International Journal of Machine Tools and Manufacture,* vol. 53, no. 1, pp. 160-169, 2012.

[21] B. Mooring, "The Effect of Joint Axis Misalignment on Robot Positioning Accuracy," in *Proccedings of the 1983 ASME Computers in Engineering Conference*, Chicago, Illinois, August 1983.

[22] B. Mooring, Z. S. Roth and M. R. Driels, Fundamentals of Manipulator Calibration, John Wiley & Sons, Inc. , 1991.

[23] H. Stark and J. W. Woods, "Maximum Likelihood Parameter Estimation," in *Probability, Random Processes, and Estimation Theory for Engineers*, Upper Saddle River, NJ, Prentice Hall, 1994, pp. 284-286.

[24] J. Nocedal and S. J. Wright, Numerical Optimization, Springer, 2006.

VITA

Jennifer Ruth Creamer received her Bachelor of Science in Mechanical Engineering from Montana State University in Bozeman, MT on May 7, 2010. She began working as an engineer at Boeing Research and Technology in November of 2015. She received her Doctor of Philosophy in Mechanical Engineering from Missouri University of Science and Technology in May of 2017.